UCLouvain
Institute for Information
and Communication Technologies,
Electronics and Applied Mathematics

Joint coverage and EMF exposure analysis in cellular and cell-free networks

A stochastic geometry perspective

Charles Wiame

Thesis submitted in partial fulfillment
of the requirements for the degree of
Docteur en sciences de l'ingénieur

Dissertation committee:

Prof. Claude Oestges (UCLouvain, advisor)
Prof. Luc Vandendorpe (UCLouvain, advisor)
Prof. Jérôme Louveaux (UCLouvain, secretary)
Prof. François Baccelli (INRIA)
Prof. Marco Di Renzo (CentraleSupelec, Université Paris-Saclay)
Prof. Christophe Craeye (UCLouvain, chairman)

Version of June 22, 2023.

Abstract

The objective of this thesis consists in analysing the global statistics of the coverage and EMF exposure in wireless communication networks. To this purpose, stochastic geometry theory is employed as mathematical framework to model the randomness in the network topology. A number of novel performance metrics are introduced to characterize the exposure in large-scale environments. Two categories of wireless architectures are then studied: cellular and cell-free systems. Finally, an optimization problem is proposed to minimize the exposure in a heterogeneous network for a scenario of tier addition.

Acknowledgements

My first words are naturally dedicated to Prof. Claude Oestges and Prof. Luc Vandendorpe, to whom I am grateful for hiring me as a their student and for their availability during my PhD years.

I also would like to express my gratitude to the other members of the jury: Prof. Jérôme Louveaux, Prof. François Baccelli, Prof Marco Di Renzo and Prof. Christophe Craeye, for participating to the evaluation of my work.

The outcome of this thesis would not have been possible without all the colleagues who had the craziness of collaborating with me on research projects! In addition to the professors cited here above, a number of co-authors have to be to be mentioned here: Quentin Gontier, Dr. Shanshan Wang, Prof. Joe Wiart, Prof. F. Horlin, Dr. C. Tsigros, Prof. P. De Doncker, Dr. Simon Demey, Julien Pirard, François De Saint Moulin, Martin Willame, Dr. Hussein Kassab, Dr. François Rottenberg, Dr. Thomas Feuillen and Nicolas Rorive. Thank you to all of you!

On a more human level, I am more than grateful to two people in particular:

- among all the people mentioned in this section, my biggest thank is without a doubt addressed to Dr. Simon Demey. My appreciation for your friendship and for putting up with my good and bad sides goes beyond infinity!

- a big up to Dr. Thomas Pairon, who was a more than amazing office mate during my first PhD years.

Many other colleagues should be mentioned here as well. Acknowledging each of them in an exhaustive manner is unfortunately not possible given the format of this manuscript. Resorting to a global formulation, I would like to thank all colleagues from UCLouvain (professors, researchers, support staff, ...) for the nice moments we shared, and for any help provided to me during my stay in ICTEAM.

My last thanks finally go to my loved ones, whose names are clearly not needed to be mentioned here.

Contents

List of Figures . . . . . **ix**

List of Tables . . . . . **xi**

Acronyms . . . . . **xi**

List of symbols **1**

1 Introduction **1**

1.1 Context: EMF exposure in wireless networks 1

1.2 Fundamentals of stochastic geometry 4

1.2.1 Stochastic geometry for wireless networks 4

1.2.2 General results 5

1.2.3 Void probability and contact distribution 7

1.2.4 Slivnyak–Mecke's theorem 8

1.2.5 Campbell's theorem 8

1.2.6 Probability generating functional 9

1.2.7 Gil-Pelaez's inversion theorem 10

1.3 Review of related literature 10

1.3.1 Wireless power transfer 11

1.3.2 EMF monitoring 11

1.4 Stochastic geometry at UCLouvain 12

1.4.1 EMF exposure monitoring 13

1.4.2 Sensing applications 16

1.4.3 SWIPT systems 17

1.4.4 Beyond 5G technologies 17

1.5 Outline and contributions of the thesis 18

2 Definition of novel performance metrics . . . 21
2.1 Introduction . . . 21
2.1.1 Notations . . . 21
2.1.2 Related works . . . 22
2.1.3 Contributions . . . 27
2.2 System model . . . 27
2.3 Novel performance metrics . . . 29
2.3.1 Joint coverage-exposure distribution with exposure limitation . . . 29
2.3.2 Meta distribution of the exposure . . . 32
2.3.3 Meta distribution of the coverage-exposure . . . 36
2.3.4 Joint spatial distributions . . . 38
2.3.5 Efficiency ratios . . . 41
2.4 Conclusions of the chapter . . . 42
2.4.1 Summary . . . 42
2.4.2 Further research directions . . . 42

3 Analysis of cellular networks . . . 47
3.1 Introduction . . . 47
3.1.1 Point processes for cellular network modelling . . . 47
3.1.2 Approximating non-Poisson point processes . . . 48
3.1.3 Contributions . . . 49
3.2 System model . . . 50
3.3 Performance analysis . . . 52
3.3.1 Notations . . . 52
3.3.2 Distance of the closest base stations . . . 53
3.3.3 Association probabilities . . . 56
3.3.4 Distance distribution of the serving base station . . . 57
3.3.5 Characteristic functions . . . 57
3.3.6 Marginal distributions . . . 60
3.3.7 Joint coverage and exposure distribution . . . 61
3.4 Numerical results . . . 63
3.5 Conclusions of the chapter . . . 63
3.5.1 Summary . . . 63
3.5.2 Further research directions . . . 64

4 Analysis of cell-free networks . . . 67
4.1 Introduction . . . 67
4.1.1 Related works . . . 69
4.1.2 Contributions . . . 69

4.2 System Model . . . 70
4.2.1 Network topology . . . 70
4.2.2 Channel model . . . 71
4.2.3 Association policy . . . 72
4.2.4 Downlink signal model . . . 72
4.2.5 Beamforming strategy and power allocation . . . 73
4.3 Performance Analysis . . . 74
4.3.1 Signal model simplification . . . 75
4.3.2 Statistics of the incident power coming from the centric cluster 76
4.3.3 Statistics of the power coming from outside the centric cluster 80
4.3.4 Global metrics . . . 81
4.4 Numerical Results . . . 82
4.4.1 Impact of the cluster overlaps . . . 82
4.4.2 Marginal distributions and RRH density . . . 83
4.4.3 Rate-IPD trade-offs . . . 84
4.4.4 Existence of an optimal node density . . . 85
4.5 Conclusions of the chapter . . . 86
4.5.1 Summary . . . 86
4.5.2 Further research directions . . . 86

5 Constrained minimization of the EMF exposure . . . 91
5.1 Introduction . . . 91
5.2 System model . . . 93
5.3 Analytical framework . . . 94
5.4 Formulation of the optimization problem . . . 95
5.5 Solutions of the optimization problem . . . 96
5.6 Numerical results . . . 102
5.7 Conclusions of the chapter . . . 103
5.7.1 Summary . . . 103
5.7.2 Further research directions . . . 104

6 Conclusions . . . 111
6.1 Summary of the thesis . . . 111
6.2 Future work . . . 112
6.2.1 Extensions of the current models . . . 112
6.2.2 About stochastic geometry . . . 113
6.2.3 Further research directions . . . 113

Appendices . . . 117

A On the units of the EMF exposure 117
B On the computational complexity of SG results 118
C Proof of Proposition 2.3 120
D Proof of Proposition 2.6 123
E Proof of Proposition 2.12 128
F Proof of Proposition 2.14 129
G Proof of Assumption 4.1 130
H Proof of Assumption 4.2 133
I Proof of Proposition 4.3 136
J Proof of Proposition 4.4 138
K Proof of Proposition 4.6 140
L Proof of Proposition 4.9 142

Appendix Bibliography 143

List of Figures

1.1 Overview of the research projects related to stochastic geometry conducted at UCLouvain. 12
1.2 Average EMF exposure from the LTE 1800 network of one major Belgian operator around the Brussels center. 14
1.3 Illustration of two examples of Poisson line processes. 15

2.1 Bidimensional representation of the metric $\mathcal{J}_{\text{lim}}(T, T')$ 31
2.2 Conditional coverage probability 31
2.3 Mean and variance of the conditional IPD distribution 34
2.4 Illustration of IPD Meta distribution $\tilde{\mathcal{F}}_{\mathcal{P}_{\text{IPD}}}(s, T')$ 43
2.5 Illustration of the metrics $\mathcal{J}_s^{\text{IPD}}(T_1', T_2'; d)$ and $\mathcal{T}_s^{\text{IPD}}(T_1', T_2'; d)$ in the absence of fading 44
2.6 Illustration of the metrics $\mathcal{J}_s^{\text{IPD}}(T_1', T_2'; d)$ and $\mathcal{T}_s^{\text{IPD}}(T_1', T_2'; d)$ in the presence of fading 45

3.1 Illustration of the zones associated the four subtiers. 53
3.2 Illustration of the IDT results obtained for several French operators in Paris. 65

4.1 Cell-free versus user-centric cell-free networks. 68
4.2 Illustration of the cluster overlaps with distance-based clusters. 72
4.3 Structure of Section 4.3. 75
4.4 Geometrical representation of the quantities n_U and n_U' 77
4.5 Geometrical representation of the quantities n_R and n_R' 78
4.6 Impact of the cluster overlaps 84
4.7 Coverage and exposure CDFs for several RRH densities 87
4.8 Rate-IPD trade-offs 88

4.9 Evolution of the metric $\mathcal{J}_{\text{lim}}(T, T')$ as function of the average number of RRHs per cluster 89
4.10 Illustration of the optimal RRH densities maximizing $\mathcal{J}_{\text{lim}}(T, T')$ 90

5.1 Illustration of the CDF of the useful received power as function of the densities λ_1 and λ_2 97
5.2 Representation of the constraints $c2a$ and $c2b$. 97
5.3 Representation of domains associated to cases I to IV. 105
5.4 Representation of domains associated to cases VI and VIII . . . 106
5.5 Optimal CDF $\mathcal{P}^*_{P_S}(T')$ of the useful received power illustrated for several coverage constraints 106
5.6 Optimal CDF of the useful received power $\mathcal{P}^*_{P_S}(T' = -85dBm)$ as function of the coverage constraint (p, T) 107
5.7 Optimal CDF of the useful received power $\mathcal{P}^*_{P_S}(T' = -75dBm)$ as function of the coverage constraint (p, T) 107
5.8 Optimal CDF of the useful received power $\mathcal{P}^*_{P_S}(T' = -65dBm)$ as function of the coverage constraint (p, T) 108
5.9 Optimal CDF of the useful received power $\mathcal{P}^*_{P_S}(T' = -75dBm)$ with $\alpha = 4.5$ 108
5.10 Influence of the path loss exponent on the optimal $\mathcal{P}^*_{P_S}(T')$ . . 109

6.1 Examples of metrics considered in the deployment of future mobile generations 115
2 Illustration of the distances with two users. 128
3 Illustration of the approximation employed to obtain (63). . . . 132
4 Intersections considered to compute the conditional probabilities. 133

List of Tables

2.1 Overview of the new performance metrics 27

3.1 Comparison of the model of Chapter 3 with existing works. 50
3.2 Table of parameters for urban Paris case. 63

5.1 Summary of the solutions of (5.11) 101

1 Comparison of the runtimes required to evaluate equations (5.7) and (2.37) via MC simulations and SG. 118

1 Introduction

1.1 Context: EMF exposure in wireless networks

Electromagnetic waves carry energy. In 1884, John Henry Poynting [1] introduced a vector (later named *Poynting's vector*) representing the direction of the energy flux generated by these waves. The same author also developed a theorem describing the energy conservation for these electromagnetic (EM) fields.

Since the 20th century, EM waves have been employed in plethora of scientific inventions, ranging from medical imaging and treatments to home appliances. Among these inventions, wireless communications is probably the most ubiquitous application in our everyday lifes. In that context, EM waves transmit information to mobile users in addition to energy. Due to the broadcast nature of these waves, mobile devices of current wireless networks can receive various types of signals. The following classification is possible, distinguishing:

- the useful data stream intended to a device and transmitted by its serving base station;
- other information sequences sent by other base stations and intended to different devices. These signals constitute *interference* and can potentially affect the useful data.

Independently of this classification, mobile users experience an electromagnetic field (EMF) exposure coming from their surrounding base stations. We define the *incident power density* (IPD) as the sum of the contributions from all of these base stations (independently of their serving or interfering role). This incident power density is the central concept analyzed in this thesis. At the time of writing this manuscript, its study can be motivated in three different contexts:

1. *EMF monitoring for public health*: the EMF exposure caused by communication networks is regulated in many countries [2]. An important issue for mobile operators therefore consists in optimizing the performance of their networks while meeting these regulations. Two remarks can be mentioned regarding this first context:

    - One will note that the IPD is actually not strictly equal to the exposure absorbed by the users. More information absorption mechanisms and about the units of the exposure can respectively be found in the references of [3] and in Appendix A. In the context of this manuscript, the proposed level of abstraction restricts the analysis to the IPD only. A slight abuse of language will therefore be employed in this text, using the two wordings as synonyms.
    - At the time of writing this manuscript, the above regulations are subject to debates and controversy in Belgium due to the deployment of 5G networks. The objective of this manuscript is not to discuss the relevance of the actual limits, neither to assess the hypothetical impact of the EMF on the public health. The point of view taken taken in this dissertation rather considers the analysis and optimization of the performance of current networks given this legal constraint.

    The vast majority of this thesis is dedicated to this first aspect. In particular, the *joint statistics* of the exposure and of the quality of service are investigated. Indeed, both these quantities are statistically correlated, yet often independently analysed. This claim is easily explained in the following lines. Building up on the previous classification, let us define

    - S, the signal containing the useful data sequence intended to this user. We denote by P_S the average power of this signal.

- I, the total interference due to information signals dedicated to other user equipments. We denote by P_I the associated power.

The quality of service experienced by this mobile user can be quantified in terms of *signal-to-inference-plus-noise ratio* (SINR):

$$SINR = \frac{P_S}{P_I + P_N} \tag{1.1}$$

where P_N denotes the noise power. Using the same notations, the total IPD arriving at the user is given by

$$IPD = P_S + P_I \tag{1.2}$$

Current mobile networks often manage to operate in *high SINR conditions*. Such operating points implies that $P_S \gg P_I$, resulting in a strong correlation between the two quantities.

2. *Wireless power transfer*: in a different context, the IPD can be viewed as an energy resource to be harvested. During the last decade, a number of studies have explored this direction [4–6]. Such a harvested energy can for instance be employed to recharge the battery of a mobile device. A number of works also investigate *simultaneous information and power transfer* (SWIPT). In this framework, multiple techniques have been developed at the receiver to perform both information decoding and energy harvesting [6]: time switching, power splitting, antenna switching, etc. For these SWIPT systems, performance studies typically include the analyses of trade-offs between the data rate and the harvested energy.

3. *Radar applications*: in the case of sensing scenarios, the useful signal S is not a wave sent by a base station, but a radar echo coming from a target to be detected. The measured IPD is then employed as a decision variable associated to the potential presence of the target. This IPD also contains a form of interference present in these systems due to the background clutter, or to applications operating in the same bands as the radar. The *detection probability* is the metric associated to CDF of this radar IPD [7]. Likewise, the *radar success probability* is defined as the CDF of the *radar* SINR based on the radar echo [8]. Thanks to these similarities, parts of the framework developed in this thesis for EMF monitoring can be transposed to radar applications.

An additional argument motivating the study of the IPD is its likelihood of significantly changing in future mobile networks. Several factors explain this expected evolution:

- the massive densification of access points predicted for the upcoming years [9];
- the new frequency bands (mmWave and THz), expected to be exploited by future cellular generations [10].

Regarding the methodology, multiple tools are possible to model these future networks. Depending on the desired study (large-scale or site specific), a number of approaches are more or less suitable: ray-tracing, full-wave techniques, etc. Further information about these methods is available in [11]. In the particular case of this thesis, **the proposed objective consists in analytically describing the global statistics of the IPD in large-scale environments**. To this purpose, *stochastic geometry* theory is selected to meet these requirements. The next section provides an introduction to this mathematical framework.

1.2 Fundamentals of stochastic geometry

Stochastic geometry (SG) is a branch of spatial statistics dedicated to the study of random irregular patterns. In addition to telecommunications, this theory has been applied in various fields: astronomy, material science, image analysis, etc. A mathematical introduction on the topic (independent of the context of telecommunications) is available in [12].

1.2.1 Stochastic geometry for wireless networks

Considering the application of telecommunications, SG is employed to capture the randomness in the positions of the network nodes (base stations and mobile users). In all generality, the quality of service experienced by any user depends on its location with respect the base stations of the network. From the point of view of mobile operators, it is interesting to know the statistics of this quality of service, averaged out over possible spatial configurations of these network nodes. As an alternative to Monte Carlo simulations, SG is used to derive analytical expressions

describing this global performance as function of the network's macro parameters (e.g. node densities).

At the time of writing this dissertation, a few thousand publications have been written on the topic of SG for wireless networks. A number of aspects have been analysed regarding:

- the metrics describing the performance. A survey detailing these metrics is provided in section 2.1.2.
- the topology of the network, which can be modelled by means of different point processes. These point processes can exhibit various behaviours such as correlation, attraction or repulsion between the nodes.
- the propagation model, with degrees of freedom in the selection of the path loss, shadowing and fading models.
- the technologies employed by the network. A non-exhaustive list of studied techniques include MIMO beamforming, multihop relays, cognitive networks, ...

Examples of associated surveys are available in [13–15].

1.2.2 General results

This subsection summarizes fundamental definitions and theorems necessary for most models of this dissertation. Advanced concepts required for specific sections are covered further down, within the corresponding chapter. All the notions are based on the books [16–18], which are extensively used as references for many works of the research field.

Point processes

Definition 1.1. A point process (PP) Ψ can be defined as a countable random collection of points residing in a measure space. In the framework of this dissertation, the selected space is the Euclidean plane $\mathbb{R}^2$.

Point processes are classically characterized by counting the number of points contained within sets $B \in \mathbb{R}^2$. The non-negative random variable corresponding to this number of points is called *random counting measure* and is denoted by $N(B)$. In addition, the deterministic equivalent of the

random counting measure is the *intensity measure*, defined as the expected number of points in the set B:

$$\Lambda(B) = \mathbb{E}\big[N(B)\big] \tag{1.3}$$

Poisson point processes

Definition 1.2. A Poisson point process (PPP) Ψ of intensity measure $\Lambda(\cdot)$ is a PP satisfying the two following properties:

1. for every compact set $B \in \mathbb{R}^2$, $N(B)$ follows a Poisson distribution of mean $\Lambda(B)$.
2. for any mutual disjoint sets $B_1, \ldots, B_n$, the random variables $N(B_1)$, $\ldots$, $N(B_n)$ are independent.

Instead of characterizing a PPP by means of its intensity measure $\Lambda(\cdot)$, one can also describe it as function of its *density* $\lambda(x, y)$ or $\lambda(r, \theta)$. This density function is mathematically defined by the following equality:

$$\Lambda(B) = \int_{(x,y)\in B} \lambda(x, y) dx dy \tag{1.4}$$

$$\text{or } \Lambda(B) = \int_{(r,\theta)\in B} \lambda(r, \theta) r dr d\theta. \tag{1.5}$$

As additional classification, a PPP is *homogeneous* (resp: *inhomogeneous*) if this density is constant (resp: depends on r/θ or x/y).

PPPs are studied in the majority of the publications associated to SG for wireless networks. All PPs employed in this thesis belong to this category. Several reasons can explain their prevalence in the literature:

- They benefit from remarkable properties: invariance under translation and rotation[1], preservation (under superposition, thinning and transformation with a kernel), etc. For this reason, the PPP is often considered as the 'Gaussian' of point processes.
- They enable to derive to expressions which are more tractable than using other PPs. Such a tractability is obtained thanks to notable theorems and results: Campell's theorem, probability generating functional, ... (see below);

[1] the properties of invariance under translation and rotation are also called *stationarity* and *isotropy* respectively

- Their distribution was historically shown to be provide a good fit to several real network deployments [19].

1.2.3 Void probability and contact distribution

In telecommunications, mobile users are often served by the closest base station of their operator's network. This base station provides in that case the useful information signal to the user. Other base stations of the network are then either silent, or provide some interference if they are serving other users on the same resources (time,space,frequency). Since base stations are here represented via PPPs, it is relevant to derive the distribution of the distance from an arbitrary user location to the closest point for these PPPs. By convention, this arbitrary user location is usually assumed to be $(0,0)$. In the case of a HPPP, this choice has no impact since the HPPP is translation and rotation invariant.

Definition 1.3. Given a compact set $B \in \mathbb{R}$, the *void probability* of a PP Ψ is the probability that no point of Ψ lies in B. For a PPP, its expression is given by

$$\mathbb{P}\Big[N(B)=0\Big] = \exp\Big(-\Lambda(B)\Big). \tag{1.6}$$

Definition 1.4. The *contact distribution* of a PP Ψ is defined as the probability density function (PDF) from $(0,0)$ to the closest point of Ψ. For a PPP of intensity function $\lambda(r,\theta)$, its expression is given by

$$f_R(r) = \frac{\partial}{\partial r}\left(\int_0^{2\pi}\int_0^r \lambda(r',\theta)r'dr'd\theta\right)\exp\left(-\int_0^{2\pi}\int_0^r \lambda(r',\theta)r'dr'd\theta\right) \tag{1.7}$$

Proof. Let $D(\mathbf{o},r)$ be the disk of radius r centered around $(0,0)$. The void probability associated to this set is given by

$$\mathbb{P}\Big[N(B)=0\Big] = \exp\Big[-\Lambda\Big(D(\mathbf{o},r)\Big)\Big]. \tag{1.8}$$

For the HPPP, this expression becomes

$$\mathbb{P}\Big[N\Big(D(\mathbf{o},r)\Big)=0\Big] = \exp\left(-\int_0^{2\pi}\int_0^r \lambda(r',\theta)r'dr'd\theta\right). \tag{1.9}$$

Using the definition of the void probability, the cumulative distribution (CDF) of the distance to the closest point of Ψ is by definition given by

$$F_r(r) = 1 - \mathbb{P}\left[N\Big(D(\mathbf{o}, r)\Big) = 0\right] \tag{1.10}$$

The contact distribution is then obtained by deriving the last expression with respect to r.

□

Corollary 1.5. *For a HPPP of density λ, the expression of the contact distributions becomes*

$$f_R(r) = 2\pi r \exp(-\lambda \pi r^2) \tag{1.11}$$

1.2.4 Slivnyak–Mecke's theorem

In addition to characterizing the useful power received by the user, it is important to properly model the aggregate interference coming from the other base stations of the network. This set of interfering nodes is equal to the realization of PP Ψ from which the closest node (providing the useful signal) has been retrieved.

Slivnyak–Mecke's theorem states that the *reduced Palm distribution* of PPP is equal to its original distribution [16]. As explained in [20], this theorem means that conditioning on a particular point of the process has no impact on the distribution and statistical properties of the rest of the process. As a consequence, the interference of the network can be analyzed as a PPP despite removing the service base station from the process.

1.2.5 Campbell's theorem

Theorem 1.6. *Let Ψ be a PPP on $\mathbb{R}^2$, $f : \mathbb{R}^2 \to \mathbb{R}$ and S the random variable defined as*

$$S = \mathbb{E}\left[\sum_{\underline{x}_i \in \Psi} f(\underline{x}_i)\right] \tag{1.12}$$

If the mean of S is finite, the following equality can be written:

$$\mathbb{E}[S] = \int_{\mathbb{R}^2} f(\underline{x}) \Lambda(d\underline{x}) \tag{1.13}$$

If the intensity function of Ψ is defined, this expression can also be rewritten as

$$\mathbb{E}[S] = \int_{(x,y)\in\mathbb{R}^2} f(x,y)\lambda(x,y)dxdy \tag{1.14}$$

$$or\ \ \mathbb{E}[S] = \int_{(r,\theta)\in\mathbb{R}^2} f(r,\theta)\lambda(r,\theta)rdrd\theta \tag{1.15}$$

This theorem will be here employed to compute the moments of the total EMF exposure affecting a mobile user (i.e. the *sum* of the individual incident power densities coming from each base station).

1.2.6 Probability generating functional

Campbell's theorem enables to derive the mean of sums performed over a PPP. With the same line of thought, the notion of *probability generating functional* (PGFL) enables to compute products over the points of the PP.

Definition 1.7. Let $\mathcal{F}$ be the family of measurable functions $f : \mathbf{R}^2 \to [0,1]$ such that $1-f$ has a bounded support. For $f \in \mathcal{F}$, the PGFL of a PP Ψ is defined as

$$G[f] \triangleq \mathbb{E}\left[\prod_{\underline{x}_i\in\Psi} f(\underline{x}_i)\right] \tag{1.16}$$

If Ψ is a PPP, this expression can be evaluated by means of the intensity measure:

$$G[f] = \exp\left[-\int_{\mathbb{R}^2}[1-f(\underline{x})]\Lambda(d\underline{x})\right] \tag{1.17}$$

Therefore,

$$G[f] = \exp\left(-\int_{(x,y)\in\mathbb{R}^2}[1-f(x,y)]\lambda(x,y)dxdy\right) \tag{1.18}$$

$$\text{or}\ \ G[f] = \exp\left(-\int_{(r,\theta)\in\mathbb{R}^2}[1-f(r,\theta)]\lambda(r,\theta)rdrd\theta\right) \tag{1.19}$$

In the context of wireless networks, the PGFL enables to derive the *Laplace transform* (LT) of the aggregate interference I. Defining $P(\underline{x}_i)$, the

power received at $(0,0)$ from node $\underline{x}_i \in \Psi$, one has

$$\mathcal{L}_I(s) \triangleq \mathbb{E}\left[e^{-sI}\right] = \mathbb{E}\left[e^{-s\sum_{\underline{x}_i\in\Psi} P\left(\underline{x}_i\right)}\right] = \mathbb{E}\left[\prod_{\underline{x}_i\in\Psi} e^{-sP\left(\underline{x}_i\right)}\right] \tag{1.20}$$

Similarly, the characteristic function (CF) of the aggregate interference is defined as

$$\phi_I(t) \triangleq \mathbb{E}\left[e^{jtI}\right] = \mathbb{E}\left[e^{jt\sum_{\underline{x}_i\in\Psi} P\left(\underline{x}_i\right)}\right] = \mathbb{E}\left[\prod_{\underline{x}_i\in\Psi} e^{jtP\left(\underline{x}_i\right)}\right] \tag{1.21}$$

1.2.7 Gil-Pelaez's inversion theorem

In wireless communications, many performance metrics depend on the aggregate interference introduced here above. In order to derive the statistical distribution of these metrics, Gil-Pelaez inversion theorem [21] is employed several times in this dissertation. This theorem enables to retrieve the probability density function (PDF) and the cumulative distribution (CDF) of a random variable on the basis of its CF:

Theorem 1.8. *Let X be a random variable of CF $\phi_X(t)$. The CDF and PDF of X can be expressed as*

$$F_X(x) = \frac{1}{2} - \frac{1}{\pi}\int_0^\infty Im\left[\phi_X(t)e^{-jtx}\right]t^{-1}dt \tag{1.22}$$

$$f_X(x) = \frac{1}{\pi}\int_0^\infty Re\left[\phi_X(t)e^{-jtx}\right]dt \tag{1.23}$$

provided that

- *x is a continuity point of the above distributions;*
- *the above integrals are Lebesgue-integrable.*

1.3 Review of related literature

This section highlights existing works dedicated to EMF exposure modelling using SG. Publications written in the context of energy harvesting and EMF monitoring for health are successively described. It is important

to note the state of the art provided here is general and non-exhaustive. More related works specific to particular parts of the thesis are detailed later within the corresponding chapters of the dissertation.

1.3.1 Wireless power transfer

The authors of [22] consider opportunistic wireless energy harvesting in cognitive radio networks. [23] derives the joint coverage-IPD distribution of a network including directional beamforming, as well as line-of-sight (LoS) and non-line-of-sight (nLoS) links. This joint distribution is also derived in [24] in the case of a multiple input/multiple output (MIMO) network. Another MIMO system, employing maximum ratio transmission (MRT) is also considered in [25]. The work in [26] separately investigates simultaneous information and power transfer (SWIPT) in a K-tier network. The authors of [27] introduce a cooperative SWIPT protocol applied in the framework of non orthogonal multiple access (NOMA) transmissions. In [28], the node density of an ad-hoc network is optimized to maximize the area energy harvested, given a constraint on the capacity. In [29], the deployment of a SWIPT-MIMO network is considered in an indoor environment. The framework introduced in [30] aims at analyzing a relay selection problem in a network with wireless powered nodes.

1.3.2 EMF monitoring

Analyses of the IPD in a HPPP, Manhattan Poisson line process and in a β-Ginibre PP are respectively available in [31], [32] and [33]. The authors of [34] perform a fitting of a 5G massive MIMO antenna pattern using a multimodal normal law. The resulting distribution is then incorporated in a SG analysis. The framework of [35] considers a downlink max-min fairness power control protocol. The impact of this protocol on the EMF exposure in a MIMO network is quantified. In [36], an analysis of the global exposure of both uplink and downlink bands is proposed for a HPPP. Finally, the model of [37] studies the IPD in scenarios including antennas operating at both mmWave and sub-6 GHz frequencies. To the best of the authors' knowledge, no other SG publication studies the EMF exposure in a health monitoring context.

1.4 Stochastic geometry at UCLouvain

During this PhD thesis, the author of this manuscript supervised and collaborated in a number of research projects associated to stochastic geometry. The objective of this section is therefore to provide a contextual overview of these works, and to identify those included within this dissertation. The different projects are grouped into the four categories illustrated in Fig. 1.1.

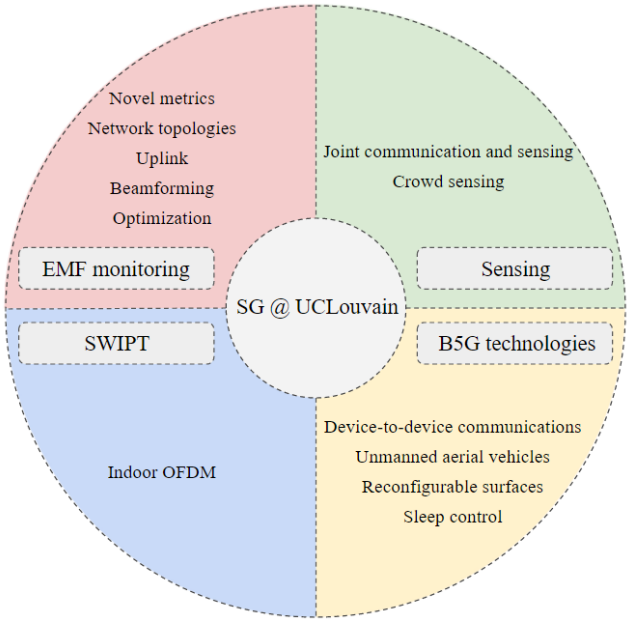

Fig. 1.1 Overview of the research projects related to stochastic geometry conducted at UCLouvain.

Three of these categories are dedicated to the applications motivating the study of EMF exposure mentioned in section 1.1 (SWIPT, sensing and EMF monitoring). The fourth group gathers novel communication technologies investigated for beyond 5G. The content of each individual project is summarized in the following subsections. In terms of publications, the majority of these works is associated to at least one future journal publication (submitted or in preparation), featuring the author of this thesis as first or second author.

1.4.1 EMF exposure monitoring

Novel performance metrics

(C. Wiame, Prof. C. Oestges, Prof. L. Vandendorpe)

This work consists in the development of new metrics to jointly evaluate the statistics of the coverage and exposure in general wireless networks. The associated content is available in Chapter 2.

The next five collaborations are dedicated to the analysis of specific network topologies, modelled using different point processes. The same set of performance metrics characterizing the exposure has been systematically derived for each of these topologies.

Analysis of cellular networks: inhomogenous double thinning approach

(C. Wiame, Q. Gontier, Dr. S. Wang, Prof. M. Di Renzo, Prof. C. Oestges)

The objective of this project is to generalize the framework proposed in [38] for modelling real-world network deployments by means of two inhomogeneous PPPs. This framework was originally developed to perform a coverage analysis only. The main contribution of this project was the extension of existing results to study the statistics of the exposure. The outcomes of this project are presented in Chapter 3.

Analysis of cellular networks: β-Ginibre point processes

(Q. Gontier, C. Wiame, Dr. S. Wang, Prof. M. Di Renzo, Prof. J. Wiart, Prof. F. Horlin, Dr. C. Tsigros, Prof. C. Oestges, Prof. P. De Doncker)

β-Ginibre point processes (βGPP) form another class of processes that can also be employed to approximate networks of real operators. The joint statistics of coverage and exposure have been studied for this particular topology as well.

Analysis of cellular networks: motion variant point processes

(Q. Gontier, C. Wiame, Dr. S. Wang, Prof. M. Di Renzo, Prof. J. Wiart, Prof. F. Horlin, Dr. C. Tsigros, Prof. C. Oestges, Prof. P. De Doncker)

The vast majority of PPs studied in the literature respect the motion invariance property. In practical scenarios, most metropolises are however characterized by a historical center featuring a higher density of base stations. The signal strength measured at a given user might therefore depend on its location with respect to that center. In order to model such an effect,

motion variant PPPs have been developed, featuring an inhomogeneous density $\lambda(r, \theta)$ accounting for such denser locations. An example of result is provided in Fig. 1.2.

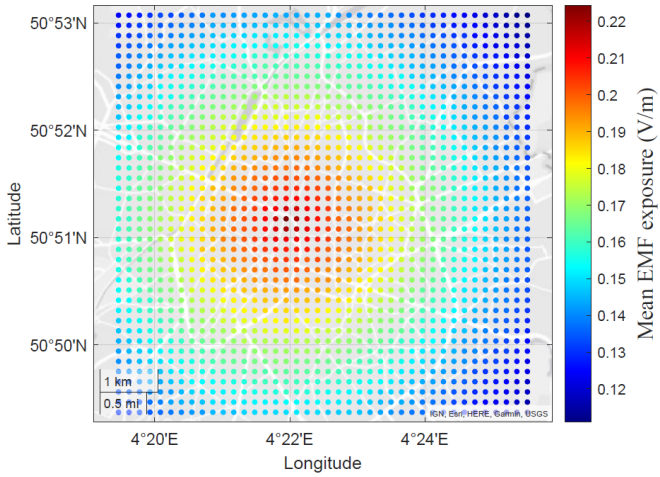

Fig. 1.2 From [39]. Average EMF exposure from the LTE 1800 network of one major Belgian operator around the Brussels center.

Analysis of cellular networks: Poisson line processes

(S. Demey, C. Wiame*, Prof. L. Vandendorpe, Prof. P. De Doncker, Prof. C. Oestges)*

Poisson line processes (PLPs) are part of the class of doubly stochastic PPs. These PLPs are here employed to randomly generate streets as well as users within each of these streets. Two examples are depicted in Fig. 1.3.

Several research directions have been investigated within this project:

- the performance values obtained via SG analysis have been compared with a ray-tracing tool. Conditioned on a coherent selection of the model parameters, the two approaches are shown to yield similar results.
- Cox-based models (see Fig. 1.3b) existing in the literature have been generalized to incorporate novel features: non-uniform street deployments, diffraction mechanisms, etc.

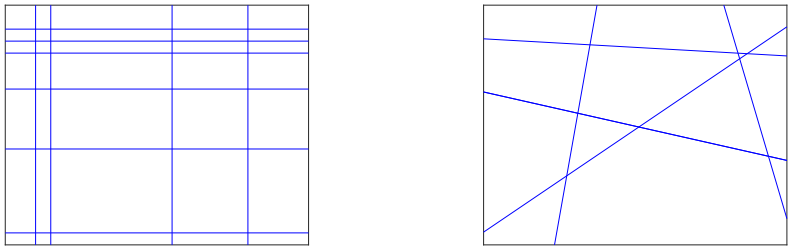

(a) Manhattan Poisson line process. **(b)** Poisson Cox line process.

Fig. 1.3 Illustration of two examples of Poisson line processes.

Analysis of cell-free networks

(C. Wiame, Prof. C. Oestges, Prof. L. Vandendorpe)

User-centric cell-free networks (UCCFNs) are characterized by the joint transmission (JT) of multiple access points to serve each individual user [40]. In that sense, UCCFNs can be considered as an evolution of Cooperative Multi-Point (CoMP) systems. Although this architecture is present in a large number of publications, the assessment of the EMF exposure for this architecture has been subject to fewer studies. The results presented in Chapter 4 of this dissertation attempt to bridge this gap.

Analysis of uplink communications

(Q. Gontier, C. Wiame, Prof. C. Oestges, Prof. P. De Doncker)

All the works previously mentioned consider the downlink exposure exclusively. In practical scenarios, the uplink exposure (mostly coming from the user's cellphone) can also be significant. This project hence features another new group of joint metrics, considering both coverage and exposure in the uplink and downlink.

Beamforming strategies

(Q. Gontier, C. Wiame, Prof. C. Oestges, Prof. P. De Doncker)

Novel technologies for 5G and beyond are expected to include massive MIMO networks, offering a high number of directional antennas in the downlink. These antennas enable to employ various beamforming strategies to maximize the useful received signal and/or to reduce the multi-user interference. In addition to the benefits to the coverage, the use of direc-

tional beams also impacts the EMF exposure. The objective of this work is to quantify this impact.

Development of tractable optimization problems

(J. Pirard, C. Wiame, Prof. C. Oestges, Prof. L. Vandendorpe)

All the research projects previously mentioned include analyses remaining at a descriptive level. The work of the master thesis [41] associated to this project attempts at going one step further and proposes optimization problems jointly considering the coverage and the exposure.

1.4.2 Sensing applications

Joint communication and sensing (JCAS)

(F. De Saint Moulin, C. Wiame, Prof. C. Oestges, Prof. L. Vandendorpe)

Two work packages are considered within this project:

- In a way similar to Chapter 2, novel metrics have been developed for radar-communication systems. Joint probabilities have been derived to simultaneously assess the communication function (coverage or rate) and the radar function (detection or success probability). These metrics have been evaluated for the particular case of an automotive scenario, featuring mutual interference cancellation capabilities between the two functions.

- Cooperative JCAS has been studied for vehicular applications as well. The coordination of multiple roadside units has been considered to jointly serve and detect a vehicle located at a crossroad within a Poisson Cox line process.

Crowd sensing

(M. Willame, C. Wiame)

The objective of this work is to evaluate the performance of sensing systems simultaneously detecting multiple targets. In particular, the impact of the radar clutter and of the mutual interference between adjacent targets is quantified. SG is here employed to account for the randomness in the targets' positions and in the static elements of the clutter.

1.4.3 SWIPT systems

On the deployment of an indoor SWIPT-OFDM system

(Dr. H. Kassab, Dr. F. Rottenberg, Dr. T. Feuillen, C. Wiame, Prof. J. Louveaux)

This collaboration is dedicated to the study of a new waveform for SWIPT. This waveform was considering the superposition of a rectangular power pulse with the cylic prefix of an OFDM symbol. Since cyclic prefixes are discarded at OFDM receivers, it is possible to transmit this power pulse without affecting data symbols for channels with sufficiently low frequency selectivity. Two research directions have been explored:

- the hardware implementation of this waveform;
- the study of the mutual interference between multiple setups employing this waveform. The SG model employed to that purpose considers an indoor environment generated by means of a PLP. The outcomes of the analysis include the derivation of trade-offs between the data rate and the harvested power, the impact of the synchronization between the setups, as well as the frequency selectivity of the channels.

1.4.4 Beyond 5G technologies

Reconfigurable intelligent surfaces

(N. Rorive, C. Wiame, Prof. C. Oestges, Prof. L. Vandendorpe)

Two research directions have been considered for this research project:

- the use of multiple reconfigurable intelligent surfaces (RIS) to improve the quality of one non line-of-sight (NLoS) link. Both cases of a deterministic and random number of available RIS are investigated. This objective of this direction was to answer questions such as: *"Given a budget of available RIS elements, should these elements be deployed on a low number of large surfaces, or distributed on a high number of smaller RIS?*
- the development of association rules and protocols in networks featuring line-of-sight (LoS) and non line-of-sight (NLoS) links, some of them involving a RIS. This objective of this direction was to answer

questions such as: *"Given a cellular network, should a mobile user connect to a NLoS base station aided by a RIS, or to a LoS base station located further away?*

Sleep control strategies

(M. Willame, C. Wiame, Prof. J. Louveaux, Prof. C. Oestges, Prof. L. Vandendorpe)

This research project is dedicated to the modelling of realistic sleep strategies in practical scenarios. In this work, base stations are given the ability to reduce their transmit power or to be fully turned off depending on the number of active users within their individual cell. Two major contributions of the study are the incorporation within a SG framework of a load dependent sleep control and the definition of multiple power levels.

Unmanned aerial vehicles

(F. De Saint Moulin, C. Wiame, Prof. C. Oestges, Prof. L. Vandendorpe)

This master thesis considers the use of drones as relays within a terrestrial network. A realistic propagation model is employed for the corresponding air-to-ground links: Ricean fading, a line-of-sight model based on the 3rd Generation Partnership Project (3GPP), etc. The mobility of the drone is also studied by considering the scenario of a UAV moving from the base station towards the user to be served. The temporal evolution of the coverage is derived for this dynamic case.

Device-to-device communications

(S. Demey, C. Wiame, Prof. C. Oestges, Prof. L. Vandendorpe)

The objective of this master project is to study the mutual interference between cellular networks and device-to-device (D2D) communications employing cellular bands. Semi-closed form expressions of the outage probability are derived and incorporate Rician fading on the D2D links. Both cases of D2D communications operating in the downlink and uplink bands of the cellular network are considered.

1.5 Outline and contributions of the thesis

The contributions of this text can be summarized into three main claims:

1. Novel performance metrics centered around the exposure and coverage are introduced in Chapter 2. These metrics include:
    - A *joint coverage-exposure distribution* featuring an inequality requiring the exposure to remain below a given threshold.
    - *Joint spatial distributions* characterizing the statistical dependency between the coverage and exposure measured at two adjacent mobile users.
    - *Meta distributions*, decoupling the effects of the small-scale fading and path loss coefficients on the EMF exposure.
    - *Efficiency ratios* between the average data rate and average EMF exposure experienced by the users of the network.
2. On the basis of the first of these new metrics, two major communication architectures are analyzed:
    - *Cellular networks*, covered in Chapter 3. The motivation behind this choice of architecture is naturally justified by its prevalence in the SG literature, and by its use by current mobile operators.
    - *User-centric cell-free networks*, studied in chapter 4 and considered as a promising paradigm for beyond 5G.

    The contributions of this text are two-fold for both chapters:
    - Independently of the context of EMF exposure, system models with new features are proposed to study these architectures within the SG framework.
    - The statistics of the EMF exposure are analyzed in a comprehensive manner. In addition to highlighting coverage-exposure trade-offs, further analyses specific to each architecture are proposed. On the one hand, the framework proposed for cellular networks enables to study the exposure in topologies close to real-world deployments in cities. On the other hand, the optimality of macro parameters is studied for cell-free networks.
3. A first attempt to incorporate the developed frameworks within an optimization problem is presented in Chapter 5. The proposed problem consists in minimizing the EMF exposure in a multi-tier network while meeting coverage constraints.

2

Definition of novel performance metrics

This chapter is organized as follows: performance metrics existing in the literature are detailed in section 2.1. The system model employed in this chapter is then described in section 2.2. Our new metrics are finally introduced and analysed in section 2.3.

2.1 Introduction

2.1.1 Notations

In this chapter, the following notations are employed:

- $\mathcal{P}(\cdot)$ denotes a CDF or a cumulative CDF;
- $\mathcal{J}(\cdot,\cdot)$ represents a joint distribution;
- $\mathcal{F}_{\mathcal{G}}(\cdot,\cdot)$ denotes the meta distribution associated to function $\mathcal{G}(\cdot)$;
- $\mathcal{M}_{\mathcal{G}}(b,\cdot)$ represents the moment of order b of $\mathcal{G}(\cdot)$.

The quantities associated to these distributions are indicated in subscript or superscript. Regarding the thresholds employed in these distributions:

- T is used to denote a SINR threshold;
- T' is used to denote an IPD threshold.

2.1.2 Related works

The objective of this section is to provide an overview of existing performance metrics derived using stochastic geometry. These metrics are here classified into three categories: classical metrics (considered in the majority of SG publications), spatio-temporal metrics, and metrics related to the EMF exposure. Most of following definitions are detailed in [15] and [42].

Classical metrics

As a reminder, the SINR is expressed as

$$\mathrm{SINR} = \frac{P_S}{P_I + P_N} \tag{2.1}$$

where P_S, P_I and P_N respectively denote the powers of the useful signal, of the aggregate interference, and of the noise. On the basis of this quantity, the following metrics can be detailed:

- the *conventional coverage probability*, defined as

$$\mathcal{P}_{\mathrm{cov}}(T) = \mathbb{P}\Big[\mathrm{SINR} > T\Big] \tag{2.2}$$

- the *mean spectral efficiency*, written as

$$\mathrm{SE} = \mathbb{E}\Big[\log(1+\mathrm{SINR})\Big]. \tag{2.3}$$

  If the above expression is multiplied by the system bandwidth B, the above definition corresponds in that case to the *mean data rate*.

- the energy efficiency, expressed as

$$\mathrm{EE} = \frac{\mathrm{SE}}{P_{\mathrm{tot}}} \tag{2.4}$$

  where P_{tot} is the power consumed by the network.

Note that these statistical quantities are most of the time defined for a user located at the reference point $(0,0)$. In the literature, this user is hence

referred to as *centric user* or *typical user*. In the case of a HPPP, it is well established that the above metrics are agnostic to this choice of reference.

More specific metrics are also detailed in [15]: mean rate utility, finite block length ergodic rate, area spectral efficiency, potential throughput as well as the paired and mobility aware coverage probabilities. These metrics are not employed in this thesis and will hence not be described here due to space limitations.

Spatio-temporal metrics

In the vast majority of SG models, two sources of randomness can be distinguished in the power received from base stations:

- the variable *path loss attenuations*, which depend on the realizations of the point process.
- the *small-scale fading* effects. In most studies, a fading coefficient is associated to each base station. Let $\{h_i\}_{i\in\Psi}$ be the set of these coefficients. These quantities are generally independent and identically distributed random variables and are independent of the path loss.

The objective of the next metrics is to decouple the effects of these two sources of randomness. As a first remark, one will note the first of these sources is associated to spatial aspects of the SG model while the second is related to fluctuations varying over time. For these reasons, the metrics below are given the adjective *spatio-temporal*. Let us introduce the first of these metrics:

- the conditional coverage probability is defined as

$$\mathcal{P}_{\text{cov}}(T|\Psi) = \mathbb{P}_{\{h_i\}_{i\in\Psi}}\Big[\text{SINR} > T|\Psi\Big] \tag{2.5}$$

  where $\mathbb{P}_{\{h_i\}_{i\in\Psi}}\big[\,\cdot\,\big]$ is the probability operator defined with respect to the fading coefficients $\{h_i\}_{i\in\Psi}$. This distribution has an easy interpretation and enables to answer the following question:*"Given the positions of the base stations of the network, what is the statistical distribution of the SINR associated to the fluctuation of the fading?"*

  $\hookrightarrow$ *example:* let Ψ^* be a realization of Ψ representing a given set of BS locations. Considering the equality

$$\mathcal{P}_{\text{cov}}(T = 30\text{dB}|\Psi = \Psi^*) = 0.8,$$

the mobile operator can conclude that *for the fixed set of BS locations Ψ^*, the probability for the centric user to experience a SINR above 30dB is 80%*. Considering that the fading varies over time, the following conclusion can be drawn equivalently:*"the centric user will experience a SINR above 30dB during 80% of the time."*

For a fixed Ψ, this function $\mathcal{P}_{\text{cov}}(T|\Psi)$ is deterministic and provides output values in the range $\left[0,1\right]$. By contrast, if one allows Ψ to vary, it becomes a random variable distributed in the interval $\left[0,1\right]$. As for any random variable, one can define the associated moments and CDF:

- the b-moments of the conditional coverage probability are given by

$$\mathcal{M}_{\mathcal{P}_{\text{cov}}}(b,T) = \mathbb{E}_{\Psi}\left[\left(\mathcal{P}_{\text{cov}}(T|\Psi)\right)^{b}\right] \tag{2.6}$$

$$= \mathbb{E}_{\Psi}\left[\left(\mathbb{P}_{\{h_i\}_{i\in\Psi}}\left[\text{SINR} > T|\Psi\right]\right)^{b}\right] \tag{2.7}$$

  where $\mathbb{E}_{\Psi}\left[\,\cdot\,\right]$ is the expectation operator with respect to the PP Ψ.

- the SINR meta distribution is defined as the complementary CDF of the conditional coverage probability with respect to the point process. Its mathematical definition is given by

$$\mathcal{F}_{\mathcal{P}_{\text{cov}}}(s,T) = \mathbb{P}_{\Psi}\left[\mathcal{P}_{\text{cov}}(T|\Psi) > s\right] \tag{2.8}$$

$$= \mathbb{P}_{\Psi}\left[\mathbb{P}_{\{h_i\}_{i\in\Psi}}\left[\text{SINR} > T|\Psi\right] > s\right] \tag{2.9}$$

  where $\mathbb{P}_{\Psi}\left[\,\cdot\,\right]$ is the probability operator associated to the spatial realizations of the PP Ψ. This distribution enables to answer questions such as:*"Considering an entire network deployed over a large-scale area, which percentage of the users experience an SINR above a threshold T during s percent of the time?"*

  $\hookrightarrow$ *example:* considering the equality

$$\mathcal{F}_{\mathcal{P}_{\text{cov}}}(s=0.7, T=30dB) = 0.9,$$

  one can deduce that for 90 % of the PP realizations (i.e. 90 % of

the maps of BSs randomly generated), the centric user experiences an SINR above 30 dB during 70 % of the time (taking into account the fluctuations of the fading coefficients). In the case of an HPPP defined on $\mathbb{R}^2$, the two following elements are equivalent from the user's perception:

- Considering a new realization of the HPPP, i.e. generating a new map of BSs around the centric user;
- Keeping a unique realization of the HPPP (i.e. one unique map of BSs defined over $\mathbb{R}^2$), but randomly moving the centric user at a different location in the map instead of regenerating a new realization around it.

As a consequence, the above example can also be interpreted as *90 % of the users in the network will experience a SINR above 30 dB during 70 % of the time* (assuming that these users are uniformly distributed in the network map).

For the interested reader, a more progressive and formal presentation of the above definitions is also proposed in [43, 44].

As additional spatio-temporal metrics, one can mention:

- the joint spatio-temporal coverage probability, defined as

$$\mathcal{J}_s^{\text{cov}}(T_1, T_2) = \mathbb{P}\left[\text{SINR}^{(\underline{x}_1, t_1)} > T_1, \text{SINR}^{(\underline{x}_2, t_2)} > T_2\right] \tag{2.10}$$

  where $\text{SINR}^{(\underline{x}_1, t_1)}$ and $\text{SINR}^{(\underline{x}_2, t_2)}$ denote the SINRs experienced by two user equipments at times and locations $(\underline{x}_1, t_1)$ and $(\underline{x}_2, t_2)$. This metric is here presented for two receivers but can be generalized to an arbitrary number K of users (see [42]).

- the joint uplink and downlink coverage probability, given by

$$\mathcal{J}_{\text{UL,DL}}(T_{UL}, T_{DL}) = \mathbb{P}\left[\text{SINR}_{UL} > T_{UL}, \text{SINR}_{DL} > T_{DL}\right] \tag{2.11}$$

  where SINR_{DL} and SINR_{UL} denote the SINRs experienced by a user equipment for its downlink and uplink transmissions.

A few other spatio-temporal metrics are also defined in the literature: SIR gain, conditional success probability, product Meta distribution and joint SIR Meta distribution. The interested reader is referred to [42] for more details.

Metrics related to the EMF exposure

Let us first recall the definition of the incident power density:

$$\mathrm{IPD} = P_S + P_I.$$

A few metrics related to this quantity already exist:

- the (raw) moments of the IPD, given by

$$m_{\mathrm{IPD}}^{(n)} = \mathbb{E}\left[\mathrm{IPD}^n\right].$$

  The first and second moments can respectively be derived using Campbell theorem and the second order product density of the PPP [18].

- the marginal CDF of the IPD:

$$\mathcal{P}_{IPD}(T') = \mathbb{P}\left[\mathrm{IPD} < T'\right] \tag{2.12}$$

- the exposure index distribution [36], which takes into account both the uplink and the downlink exposure:

$$\mathcal{P}_{EI}(T') = \mathbb{P}\left[\beta_{DL}\mathrm{IPD}_{\mathrm{DL}} + \beta_{UL}\mathrm{IPD}_{\mathrm{UL}} < T'\right] \tag{2.13}$$

  where β_{DL} and β_{UL} are given absorption coefficients.

- the joint coverage and IPD complementary CDF, originally introduced in [45] for SWIPT applications:

$$\mathcal{J}_{\mathrm{SWIPT}}(T, T') = \mathbb{P}\left[\mathrm{SINR} > T, \mathrm{IPD} > T'\right] \tag{2.14}$$

- the energy correlation coefficient, introduced in [46]. Let us define $\mathrm{IPD}^{(\underline{x}_1,t_1)}$ and $\mathrm{IPD}^{(\underline{x}_2,t_2)}$ as the incident power densities measured locations and time instants $(\underline{x}_1, t_1)$ and $(\underline{x}_2, t_2)$. On the basis of these notations, the energy correlation coefficient is defined as

$$\rho(\underline{x}_1, \underline{x}_2, t_1, t_2) = \frac{\mathbb{E}\left[\mathrm{IPD}^{(\underline{x}_1,t_1)}\mathrm{IPD}^{(\underline{x}_2,t_2)}\right] - \mathbb{E}\left[\mathrm{IPD}^{(\underline{x}_1,t_1)}\right]\mathbb{E}\left[\mathrm{IPD}^{(\underline{x}_2,t_2)}\right]}{\sqrt{\mathrm{Var}\left[\mathrm{IPD}^{(\underline{x}_1,t_1)}\right]\mathrm{Var}\left[\mathrm{IPD}^{(\underline{x}_2,t_2)}\right]}} \tag{2.15}$$

2.1.3 Contributions

This chapter introduces no less than nine new metrics associated to the IPD and summarized in table 2.1. Analytical expressions for these metrics are derived for the canonical scenario considering an HPPP with Rayleigh fading. Building up on this canonical scenario, an performance analysis is proposed as well for some of these metrics.

	Metric	Notation	Derivation
1	Joint coverage-IPD distribution with IPD limitation	$\mathcal{J}_{\text{lim}}(T, T')$	Proposition 2.3
2	Second moment of the conditional IPD distribution	$\mathcal{M}_{\mathcal{P}_{\text{IPD}}}(2, T')$	Proposition 2.6
3	Meta distribution of the IPD	$\mathcal{F}_{\mathcal{P}_{\text{IPD}}}(s, T')$	Proposition 2.8
4	Second moment of the joint coverage-IPD distribution	$\mathcal{M}_{\mathcal{J}_{\text{lim}}}(2, T, T')$	Proposition 2.10
5	Meta distribution of the coverage-IPD	$\mathcal{F}_{\mathcal{J}_{\text{lim}}}(s, T, T')$	Proposition 2.11
6	Joint IPD-IPD spatial distribution	$\mathcal{J}_s^{\text{IPD}}(T_1', T_2')$	Proposition 2.12
7	Joint coverage-IPD spatial distribution	$\mathcal{J}_s^{\text{SINR-IPD}}(T_1, T_2')$	Proposition 2.13
8	SE-IPD ratio	χ_1	Proposition 2.14
9	IPD-SE ratio	χ_2	-

Table 2.1 Overview of the new performance metrics

2.2 System model

We consider an HPPP of BSs of intensity λ deployed in $\mathbb{R}^2$. The studied user equipment is positioned at $(0, 0)$ and will be referred to as *typical user*. This user is served by its closest BS. All other BSs generate interference by covering other users. Regarding the propagation model:

- each BS is given a constant and isotropic transmit power P_t;
- we consider the path loss model given in eq. (5) of [47]:

$$l(r) = \min\left[1, l'(r)\right]$$

where

- $l'(r) = \kappa^{-1} r^{-\alpha}$;
- α is the path loss exponent;
- $\kappa = (4\pi f/c)^2$;
- f is the carrier frequency;
- c is the speed of light.

One can note that the presence of the minimum enables to avoid singularities in this path loss definition.

- Rayleigh fading is considered on all links.

The constant noise power is denoted by P_N.

For this scenario, the following results are known from the literature:

- the CF of the useful received power conditioned on the service distance r is given by

$$\phi_{P_S}(t|r) = \frac{1}{1 - jtP_t l(r)} \tag{2.16}$$

- the PDF of the distance from the user to its closest BS is given by [17]:

$$f_r(r) = \begin{cases} 2\pi\lambda r \exp\left(-\pi\lambda r^2\right) & \text{for } r \geq 0 \\ 0 & \text{for } r < 0 \end{cases} \tag{2.17}$$

- conditioned on the service distance r, the CF of the aggregate interference is given in Appendix IV of [14]:

$$\phi_I(t|r) = \exp\left\{-2\pi\lambda \int_r^\infty \left(1 - \frac{1}{1 - jtP_t l(r')} r' dr'\right)\right\} \tag{2.18}$$

- in a similar manner, the CF of the total IPD is given by

$$\phi_{\text{IPD}}(t) = \exp\left\{-2\pi\lambda \int_0^\infty \left(1 - \frac{1}{1 - jtP_t l(r')} r' dr'\right)\right\} \tag{2.19}$$

- conditioned on the realization of Ψ (i.e. on the locations of all BSs), the CF of the interference can be expressed as in Appendix IV of [14]:

$$\phi_I(t|\Psi) = \prod_{\underline{x}_i \in \Psi \setminus \{\underline{x}_0\}} \frac{1}{1 - jtP_t l(r_i)} \tag{2.20}$$

  where $r_i = ||\underline{x}_i||$ represents the distance between the centric user and a point $\underline{x}_i$ of Ψ. $\underline{x}_0$ denotes the closest BS serving the user (which is not considered in the interference).

- in a similar manner, the CF of the IPD conditioned on Ψ can be written as

$$\phi_{\text{IPD}}(t|\Psi) = \prod_{\underline{x}_i \in \Psi} \frac{1}{1 - jtP_t l(r_i)} \tag{2.21}$$

2.3 Novel performance metrics

2.3.1 Joint coverage-exposure distribution with exposure limitation

The first novel metric enables to evaluate the probability for a mobile users to benefit from a coverage above one first given threshold while being exposed to an IPD limited below a second threshold[1]:

$$\mathcal{J}_{\text{lim}}(T, T') = \mathbb{P}\Big[\text{SINR} > T, \text{IPD} < T'\Big] \tag{2.22}$$

Remark 2.1. One will note that conditional distributions can be trivially derived from the above metric. Using Bayes' rule, one can express

$$\mathbb{P}\Big[\text{SINR} > T | \text{IPD} < T'\Big] = \frac{\mathcal{J}_{\text{lim}}(T, T')}{\mathcal{P}_{\text{IPD}}(T')} \tag{2.23}$$

$$\mathbb{P}\Big[\text{IPD} < T' | \text{SINR} > T\Big] = \frac{\mathcal{J}_{\text{lim}}(T, T')}{\mathcal{P}_{\text{cov}}(T)} \tag{2.24}$$

The first of the above distributions represents the probability for a user satisfying exposure constraints to benefit from a sufficient coverage. By contrast, the second equality corresponds to the probability for a user in sufficient coverage to meet the exposure requirements. Conditional means

[1] whose value can be fixed by the operator or by legal requirements.

can then be deduced from the above developments. As an example, one can define

$$m_{IPD|T} = \int_0^\infty 1 - \mathbb{P}\Big[\text{IPD} < T' | \text{SINR} > T\Big] dT' \tag{2.25}$$

$$= \int_0^\infty 1 - \mathcal{J}_{\text{lim}}(T, T') \mathcal{P}_{cov}^{-1}(T) dT' \tag{2.26}$$

as the mean exposure affecting users experiencing a SINR above T dB.

Remark 2.2. One will note that (2.22) can be lower and upper bounded by means of Fréchet inequalities [48]:

$$\max\Big(0, \mathcal{P}_{\text{cov}}(T) + \mathcal{P}_{\text{IPD}}(T') - 1\Big) \leq \mathcal{J}_{\text{lim}}(T, T') \leq \min\Big(\mathcal{P}_{\text{cov}}(T), \mathcal{P}_{\text{IPD}}(T')\Big) \tag{2.27}$$

Proposition 2.3. *For the system model of section 2.2, the joint coverage-exposure distribution with exposure limitation can be expressed as*

$$\mathcal{J}_{lim}(T, T') = \int_r \left[\psi(T', r) - \frac{1}{\pi} \int_0^\infty Im\left[\phi_I(q|r)\ \zeta(q, T, T', r)\right]\ q^{-1} dq\right] f_R(r) dr \tag{2.28}$$

with

$$\psi(T', r) = \frac{1}{2}\left(1 - e^{\frac{T'}{P_t l(r)}}\right)$$

$$\zeta(q, T, T', r) = \frac{1 - \exp\left(\frac{-T''}{P_t l(r)}\left(1 + jqP_t l(r)\right)\right)}{1 + jqP_t l(r) T^{-1}} e^{jqP_N} + e^{-jqT'} \frac{\exp\left(\frac{T'}{P_t l(r)}\left(-1 + \frac{jqP_t}{l^{-1}(r)}\right)\right) - \exp\left(\frac{T''}{P_t l(r)}\left(-1 + \frac{jqP_t}{l^{-1}(r)}\right)\right)}{-1 + jqP_t l(r)}$$

$$T'' = \frac{T(T' + P_N)}{1 + T}$$

Proof. see Appendix C

Figures 2.1 and 2.2 respectively illustrate the joint metric (2.28) as well as the conditional coverage probability (2.23). The trade-offs associated to SINR and the IPD are observable on both graphs. Isovalues of the joint probability can be read in Figure 2.1. In a complementary manner, Figure 2.2 depicts by definition the coverage associated to users satisfying given exposure constaints T'. The comparison of the three curves shows the decrease in SINR performance when increasing the exposure limitations.

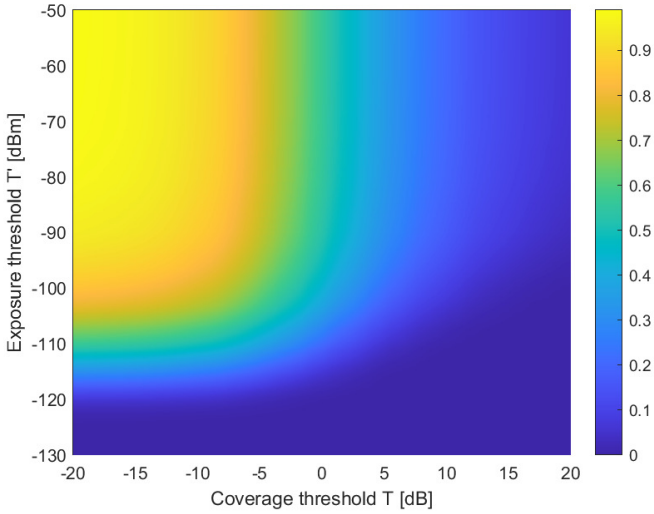

Fig. 2.1 Bidimensional representation of the metric $\mathcal{J}_{\text{lim}}(T, T')$ for $P_t = 1\ W$, $\alpha = 4$, $P_N = 0$ and $\lambda = 2.10^{-6}\ m^{-2}$.

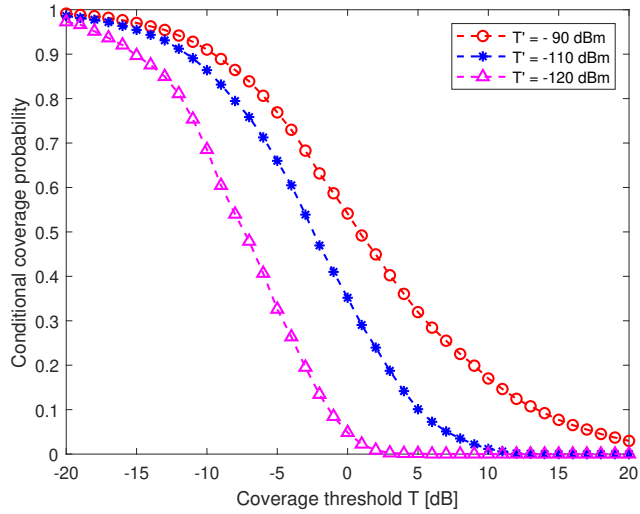

Fig. 2.2 Conditional coverage probability for fixed exposure thresholds T', with $P_t = 1\ W$, $\alpha = 4$, $P_N = 0$ and $\lambda = 2.10^{-6}\ m^{-2}$.

2.3.2 Meta distribution of the exposure

Conditional IPD distribution

As a preliminary result for this section, the conditional distribution of the IPD is defined as

$$\mathcal{P}_{\text{IPD}}(T'|\Psi) = \mathbb{P}_{\{h_i\}_{i\in\Psi}}\Big[\text{IPD} < T'|\Psi\Big]. \tag{2.29}$$

This metric represents the distribution of the IPD due the fluctuation of the fading coefficients for a given realization of Ψ.

Proposition 2.4. *For the system model of section 2.2, the conditional distribution of the IPD can be expressed as*

$$\mathcal{P}_{IPD}(T'|\Psi) = \frac{1}{2} - \frac{1}{\pi}\int_0^\infty Im\Big[\phi_{IPD}(t|\Psi)e^{-jT't}\Big]t^{-1}dt \tag{2.30}$$

Proof. the proof consists in a direct application of Gil-Pelaez theorem [21]

Moments of the conditional IPD distribution

The b-moments of the conditional IPD distribution are given by

$$\mathcal{M}_{\mathcal{P}_{\text{IPD}}}(b,T') = \mathbb{E}_\Psi\left[\Big(\mathcal{P}_{\text{IPD}}(T'|\Psi)\Big)^b\right] \tag{2.31}$$

Proposition 2.5. *For the system model of section 2.2, the first order moment of the conditional IPD distribution is trivially given by*

$$\mathcal{M}_{\mathcal{P}_{IPD}}(1,T') = \mathcal{P}_{IPD}(T') = \frac{1}{2} - \frac{1}{\pi}\int_0^\infty Im\Big[\phi_{IPD}(t)e^{-jT't}\Big]t^{-1}dt \tag{2.32}$$

Proof. the result is obtained by applying the expectation operator on (2.30):

$$\mathcal{M}_{\mathcal{P}_{\text{IPD}}}(1,T') = \mathbb{E}_\Psi\left[\frac{1}{2} - \frac{1}{\pi}\int_0^\infty \text{Im}\Big[\phi_{\text{IPD}}(t|\Psi)e^{-jT't}\Big]t^{-1}dt\right] \tag{2.33}$$

$$\overset{(a)}{=} \frac{1}{2} - \frac{1}{\pi}\int_0^\infty \text{Im}\Big[\mathbb{E}_\Psi\big[\phi_{\text{IPD}}(t|\Psi)\big]e^{-jT't}\Big]t^{-1}dt \tag{2.34}$$

$$= \frac{1}{2} - \frac{1}{\pi}\int_0^\infty \text{Im}\Big[\phi_{\text{IPD}}(t)e^{-jT't}\Big]t^{-1}dt \tag{2.35}$$

$$\overset{(b)}{=} \mathcal{P}_{IPD}(T') \tag{2.36}$$

with $\phi_{\text{IPD}}(t)$ defined in (2.19). In the above developments, (a) is obtained by linearity and (b) by identification.

Proposition 2.6. *For the system model of section 2.2, the second order moment of the conditional IPD distribution can be expressed as*

$$\mathcal{M}_{\mathcal{P}_{IPD}}(2,T') = \frac{-1}{4} + \mathcal{M}_{\mathcal{P}_{IPD}}(1,T') + \frac{1}{\pi^2}\,\Omega(T') \tag{2.37}$$

where

$$\begin{aligned}
\Omega(T') &= \int_0^\infty \int_0^\infty \Delta(t,t';T') t^{-1} t'^{-1} dt dt' \\
\Delta(t,t';T') &= \frac{1}{2} Re\Big[\Delta_-(t,t') e^{-j(t-t')T'} - \Delta_+(t,t') e^{-j(t+t')T'}\Big] \\
\Delta_+(t,t') &= \exp\left\{ -2\pi\lambda \int_0^\infty \left(1 - \frac{1}{1-jtP_t l(r)} \frac{1}{1-jt'P_t l(r)}\right) r dr \right\} \\
\Delta_-(t,t') &= \exp\left\{ -2\pi\lambda \int_0^\infty \left(1 - \frac{1}{1-jtP_t l(r)} \frac{1}{1+jt'P_t l(r)}\right) r dr \right\}
\end{aligned}$$

Proof. see Appendix D

Remark 2.7. The variance of the conditional IPD can be trivially deduced from the previous expressions:

$$\mathcal{V}_{\mathcal{P}_{\text{IPD}}}(T') \triangleq \mathcal{M}_{\mathcal{P}_{\text{IPD}}}(2,T') - \mathcal{M}_{\mathcal{P}_{\text{IPD}}}(1,T')^2 \tag{2.38}$$

The first moment and the variance of the conditional IPD distribution are illustrated in Figure 2.3. Regarding the variance, one will note that

$$\lim_{T'\to+\infty} \mathcal{V}_{\mathcal{P}_{\text{IPD}}}(T') = \lim_{T'\to 0} \mathcal{V}_{\mathcal{P}_{\text{IPD}}}(T') = 0. \tag{2.39}$$

This asymptotic behaviour can be interpreted: for very high (resp. very low) values of T', the IPD is always below (resp. above) this threshold with a value of $\mathcal{P}_{\text{IPD}}(T'|\Psi)$ tending to one (resp. zero). This observation is verified for all PP realizations, resulting in no statistical fluctuations of $\mathcal{P}_{\text{IPD}}(T'|\Psi)$ (and therefore a variance equal to zero). By contrast, the variance is maximal when the corresponding first moment takes values around 0.5. One can deduce that the impact of the spatial configuration of the net-

work is maximal when the IPD is required to be below a value in the middle of its dynamical range (around -112 dBm for $\alpha = 4$ and -98 dBm for $\alpha = 3.5$).

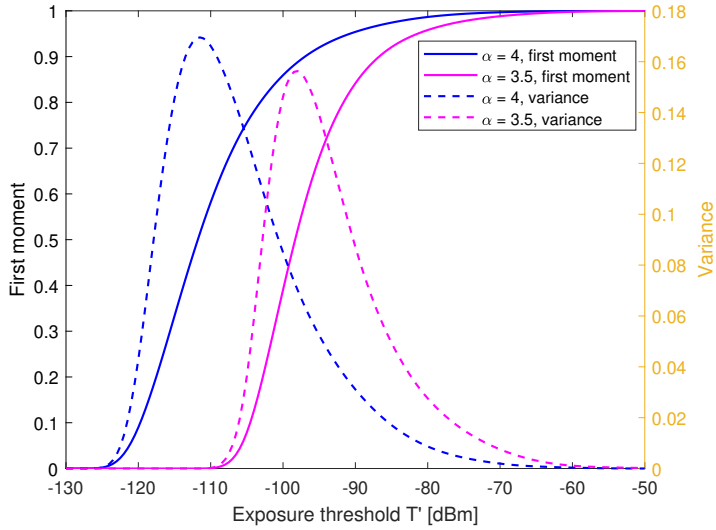

Fig. 2.3 Mean and variance of the conditional IPD distribution illustrated for two values of the path loss exponent. The following parameters were selected: $P_t = 1\ W$, $P_N = 0$ and $\lambda = 2.10^{-6}\ m^{-2}$.

IPD Meta distribution

The IPD Meta distribution is defined as

$$\mathcal{F}_{\mathcal{P}_{\text{IPD}}}(s, T') = \mathbb{P}_{\Psi}\left[\mathcal{P}_{\text{IPD}}(T'|\Psi) > s\right] \tag{2.40}$$

$$= \mathbb{P}_{\Psi}\left[\mathbb{P}_{\{h_i\}_{i\in\Psi}}\left[\text{IPD} < T'|\Psi\right] > s\right] \tag{2.41}$$

This metric follows the same line of thought as the Meta distribution of the coverage (section 2.1.2). Its definition enables to provide answers to the question *"what percentage of users experience an IPD below a threshold T' during at least s% of the time?"*.

Proposition 2.8. *Capitalizing on the methodology of [49], a tractable approximation for $\mathcal{F}_{\mathcal{P}_{IPD}}(s, T')$ is given by the beta distribution:*

$$\tilde{\mathcal{F}}_{\mathcal{P}_{IPD}}(s, T') = \mathcal{I}_s\left[\tilde{\alpha}_{\mathcal{P}_{IPD}}(T'), \tilde{\beta}_{\mathcal{P}_{IPD}}(T')\right] \tag{2.42}$$

where

- $\mathcal{I}_{(\cdot)}\left[\cdot, \cdot\right]$ *is the incomplete beta function.*
- $\tilde{\alpha}_{\mathcal{P}_{IPD}}(T')$ *and* $\tilde{\beta}_{\mathcal{P}_{IPD}}(T')$ *are the parameters of the beta distribution obtained via moment matching. Under the following condition:*

$$\mathcal{M}_{\mathcal{P}_{IPD}}(2, T') - \mathcal{M}_{\mathcal{P}_{IPD}}(1, T')^2 < \mathcal{M}_{\mathcal{P}_{IPD}}(1, T')\left[1 - \mathcal{M}_{\mathcal{P}_{IPD}}(1, T')\right], \tag{2.43}$$

their expressions are given by

$$\tilde{\alpha}_{\mathcal{P}_{IPD}}(T') = \mathcal{M}_{\mathcal{P}_{IPD}}(1, T')\left[\frac{\mathcal{M}_{\mathcal{P}_{IPD}}(1, T')\left(1 - \mathcal{M}_{\mathcal{P}_{IPD}}(1, T')\right)}{\mathcal{M}_{\mathcal{P}_{IPD}}(2, T') - \mathcal{M}_{\mathcal{P}_{IPD}}(1, T')^2} - 1\right] \tag{2.44}$$

$$\tilde{\beta}_{\mathcal{P}_{IPD}}(T') = \left[1 - \mathcal{M}_{\mathcal{P}_{IPD}}(1, T')\right]\left[\frac{\mathcal{M}_{\mathcal{P}_{IPD}}(1, T')\left(1 - \mathcal{M}_{\mathcal{P}_{IPD}}(1, T')\right)}{\mathcal{M}_{\mathcal{P}_{IPD}}(2, T') - \mathcal{M}_{\mathcal{P}_{IPD}}(1, T')^2} - 1\right] \tag{2.45}$$

The metric $\mathcal{F}_{\mathcal{P}_{\text{IPD}}}(s, T')$ is depicted as function of both s and T' in Figure 2.4 (page 43). Figure 2.4a provides a bidimensional representation while Figure 2.4b provide a cross-sectional view for fixed values of T'. Considering this second figure, the behaviour of the curves at the boundaries of their domain can be studied. One will observe that

$$\tilde{\mathcal{F}}_{\mathcal{P}_{\text{IPD}}}(0, T') = 1, \quad \forall T' \tag{2.46}$$

$$\tilde{\mathcal{F}}_{\mathcal{P}_{\text{IPD}}}(1, T') = 0, \quad \forall T' \tag{2.47}$$

These equalities can be analyzed on the basis of the definition of the IPD Meta distribution (page 34). Equation (2.46) can be interpreted as *"for any exposure threshold T', 100% of the network realizations experience an IPD below the threshold more than 0% of the time"*. In other words, there exists for any network realization a set of fading coefficients leading to an exposure satisfying the threshold. In a complementary manner, (2.46) can be read as *"for any threshold T', 0% of the network realizations experience an IPD below T' during 100% of the time"*. It is therefore impossible to find a network realization for which the exposure meets the threshold for any set of fading coeffi-

cients. Still considering Figure 2.4b, one will note that for lowest exposure threshold ($T' = -120$ dBm, in blue), the values of the Meta distribution quickly decrease from 1 to about 0.2 for low values of s. For a constraining value of T', it is therefore not possible to obtain high percentages of users for which the values of the IPD will be below T' in high probability. By contrast, the curves associated to higher thresholds (e.g. to $T' = -105$ dBm, in purple) can also be analyzed. From these curves, one deduces that the IPD Meta distribution takes relatively high values, except for very high values of s (close to 100%, for which the Meta drops to 0). For high thresholds T', a large percentage of users are able to meet the exposure requirement for a relatively large fraction of the time.

2.3.3 Meta distribution of the coverage-exposure

The framework introduced in the previous section has been derived with respect to the IPD only. The metrics presented in that section (conditional distribution, moments and meta distribution) are now redefined with respect to the joint SINR-IPD statistics.

Conditional SINR-IPD distribution

The conditional distribution of the SINR and IPD is defined as

$$\mathcal{J}_{\text{lim}}(T, T'|\Psi) = \mathbb{P}_{\{h_i\}_{i\in\Psi}}\Big[\text{SINR} > T, \text{IPD} < T'|\Psi\Big]. \tag{2.48}$$

Moments of the conditional SINR-IPD distribution

The b-moments of the conditional SINR-IPD distribution are given by

$$\mathcal{M}_{\mathcal{J}_{\text{lim}}}(b, T, T') = \mathbb{E}_{\Psi}\Big[\Big(\mathcal{J}_{\text{lim}}(T, T'|\Psi)^b\Big] \tag{2.49}$$

$$= \mathbb{E}_{\Psi}\Big[\Big(\mathbb{P}_{\{h_i\}_{i\in\Psi}}\Big[\text{SINR} > T, \text{IPD} < T'|\Psi\Big]\Big)^b\Big] \tag{2.50}$$

Proposition 2.9. *For the system model of section 2.2, the first order moment of the conditional SINR-IPD distribution is trivially given by*

$$\mathcal{M}_{\mathcal{J}_{lim}}(1, T, T') = \mathcal{J}_{lim}(T, T') \tag{2.51}$$

Proof. the derivation of this result is analogous to the proof of (2.32).

Proposition 2.10. *For the system model of section 2.2, the second order moment of the conditional SINR-IPD distribution can be expressed as*

$$\mathcal{M}_{\mathcal{J}_{lim}}(2,T,T') = \int_0^\infty \mathcal{M}_{\mathcal{J}_{lim}}(2,T,T'|r) f_r(r) dr \tag{2.52}$$

where

$$\mathcal{M}_{\mathcal{J}_{lim}}(2,T,T'|r) = \psi^2(T',r) - \frac{2}{\pi}\psi(T',r)\int_0^\infty Im\left[\phi_I(q|r)\,\zeta(T,T',r)\right]\, q^{-1}dq + \frac{1}{\pi^2}\omega(T,T',r)$$

$$\omega(T,T',r) = \int_0^\infty\int_0^\infty \delta(t,t';T,T',r)t^{-1}t'^{-1}dtdt'$$

$$\delta(t,t';T,T',r) = \frac{1}{2}Re\Big[\delta_-(t,t',r)\zeta(t,T,T',r)\zeta^*(t',T,T',r) - \delta_+(t,t',r)\zeta(t,T,T',r)\zeta(t',T,T',r)\Big]$$

$$\delta_+(t,t',r) = \exp\left\{-2\pi\lambda\int_r^\infty\left(1 - \frac{1}{1-jtP_t l(r)}\frac{1}{1-jt'P_t l(r)}\right)rdr\right\}$$

$$\delta_-(t,t',r) = \exp\left\{-2\pi\lambda\int_r^\infty\left(1 - \frac{1}{1-jtP_t l(r)}\frac{1}{1+jt'P_t l(r)}\right)rdr\right\}$$

$\psi(T',r)$ and $\zeta(t,T,T',r)$ defined in proposition 2.3.

Proof. the derivation follows the same steps as the proof of proposition 2.6 starting from (2.28), after conditioning on the distance to the serving BS.

SINR-IPD Meta distribution

The IPD Meta distribution is defined as

$$\mathcal{F}_{\mathcal{J}_{\text{lim}}}(s,T,T') = \mathbb{P}_\Psi\left[\mathcal{J}_{\text{lim}}(T,T'|\Psi) > s\right] \tag{2.53}$$

This definition provides the answer to the question *"what percentage of users simultaneously experience an SINR above a threshold T and an IPD below a threshold T' during s% of the time?*.

Proposition 2.11. *A tractable approximation for $\mathcal{F}_{\mathcal{J}_{lim}}(s,T,T')$ is given by the beta distribution:*

$$\tilde{\mathcal{F}}_{\mathcal{J}_{lim}}(s,T,T') = \mathcal{I}_s\left[\tilde{\alpha}_{\mathcal{J}_{lim}}(T,T'), \tilde{\beta}_{\mathcal{J}_{lim}}(T,T')\right] \tag{2.54}$$

where

- *$\mathcal{I}_{(\cdot)}[\cdot,\cdot]$ is the incomplete beta function.*
- *$\tilde{\alpha}_{\mathcal{J}_{lim}}(T,T')$ and $\tilde{\beta}_{\mathcal{J}_{lim}}(T,T')$ are the parameters of the beta distribution*

obtained via moment matching. Under the following condition:

$$\mathcal{M}_{\mathcal{J}_{lim}}(2,T,T') - \mathcal{M}_{\mathcal{J}_{lim}}(1,T,T')^2 < \mathcal{M}_{\mathcal{J}_{lim}}(1,T,T')\Big[1 - \mathcal{M}_{\mathcal{J}_{lim}}(1,T,T')\Big], \quad (2.55)$$

this matching is given by

$$\tilde{\alpha}_{\mathcal{J}_{lim}}(T,T') = \mathcal{M}_{\mathcal{J}_{lim}}(1,T,T')\left[\frac{\mathcal{M}_{\mathcal{J}_{lim}}(1,T,T')(1-\mathcal{M}_{\mathcal{J}_{lim}}(1,T,T')}{\mathcal{M}_{\mathcal{J}_{lim}}(2,T,T') - \mathcal{M}_{\mathcal{J}_{lim}}(1,T,T')^2} - 1\right] \quad (2.56)$$

$$\tilde{\beta}_{\mathcal{J}_{lim}}(T,T') = \Big[1 - \mathcal{M}_{\mathcal{J}_{lim}}(1,T,T')\Big]\left[\frac{\mathcal{M}_{\mathcal{J}_{lim}}(1,T,T')(1-\mathcal{M}_{\mathcal{J}_{lim}}(1,T,T'))}{\mathcal{M}_{\mathcal{J}_{lim}}(2,T,T') - \mathcal{M}_{\mathcal{J}_{lim}}(1,T,T')^2} - 1\right] \quad (2.57)$$

Graphical results are possible as well for this metric. Their interpretation would be similar to section 2.3.2.

2.3.4 Joint spatial distributions

Joint IPD-IPD spatial distribution

The joint spatial distribution of the IPD at locations $\underline{x}_1$ and $\underline{x}_2$ is defined as

$$\mathcal{J}_s^{\text{IPD}}(T_1', T_2') = \mathbb{P}\Big[\text{IPD}^{(\underline{x}_1)} < T_1', \text{IPD}^{(\underline{x}_2)} < T_2'\Big] \quad (2.58)$$

Proposition 2.12. *Still using the system model of section 2.2, let us consider the two locations $(0,0)$ and $(d,0)$ assumed to be affected by independent fading. The joint spatial distribution of the IPD evaluated at these two locations is given by*

$$\mathcal{J}_s^{IPD}(T_1', T_2'; d) = \frac{-1}{4} + \frac{1}{2}\mathcal{P}_{IPD}(T_1') + \frac{1}{2}\mathcal{P}_{IPD}(T_2') + \frac{1}{\pi^2}\,\mathcal{V}(T_1', T_2'; d) \quad (2.59)$$

where

$$\mathcal{V}(T_1', T_2'; d) = \int_0^\infty \int_0^\infty \sigma(t,t'; T_1', T_2', d) t^{-1} t'^{-1} dt dt'$$

$$\sigma(t,t'; T_1', T_2', d) = \frac{1}{2} Re\Big[\sigma_-(t,t'; d) e^{-j(tT_1' - t'T_2')} - \sigma_+(t,t'; d) e^{-j(tT_1' + t'T_2')}\Big]$$

$$\sigma_+(t,t'; d) = \exp\left\{ -\lambda \int_0^{2\pi} \int_0^\infty \left(1 - \frac{1}{1 - jtP_t l(r)} \frac{1}{1 - jt'P_t \tilde{I}(r; d, \beta)}\right) r dr d\beta \right\}$$

$$\sigma_-(t,t'; d) = \exp\left\{ -\lambda \int_0^{2\pi} \int_0^\infty \left(1 - \frac{1}{1 - jtP_t l(r)} \frac{1}{1 + jt'P_t \tilde{I}(r; d, \beta)}\right) r dr d\beta \right\}$$

$$\tilde{I}(r; d, \beta) = \min\left[1, \kappa^{-1}\Big(r^2 + d^2 - 2rd\cos(\beta)\Big)^{-\alpha/2}\right]$$

Proof. See Appendix E.

In order to provide a progressive interpretation, the analysis of following elements is proposed as well:

- the performance obtained in the absence of fading. This scenario can be analytically described by adapting the proof of (2.59): the CF associated to Rayleigh fading $\phi(t) = [1 - jtP_t l(r)]^{-1}$ must be replaced by $\phi(t) = \exp\left[jtP_t l(r)\right]$, which corresponds to the CF of a deterministic quantity (without fading fluctuation). This scenario without fading can model the exposure averaged over a large number of channel coherence times, or represent highly Ricean channels.

- the joint spatial PDF of the exposure, defined as

  $$\mathcal{T}_s^{\text{IPD}}(T_1', T_2') = \mathbb{P}\Big[T_1' < \text{IPD}^{(0,0)} < T_1' + dT_1', T_2' < \text{IPD}^{(d,0)} < T_2' + dT_2'\Big]$$

  In order to derive this expression, the first version of Gil-Pelaez theorem[2] must be replaced by the second version[3] in the proof of (2.59).

The values of $\mathcal{J}_s^{\text{IPD}}(T_1', T_2'; d)$ and $\mathcal{T}_s^{\text{IPD}}(T_1', T_2'; d)$ are shown in Figure 2.5 (page 44) in the absence of fading. To interpret the provided graphs, it is useful to consider the case $d = 0$, for which both receivers are at the same location and experience the same IPD. The joint spatial PDF in that case given by

$$\mathcal{T}_s^{\text{IPD}}(T_1', T_2'; d = 0) = \mathcal{T}^{\text{IPD}}(T_1')\delta(T_1' - T_2') \tag{2.60}$$

where

$$\mathcal{T}^{\text{IPD}}(T') = \frac{\partial \mathcal{P}_{IPD}(T')}{\partial T'} \tag{2.61}$$

is the marginal PDF of the IPD. By integrating (2.60), one can deduce

$$\mathcal{J}_s^{\text{IPD}}(T_1', T_2'; d = 0) = \mathcal{P}_{IPD}\Big(\min[T_1', T_2']\Big). \tag{2.62}$$

Figures 2.5a and 2.5b show probability values close to this particular case with $d = 5m$. In order to give an interpretation to the selected distance values, let us recall that the average distance between $(0, 0)$ to its closest

[2] eq. (1.22), expressing the CDF of a random variable.
[3] eq. (1.23), expressing the equivalent PDF.

base station is equal to $1/2\sqrt{\lambda}$ [16]. For the selected density value, this average distance is approximately equal to 350m. One can observe in Figure 2.5c that increasing d leads to more spread values of $\mathcal{T}_s^{\text{IPD}}(T_1', T_2'; d)$ since the values of the IPD measured at the two receivers become less correlated. For $d = 1km$, the obtained values become close to the other particular case $d \to \infty$. This case corresponds to two receivers perceiving different IPDs as if they were coming from two independent realizations of the HPPP. In that case, one can readily verify that

$$\lim_{d \to +\infty} \mathcal{J}_s^{\text{IPD}}(T_1', T_2'; d) = \mathcal{P}_{IPD}(T_1')\mathcal{P}_{IPD}(T_2')$$

For these results, one will note that the statistical behaviour of the two measured exposures is easier to interprete from the PDFs than the CDFs. By zooming on Figures 2.5b, 2.5d and 2.5f, one can however note that the increase in parameter d results in 'rounder' isocurves, respecting less and less the structure of (2.62). Finally, Figures 2.6a and 2.6b (page 45) illustrate the impact of the small scale fading for $d = 5m$. A quick comparison with Figures 2.5a and 2.5b confirms that the fading introduces more randomness, resulting in more decorrelation in the values measured at the two receivers.

Joint SIR-IPD spatial distribution

The joint SINR-IPD spatial distribution at locations $\underline{x}_1$ and $\underline{x}_2$ is defined as

$$\mathcal{J}_s^{\text{SINR-IPD}}(T_1, T_2') = \mathbb{P}\left[\text{SINR}^{(\underline{x}_1)} > T_1, \text{IPD}^{(\underline{x}_2)} < T_2'\right] \tag{2.63}$$

This metric can be employed by mobile operators to ensure a sufficient quality of service at a location with high user traffic, and a low exposure at a second location. An concrete application was provided in [50], considering the deployment of an indoor network in a French train station. In that example, the train company was requesting a high quality of service for travellers inside the station, and a low exposure for the company's employees working in adjacent offices.

Proposition 2.13. *For the system model of section 2.2, the joint SINR-IPD spatial distribution at locations* $(0,0)$ *and* $(d,0)$ *is given by*

$$\mathcal{J}_s^{\textit{SINR-IPD}}(T_1, T_2'; d) = \frac{-1}{4} + \frac{1}{2}\mathcal{P}_{cov}(T_1) + \frac{1}{2}\mathcal{P}_{IPD}(T_2') - \frac{1}{\pi^2}\,\Gamma(T_1, T_2'; d) \tag{2.64}$$

where

$$\Gamma(T_1, T_2'; d) = \frac{1}{2\pi}\int_0^{2\pi}\int_0^{\infty}\Gamma(T_1, T_2'; d, r, \eta) f_r(r) dr d\eta$$

$$\Gamma(T_1, T_2'; d, r, \eta) = \int_0^{\infty}\int_0^{\infty}\epsilon(t, t'; T_1, T_2', d, r, \eta) t^{-1} t'^{-1} dt dt'$$

$$\epsilon(t, t'; T_1, T_2', d, r, \eta) = \frac{1}{2} Re\Big[\epsilon_-(t, t'; T_1, T_2', d, r, \eta) - \epsilon_+(t, t'; T_1, T_2', d, r, \eta)\Big]$$

$$\epsilon_+(t, t'; T_1, T_2', d, r, \eta) = e^{-j(tP_N T_1 + t' T_2')} \frac{1}{[1 - jtP_t l(r)]} \frac{1}{[1 - jt' P_t \tilde{I}(r, d, \eta)]} \gamma_+(t, t'; d, r, \eta)$$

$$\epsilon_-(t, t'; T_1, T_2', d, r, \eta) = e^{-j(tP_N T_1 - t' T_2')} \frac{1}{[1 - jtP_t l(r)]} \frac{1}{[1 + jt' P_t \tilde{I}(r, d, \eta)]} \gamma_-(t, t'; d, r, \eta)$$

$$\gamma_+(t, t'; d, r, \eta) = \exp\left\{ -\lambda \int_0^{2\pi}\int_r^{\infty}\left(1 - \frac{1}{1 + jtT_1 P_t l(r')} \frac{1}{1 - jt' P_t \tilde{I}(r', d, \beta)}\right) r' dr' d\beta \right\}$$

$$\gamma_-(t, t'; d, r, \eta) = \exp\left\{ -\lambda \int_0^{2\pi}\int_r^{\infty}\left(1 - \frac{1}{1 + jtT_1 P_t l(r')} \frac{1}{1 + jt' P_t \tilde{I}(r', d, \beta)}\right) r' dr' d\beta \right\}$$

$$\tilde{I}(r, d) = \min\left[1, \kappa^{-1}\Big(r^2 + d^2 - 2rd\cos(\beta)\Big)^{-\alpha/2}\right]$$

Proof. the derivation is similar to the proof of proposition 2.6.

A graphical representation of this metric would not enable to make a lot of interpretations for the system model of section 2.2. This joint probability is expected to be incorporated in another research project (which is not presented in this dissertation) including beamforming aspects. For this other scenario, the use of an antenna array enables to create an antenna pattern at the transmit base station. This pattern is characterized by a primary lobe (improving the SINR of the targeted user), as well as secondary lobes of low amplitude (reducing the power transmitted in other directions). The use of (2.64) is therefore relevant in that context.

2.3.5 Efficiency ratios

Following the same line of thought as for the energy efficiency, two ratios can be defined to characterize the rate and IPD performance:

$$\chi_1 = \mathbb{E}\left[\frac{\log(1 + \text{SINR})}{\text{IPD}}\right] \tag{2.65}$$

$$\chi_2 = \mathbb{E}\left[\frac{\text{IPD}}{\log(1 + \text{SINR})}\right] \tag{2.66}$$

In the above definitions, the ratio χ_1 characterizes the average number of bits/s/Hz transmitted per W/m^2 or V/m of exposure affecting the mobile user. In a complementary way, χ_2 provides the average amount of exposure affecting the mobile user per transmitted bits/s/Hz.

Proposition 2.14. *For the system model of section 2.2, on the condition that the integral below converges, an upper bound for χ_1 at high SIR can be expressed as*

$$\bar{\chi}_1 = \int_0^\infty \int_0^\infty \frac{1}{xP_t l(r)} \left[\int_0^\infty \left(1 - e^{-sxP_t l(r)}\right) \mathcal{L}_I(s|r) \frac{e^{-sN_0}}{s} \right] e^{-x} f_r(r) dx dr \qquad (2.67)$$

where

$$\mathcal{L}_I(s|r) = \exp\left\{ -2\pi\lambda \int_r^\infty \left(1 - \frac{1}{1 + sP_t l(r')} r' dr'\right) \right\} \qquad (2.68)$$

Proof. see Appendix F

2.4 Conclusions of the chapter

2.4.1 Summary

This chapter proposes a number of novel performance metrics related to the statistics of the EMF exposure and coverage. These metrics have been evaluated in the canonical HPPP case with Rayleigh fading.

2.4.2 Further research directions

- A direct extension of this chapter would consist in deriving these metrics for other system models. Many scenarios are possible in the SG literature. In addition to the models of the next chapters, a non-exhaustive list includes B5G networks (featuring new technologies such as drones or reconfigurable surfaces), indoor deployments, etc.
- In the framework of another research project, a second category of new metrics is being developed. This project is dedicated to the simultaneous analysis of the uplink and downlink of cellular networks. Joint probabilities involving up to four arguments (coverage and exposure in both directions) are derived to this purpose.

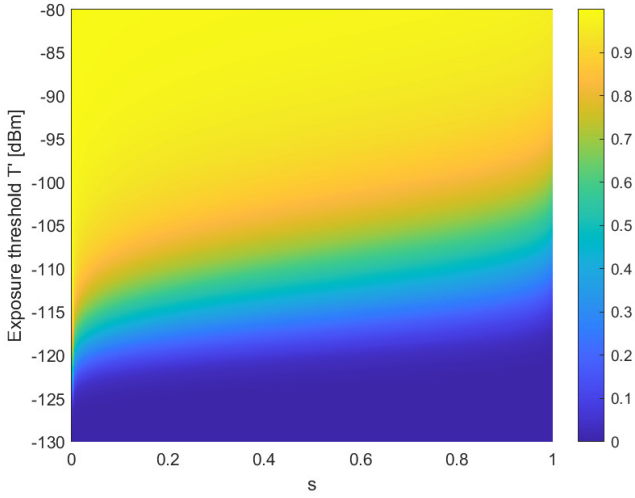

(a) Bidimensional representation of the IPD meta distribution.

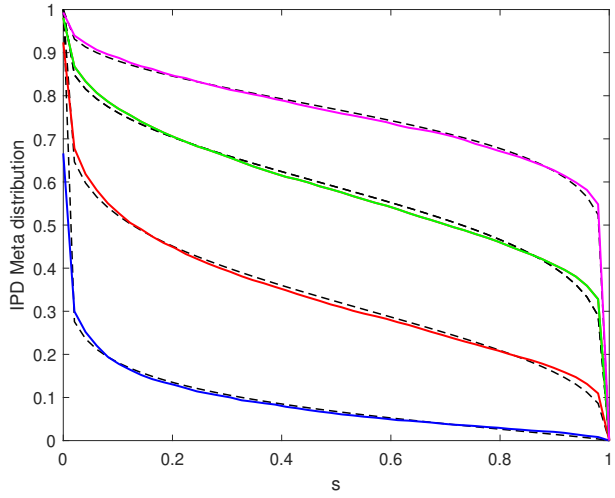

(b) IPD Meta distribution illustrated for several values of the threshold T'. The blue, red, green and purple curve correspond to $T' = \{-120, -115, -110, -105\}$ dBm. The dashed lines represent the corresponding beta approximations.

Fig. 2.4 Illustration of IPD Meta distribution $\tilde{\mathcal{F}}_{\mathcal{P}_{\text{IPD}}}(s, T')$. The following parameters were selected: $P_t = 1$ W, $\alpha = 4$, $P_N = 0$ and $\lambda = 2.10^{-6}$ m^{-2}.

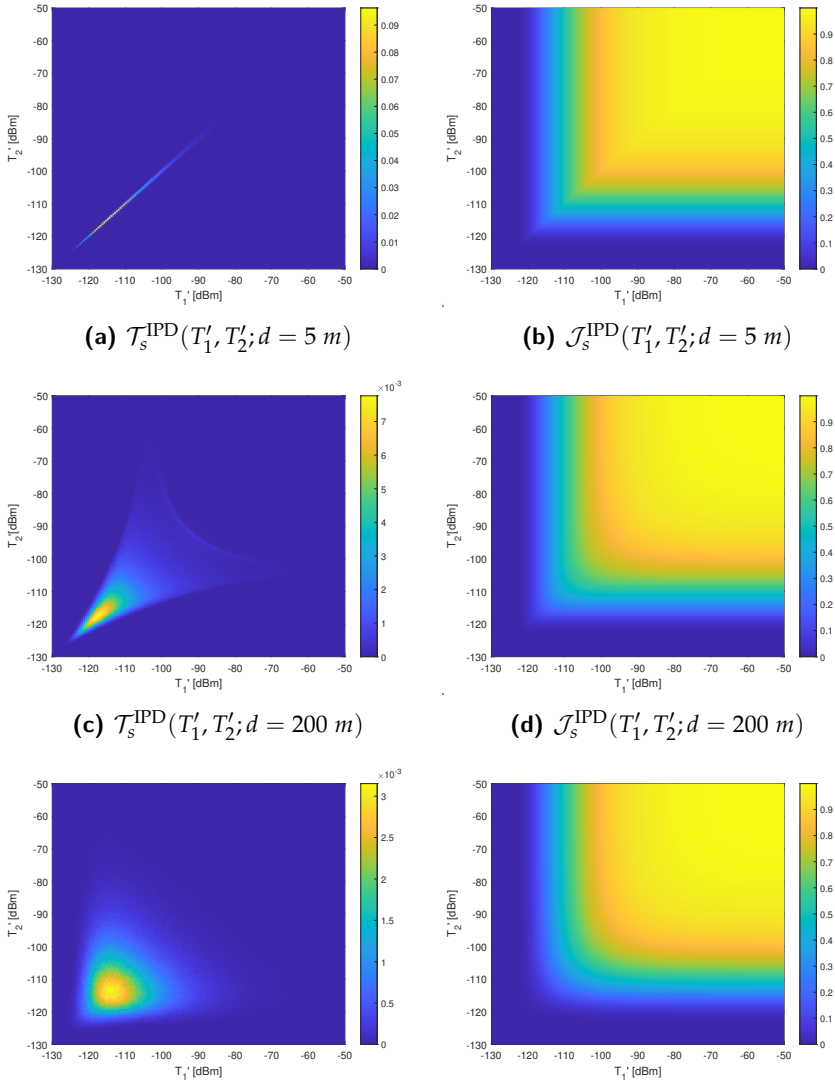

(a) $\mathcal{T}_s^{\mathrm{IPD}}(T_1', T_2'; d = 5\ m)$

(b) $\mathcal{J}_s^{\mathrm{IPD}}(T_1', T_2'; d = 5\ m)$

(c) $\mathcal{T}_s^{\mathrm{IPD}}(T_1', T_2'; d = 200\ m)$

(d) $\mathcal{J}_s^{\mathrm{IPD}}(T_1', T_2'; d = 200\ m)$

(e) $\mathcal{T}_s^{\mathrm{IPD}}(T_1', T_2'; d = 1\ km)$

(f) $\mathcal{J}_s^{\mathrm{IPD}}(T_1', T_2'; d = 1\ km)$

Fig. 2.5 Illustration of the metrics $\mathcal{J}_s^{\mathrm{IPD}}(T_1', T_2'; d)$ and $\mathcal{T}_s^{\mathrm{IPD}}(T_1', T_2'; d)$ in the absence of fading. The following parameters were selected: $P_t = 1\ W$, $\alpha = 4$, $P_N = 0$ and $\lambda = 2.10^{-6}\ m^{-2}$.

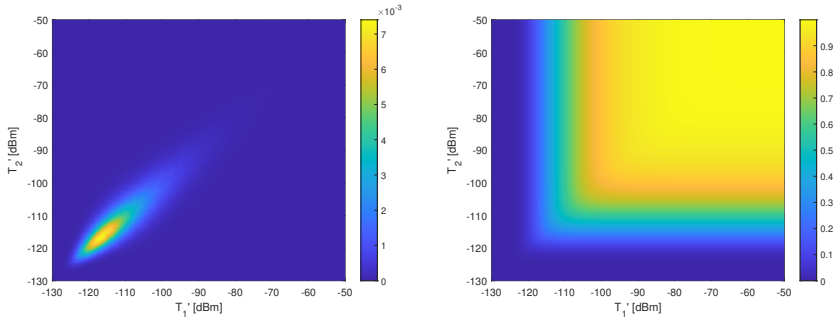

(a) $\mathcal{T}_s^{\mathrm{IPD}}(T_1', T_2'; d = 5\ m)$ **(b)** $\mathcal{J}_s^{\mathrm{IPD}}(T_1', T_2'; d = 5\ m)$

Fig. 2.6 Illustration of the metrics $\mathcal{J}_s^{\mathrm{IPD}}(T_1', T_2'; d)$ and $\mathcal{T}_s^{\mathrm{IPD}}(T_1', T_2'; d)$ in the presence of fading. The following parameters were selected: $d = 5\ m$, $P_t = 1\ W$, $\alpha = 4$, $P_N = 0$ and $\lambda = 2.10^{-6}\ m^{-2}$.

3

Analysis of cellular networks

3.1 Introduction

3.1.1 Point processes for cellular network modelling

The HPPP was the first topology employed to model cellular networks via SG theory. [13] and [51] were part of the first references dedicated to this topic. In order to analyze both macro and microcells, the notion of heterogeneous network (superposition of multiple HPPPs) was then quickly introduced [52]. Pioneering works capitalizing on these topologies mostly considered single-antenna base stations operating at sub-6 GHz frequencies. More recent publications now include more advanced features such as multi-antenna base stations [53], mmWave transmissions [54], etc.

Other categories of PPs are also employed in the wireless literature. Unlike the HPPP (for which nodes are uniformly and independently distributed), these PPs can capture other spatial behaviours:

- *Repulsion*: a non-exhaustive list of associated PPs include Matérn hard core PPs, Gibbs PPs, Poisson hole processes, ...
- *Attraction and clustering*, which can be modelled using Cox or Poisson cluster processes.

A detailed taxonomy (including references to all PPs listed above) is presented in [15].

3.1.2 Approximating non-Poisson point processes

Some of the topologies of the previous section have the disadvantage of leading to heavy or intractable expressions when deriving the associated coverage probability. In addition, the mathematical developments required to derive performance metrics for each non-Poisson PP can significantly differ from the HPPP. A unified approach (valid for any PP) would hence be of interest. Due to these drawbacks, the two methods below have been developed to approximate the performance of these non-Poisson networks.

Approximate SIR analysis based on the Poisson point process (ASAPPP)

This approach was originally proposed in [55]. Its principle is based on fact that the SIR curves of non-Poisson PPs are often similar to curve of a HPPP, up to a scaling factor. This scaling factor is computed in [56] and shown to be equal to the quotient of the *mean interference-to-signal ratios* (MISR) of the HPPP and of the non-Poisson PP.

The method is employed in [57] to approximate multi-tier and β-Ginibre networks. It is also used in [58] to establish optimization problems related to spectrum allocation.

Inhomogeneous double thinning approach (IDT)

The IDT approach relies on a different observation: general PPs can be characterized by two spatial functions:

- the *contact distance distribution* (also called *F-function*), which is the CDF of the distance betwen the mobile user and its closest BS;
- *Ripley's function* (also called *K-function*) representing the average number of points lying inside a given ball in $\mathbb{R}^2$ (without counting the BS at its center).

From the above definitions, one can observe that these functions respectively have close connections to the notions of void probability and intensity measure presented in section 1.2.2 for PPPs. The behaviour of these functions significantly vary depending on the repulsion or attraction nature of the process. In all generality, it is possible to show (see [38], section II) that the coverage probability of motion invariant-PP depends on these

two functions[1]. Capitalizing on this observation, the IDT approach employs two inhomogeneous Poisson processes (IPPPs) to model the network topology:

- One first IPPP whose parameters are selected to approximate at best the F-function of the original PP (to capture the spatial statistics of the serving BS).
- One second IPPP whose parameters are tuned to reproduce the behaviour of the K-function (to model the spatial distribution of the interfering BSs).

Two advantages of these IPPPs can be mentioned:

- their ability to fit a significant number of K and F-functions (thanks to the degrees of freedom offered by their spatial parameters). In [38], the approach is shown to provide accurate results for a large proportion of theoretical PPs and real BS datasets.
- their mathematical tractability, which is maintained since the properties of PPPs of section 1.2.2 can still be applied.

The original work presenting the IDT [38] derived the expression of the coverage probability. In addition to this work, the framework was then employed to compute the Meta distribution of the coverage [59] as well as the MISR [60] in spatially correlated networks.

3.1.3 Contributions

The objectives of this chapter can be summarized into two main contributions:

- *System modelling*: this developments of the next sections attempt to describe the joint statistics of the coverage and exposure of a cellular network as general as possible. To this purpose, the proposed system model encompasses the following aspects:
  - a representation of the serving and interfering base stations based on the IDT approach. As explained in the previous section,

[1] This result makes sense from intuition: if the user is served by its closest BS, the path loss affecting the useful received power statistically depends on the F-function. In addition, the K-function describes the spatial distribution of the interfers.

this methodology provides a tractable framework for modelling non-uniform BS deployments.

- the use of multiple tiers to represent networks of different operators coexisting in the same area.
- the inclusion of tiers operating in both sub-6 GHz and mmWave bands, as a first step to model beyond 5G networks.

A comparison of these aspects with a few existing related works is provided in Table 3.1.

- *Performance analysis:* beyond classical parameters studies, the developed model enables to analyze the joint coverage-exposure statistics in real network deployments. A case study dedicated to several French mobile operators is presented in section 3.4.

	IDT approach	General K-tier network	Coexisting sub-6 & mmWave bands	Marginal distribution of the exposure	Joint coverage & exposure statistics
[38]	✓				
[33]				✓	✓
[37]			✓	✓	
This work	✓	✓	✓	✓	✓

Table 3.1 Comparison of the model of Chapter 3 with existing works.

3.2 System model

A heterogeneous network is deployed in the disk $\mathcal{D}(\mathbf{o}, R)$ of radius R centered around $(0, 0)$. This network consists in two categories of tiers of BSs:

1. Sub-6GHz tiers

   N_1 tiers operate at sub-6GHz frequencies and are modelled via the IDT approach. Regarding the notations associated to these tiers, let us define

   - $\Psi_n^{(F,1)}$ and $\Psi_n^{(K,1)}$, the two IPPPs modelling tier n;

- $\lambda_n^{(1)}$, $[a_n^{(F,1)}, b_n^{(F,1)}, c_n^{(F,1)}]$ and $[a_n^{(K,1)}, b_n^{(K,1)}, c_n^{(K,1)}]$, the IDT parameters associated to tier n and defined in [38];
- $P_{t,n}^{(1)}$, the transmit power associated to the BSs of tier n.

The fading coefficients of these sub-6GHz frequencies are assumed to be Rayleigh, in accordance with the literature [37]. The single slope path loss of the form $l(r) = \kappa^{-1} r^{-\alpha}$ is considered with an exclusion distance r_0 around $(0,0)$ to avoid singularities in the vincinity of the centric user. The variables $\kappa_n^{(1)}$ and $\alpha_n^{(1)}$ are used to denote the path loss intercept and exponent related to tier n.

2. MmWave tiers

N_2 tiers operate in mmWave bands and are characterized by the following elements:

- As for the first category, the notations $\Psi_n^{(F,2)}$, $\Psi_n^{(K,2)}$, $P_{t,n}^{(2)}$, and IDT parameters $\lambda_n^{(2)}$, $[a_n^{(F,2)}, b_n^{(F,2)}, c_n^{(F,2)}]$,$[a_n^{(K,2)}, b_n^{(K,2)}, c_n^{(K,2)}]$ are defined for each of these tiers.
- In order to properly model the propagation at mmWave frequencies [37], the small-scale fading is represented via normalized Nakagami coefficients, with $|h_i|^2 \sim \Gamma(M_n, 1/M_n)$.
- Large-scale effects are modelled via the single-ball model [61]:

$$l(r) = \begin{cases} \begin{cases} \kappa_n^{(2,I,L)}\ r^{-\alpha_n^{(2,I,L)}} & \text{with prob. } p_n^{(I)} \\ \kappa_n^{(2,I,N)}\ r^{-\alpha_n^{(2,I,N)}} & \text{with prob. } 1 - p_n^{(I)} \end{cases} & \text{if } r \leq D_n \\ \begin{cases} \kappa_n^{(2,o,L)}\ r^{-\alpha_n^{(2,o,L)}} & \text{with prob. } p_n^{(o)} \\ \kappa_n^{(2,o,N)}\ r^{-\alpha_n^{(2,o,N)}} & \text{with prob. } 1 - p_n^{(o)} \end{cases} & \text{if } r > D_n \end{cases} \tag{3.1}$$

In the above definition, $D_n \in [r_0, R]$ represents the radius of the ball associated to tier n, the indices I and o indicated whether the BS is located inside or outside the ball, and the indices L and N refer to LOS and NLOS propagation conditions.

Regarding the association policy, the centric user connects to the BS providing the *strongest average received power*[2]. The other BSs of the network act as interferers. The noise power is finally denoted by P_N.

[2] taking into account the associated transmit power and path loss

3.3 Performance analysis

3.3.1 Notations

Splitting mmWave tiers

In order to take the single-ball model of eq. (3.1) into account, each mmWave tier n is virtually split into four subtiers:

- Base stations located at distance $r < D_n$ from the centric user and experiencing LOS propagation conditions. One will denote by $\Psi_n^{(F,2,I,L)}$ and $\Psi_n^{(K,2,I,L)}$ the associated IPPPs. The IDT density parameter of these IPPPs is trivially obtained via thinning [17] and is given by

$$\lambda_n^{(2,I,L)} = p_n^{(I)} \lambda_n^{(2)}. \tag{3.2}$$

  The corresponding IDT parameters are unchanged.

- Base stations located at distance $r < D_n$ and in NLOS conditions. The associated IPPPs, $\Psi_n^{(F,2,I,N)}$ and $\Psi_n^{(K,2,I,N)}$ are characterized by an IDT density parameter given by

$$\lambda_n^{(2,I,N)} = \left(1 - p_n^{(I)}\right) \lambda_n^{(2)}. \tag{3.3}$$

- Base stations located at distance $r > D_n$ and in LOS conditions. The associated IPPPs, $\Psi_n^{(F,2,o,L)}$ and $\Psi_n^{(K,2,o,L)}$ are characterized by an IDT density parameter given by

$$\lambda_n^{(2,o,L)} = p_n^{(o)} \lambda_n^{(2)}. \tag{3.4}$$

- Base stations located at distance $r > D_n$ and in NLOS conditions. The associated IPPPs, $\Psi_n^{(F,2,o,N)}$ and $\Psi_n^{(K,2,o,N)}$ are characterized by an IDT density parameter given by

$$\lambda_n^{(2,o,N)} = \left(1 - p_n^{(o)}\right) \lambda_n^{(2)}. \tag{3.5}$$

The zones of these four tiers are illustrated in Figure 3.1. Building up on the above notations, the tuple $\{n, p, l\}$ will be employed to uniquely identify each mmWave subtier in the following developments. Finally, prod-

ucts and sums over the four categories will be written using the notations $\prod_{\substack{p=\{I,o\}\\ l=\{L,N\}}}$ and $\sum_{\substack{p=\{I,o\}\\ l=\{L,N\}}}$.

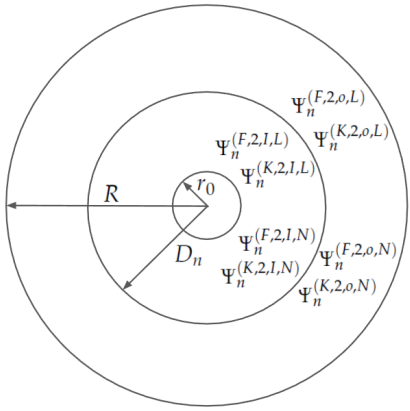

Fig. 3.1 Illustration of the zones associated the four subtiers.

Fifth IDT parameter

In order to obtain more compact expressions in the developments of the next sections, a fifth (redundant) IDT parameter is introduced:

$$d_n^{(F,1)} = (c_n^{(F,1)} - b_n^{(F,1)})/a_n^{(F,1)} \tag{3.6}$$
$$d_n^{(K,1)} = (c_n^{(K,1)} - b_n^{(K,1)})/a_n^{(K,1)} \tag{3.7}$$
$$d_n^{(F,2)} = (c_n^{(F,2)} - b_n^{(F,2)})/a_n^{(F,2)} \tag{3.8}$$
$$d_n^{(K,2)} = (c_n^{(K,2)} - b_n^{(K,2)})/a_n^{(K,2)} \tag{3.9}$$

3.3.2 Distance of the closest base stations

As presented in [38], the intensity measure of the IPPPs employed in this chapter is of the form

$$\mathcal{U}(r;a,b,c,d,\lambda_{BS}) = 2\pi\lambda_{BS}\left[\left(\frac{a}{3}r^3 + \frac{b}{2}r^2\right)\mathbb{1}(r \le d) + \left(\frac{c}{2}r^2 - \frac{(c-b)^2}{6a^2}\right)\mathbb{1}(r > d)\right] \tag{3.10}$$

where λ_{BS} and (a, b, c, d) are the IDT parameters of the considered IPPP. By taking the first order derivative of this result, the corresponding intensity function can be expressed as

$$\begin{aligned}\mathcal{U}^{(1)}(r; a, b, c, d, \lambda_{BS}) &= \frac{\partial \Lambda(r; a, b, c, d, \lambda_{BS})}{\partial r} \\ &= 2\pi\lambda_{BS}\Big[(ar^2 + br)\mathbb{1}(r \leq d) + cr\mathbb{1}(r > d)\Big]\end{aligned} \tag{3.11}$$

Capitalizing on these notations, the non-normalized CDF, CCDF and PDF of the distance between $(0, 0)$ and the closest BS of the tier are given by

$$F_C(r) = 1 - \exp\Big[-\mathcal{U}(r; a, b, c, d, \lambda)\Big] \tag{3.12}$$

$$\overline{F}(r) = \exp\Big[-\mathcal{U}(r; a, b, c, d, \lambda)\Big] \tag{3.13}$$

$$f_C(r) = \mathcal{U}^{(1)}(r; a, b, c, d, \lambda)\exp\Big[-\mathcal{U}(r; a, b, c, d, \lambda)\Big] \tag{3.14}$$

One the basis of the above developments, distance distributions can be derived for each (sub)tier by replacing by the corresponding IDT parameters and by normalizing with respect to the different zones. The following notations are therefore introduced:

- Distances distributions related to $\Psi_n^{(F,1)}$:

$$F_{C,n}^{(1)}(r) = \frac{1 - \exp\Big[-\mathcal{U}\Big(r; a_n^{(F,1)}, b_n^{(F,1)}, c_n^{(F,1)}, d_n^{(F,1)}, \lambda_n^{(1)}\Big)\Big]}{N_{C,n}^{(1)}}\,\mathbb{1}(r_0 < r < R)$$

$$\overline{F}_{C,n}^{(1)}(r) = \frac{\exp\Big[-\mathcal{U}\Big(r; a_n^{(F,1)}, b_n^{(F,1)}, c_n^{(F,1)}, d_n^{(F,1)}, \lambda_n^{(1)}\Big)\Big]}{N_{C,n}^{(1)}}\,\mathbb{1}(r_0 < r < R)$$

$$\begin{aligned}f_{C,n}^{(1)}(r) = &\frac{\mathcal{U}^{(1)}\Big(r; a_n^{(F,1)}, b_n^{(F,1)}, c_n^{(F,1)}, d_n^{(F,1)}, \lambda_n^{(1)}\Big)}{N_{C,n}^{(1)}} \\ &\times \exp\Big[-\mathcal{U}\Big(r; a_n^{(F,1)}, b_n^{(F,1)}, c_n^{(F,1)}, d_n^{(F,1)}, \lambda_n^{(1)}\Big)\Big]\mathbb{1}(r_0 < r < R)\end{aligned}$$

  where $N_{C,n}^{(1)}$ is the normalization factor given by

$$\begin{aligned}N_{C,n}^{(1)} = &\exp\Big[-\mathcal{U}\Big(r_0; a_n^{(F,1)}, b_n^{(F,1)}, c_n^{(F,1)}, d_n^{(F,1)}, \lambda_n^{(1)}\Big)\Big] \\ &- \exp\Big[-\mathcal{U}\Big(R; a_n^{(F,1)}, b_n^{(F,1)}, c_n^{(F,1)}, d_n^{(F,1)}, \lambda_n^{(1)}\Big)\Big]\end{aligned}$$

- Distances distributions related to $\Psi_n^{(F,2,I,l)}$:

$$F_{C,n}^{(2,I,l)}(r) = \frac{1-\exp\left[-\mathcal{U}\left(r;a_n^{(F,2)},b_n^{(F,2)},c_n^{(F,2)},d_n^{(F,2)},\lambda_n^{(2,I,l)}\right)\right]}{N_{C,n}^{(2,I,l)}}\mathbb{1}(r_0<r<D_n)$$
$$+\mathbb{1}(r>D_n)$$
$$\overline{F}_{C,n}^{(2,I,l)}(r) = \frac{\exp\left[-\mathcal{U}\left(r;a_n^{(F,2)},b_n^{(F,2)},c_n^{(F,2)},d_n^{(F,2)},\lambda_n^{(2,I,l)}\right)\right]}{N_{C,n}^{(2,I,l)}}\mathbb{1}(r_0<r<D_n)$$
$$f_{C,n}^{(2,I,l)}(r) = \frac{\mathcal{U}^{(1)}\left(r;a_n^{(F,2)},b_n^{(F,2)},c_n^{(F,2)},d_n^{(F,2)},\lambda_n^{(2,I,l)}\right)}{N_{C,n}^{(2,I,l)}}$$
$$\times\exp\left[-\mathcal{U}\left(r;a_n^{(F,2)},b_n^{(F,2)},c_n^{(F,2)},d_n^{(F,2)},\lambda_n^{(2,I,l)}\right)\right]\mathbb{1}(r_0<r<D_n)$$

  where $N_{C,n}^{(2,I,l)}$ is the normalization factor given by

$$N_{C,n}^{(2,I,l)} = \exp\left[-\mathcal{U}\left(r_0;a_n^{(F,2)},b_n^{(F,2)},c_n^{(F,2)},d_n^{(F,2)},\lambda_n^{(2,I,l)}\right)\right]$$
$$-\exp\left[-\mathcal{U}\left(D_n;a_n^{(F,2)},b_n^{(F,2)},c_n^{(F,2)},d_n^{(F,2)},\lambda_n^{(2,I,l)}\right)\right]$$

- Distances distributions related to $\Psi_n^{(F,2,o,l)}$:

$$F_{C,n}^{(2,o,l)}(r) = \frac{1-\exp\left[-\mathcal{U}\left(r;a_n^{(F,2)},b_n^{(F,2)},c_n^{(F,2)},d_n^{(F,2)},\lambda_n^{(2,o,l)}\right)\right]}{N_{C,n}^{(2,I,o)}}\mathbb{1}(D_n<r<R)$$
$$\overline{F}_{C,n}^{(2,o,l)}(r) = \frac{\exp\left[-\mathcal{U}\left(r;a_n^{(F,2)},b_n^{(F,2)},c_n^{(F,2)},d_n^{(F,2)},\lambda_n^{(2,o,l)}\right)\right]}{N_{C,n}^{(2,o,l)}}\mathbb{1}(D_n<r<R)$$
$$+\mathbb{1}(r<D_n)$$
$$f_{C,n}^{(2,o,l)}(r) = \frac{\mathcal{U}^{(1)}\left(r;a_n^{(F,2)},b_n^{(F,2)},c_n^{(F,2)},d_n^{(F,2)},\lambda_n^{(2,o,l)}\right)}{N_{C,n}^{(2,o,l)}}$$
$$\times\exp\left[-\mathcal{U}\left(r;a_n^{(F,2)},b_n^{(F,2)},c_n^{(F,2)},d_n^{(F,2)},\lambda_n^{(2,o,l)}\right)\right]\mathbb{1}(D_n<r<R)$$

  where $N_{C,n}^{(2,o,l)}$ is the normalization factor given by

$$N_{C,n}^{(2,o,l)} = \exp\left[-\mathcal{U}\left(D_n;a_n^{(F,2)},b_n^{(F,2)},c_n^{(F,2)},d_n^{(F,2)},\lambda_n^{(2,o,l)}\right)\right]$$
$$-\exp\left[-\mathcal{U}\left(R;a_n^{(F,2)},b_n^{(F,2)},c_n^{(F,2)},d_n^{(F,2)},\lambda_n^{(2,o,l)}\right)\right]$$

3.3.3 Association probabilities

Proposition 3.1. *The probability for the centric user to connect to a BS of tier n operating at sub-6 GHz is given by*

$$\mathcal{A}_n^{(1)} = \int_0^\infty \left\{ \prod_{\substack{j=1 \\ j\neq n}}^{N_1} \overline{F}_{C,j}^{(1)} \left[\left(\frac{P_{t,j}^{(1)} \kappa_n^{(1)}}{P_{t,n}^{(1)} \kappa_j^{(1)}} r^{\alpha_n^{(1)}} \right)^{1/\alpha_j^{(1)}} \right] \right\} \tag{3.15}$$
$$\times \left\{ \prod_{j=1}^{N_2} \prod_{\substack{p=\{I,o\} \\ l=\{L,N\}}} \overline{F}_{C,j}^{(2,p,l)} \left[\left(\frac{P_{t,j}^{(2)} \kappa_n^{(1)}}{P_{t,n}^{(1)} \kappa_j^{(2,p,l)}} r^{\alpha_n^{(1)}} \right)^{1/\alpha_j^{(2,p,l)}} \right] \right\} f_{C,n}^{(1)}(r) dr$$

Likewise, the probability for the centric user to connect to a BS of mmWave subtier $\{n, p, l\}$ can be expressed as

$$\mathcal{A}_n^{(2,p,l)} = \int_0^\infty \left\{ \prod_{j=1}^{N_1} \overline{F}_{C,j}^{(1)} \left[\left(\frac{P_{t,j}^{(1)} \kappa_n^{(2,p,l)}}{P_{t,n}^{(2)} \kappa_j^{(1)}} r^{\alpha_n^{(2,p,l)}} \right)^{1/\alpha_j^{(1)}} \right] \right\} \tag{3.16}$$
$$\times \left\{ \prod_{j=1}^{N_2} \prod_{\substack{p'=\{I,o\} \\ l'=\{L,N\}}} \overline{F}_{C,j}^{(2,p',l')} \left[\left(\frac{P_{t,j}^{(2)} \kappa_n^{(2,p,l)}}{P_{t,n}^{(2)} \kappa_j^{(2,p',l')}} r^{\alpha_n^{(2,p,l)}} \right)^{1/\alpha_j^{(2,p',l')}} \right] \right\}$$
$$\times \left\{ \overline{F}_{C,n}^{(2,p,l)}[r] \right\}^{-1} f_{C,n}^{(2,p,l)}(r) dr$$

Proof. The proof is derived by adapting Appendix A of [62].

3.3.4 Distance distribution of the serving base station

Proposition 3.2. *With the defined association rule, if the user is connected to tier n operating at sub-6 GHz, the PDF of the distance to its closest BS is given by*

$$f_{S,n}^{(1)}(r) = \frac{1}{\mathcal{A}_n^{(1)}} \left\{ \prod_{\substack{j=1 \\ j\neq n}}^{N_1} \overline{F}_{C,j}^{(1)} \left[\left(\frac{P_{t,j}^{(1)} \kappa_n^{(1)}}{P_{t,n}^{(1)} \kappa_j^{(1)}} r^{\alpha_n^{(1)}} \right)^{1/\alpha_j^{(1)}} \right] \right\} \tag{3.17}$$
$$\times \left\{ \prod_{j=1}^{N_2} \prod_{\substack{p=\{I,o\} \\ l=\{L,N\}}} \overline{F}_{C,j}^{(2,p,l)} \left[\left(\frac{P_{t,j}^{(2)} \kappa_n^{(1)}}{P_{t,n}^{(1)} \kappa_j^{(2,p,l)}} r^{\alpha_n^{(1)}} \right)^{1/\alpha_j^{(2,p,l)}} \right] \right\} f_{C,n}^{(1)}(r)$$

Similarly, if the user is connected to mmWave subtier $\{n,p,l\}$ the PDF of the distance to its closest BS is given by

$$f_{S,n}^{(2,p,l)}(r) = \frac{1}{\mathcal{A}_n^{(2,p,l)}} \left\{ \prod_{j=1}^{N_1} \overline{F}_{C,j}^{(1)} \left[\left(\frac{P_{t,j}^{(1)} \kappa_n^{(2,p,l)}}{P_{t,n}^{(2)} \kappa_j^{(1)}} r^{\alpha_n^{(2,p,l)}} \right)^{1/\alpha_j^{(1)}} \right] \right\} \tag{3.18}$$
$$\times \left\{ \prod_{j=1}^{N_2} \prod_{\substack{p'=\{I,o\} \\ l'=\{L,N\}}} \overline{F}_{C,j}^{(2,p',l')} \left[\left(\frac{P_{t,j}^{(2)} \kappa_n^{(2,p,l)}}{P_{t,n}^{(2)} \kappa_j^{(2,p',l')}} r^{\alpha_n^{(2,p,l)}} \right)^{1/\alpha_j^{(2,p',l')}} \right] \right\}$$
$$\times \left\{ \overline{F}_{C,n}^{(2,p,l)}[r] \right\}^{-1} f_{C,n}^{(2,p,l)}(r)$$

Proof. This result is derived by adapting the proof of Lemma 3 in [62].

3.3.5 Characteristic functions

Characteristic function of the useful received signal

Proposition 3.3. *If the centric user connects to a BS of sub-6 GHz tier n located at distance r, the CF of its useful received power will be given by*

$$\phi_{S,n}^{(1)}(t|r) = \left(1 - \frac{jtP_{t,n}^{(1)} r^{-\alpha_n^{(1)}}}{\kappa_n^{(1)}} \right)^{-1} \tag{3.19}$$

If the centric user connects to a BS of mmWave subtier $\{n,p,l\}$ located at distance r, the CF of its useful received power will be given by

$$\phi_{S,n}^{(2,p,l)}(t|r) = \left(1 - \frac{jtP_{t,n}^{(2)} r^{-\alpha_n^{(2,p,l)}}}{\kappa_n^{(2,p,l)} M_n}\right)^{-M_n} \tag{3.20}$$

Proof. These results are trivially obtained from the definitions of the CFs of the exponential and Gamma distributions.

Characteristic function of the aggregate interference

Proposition 3.4. *If the centric user is served by a BS of sub-6 GHz n, the characteristic function of the aggregate interference conditioned on the service distance r is then given by*

$$\phi_{I_{tot}}^{\{n,1\}}(t|r) = \left\{\prod_{n'=1}^{N_1} \phi_{I,n'}^{(1)}\left[t\middle|\beta_{n',1}^{\{n,1\}}(r)\right]\right\}\left\{\prod_{n'=1}^{N_2}\prod_{\substack{p=\{I,o\}\\ l=\{L,N\}}} \phi_{I,n'}^{(2,p,l)}\left[t\middle|\beta_{n',(2,p,l)}^{\{n,1\}}(r)\right]\right\} \tag{3.21}$$

where

$$\beta_{n',1}^{\{n,1\}}(r) = \left(\frac{P_{t,n}^{(1)}\kappa_{n'}^{(1)}}{P_{t,n'}^{(1)}\kappa_n^{(1)}} r^{-\alpha_n^{(1)}}\right)^{-1/\alpha_{n'}^{(1)}} \tag{3.22}$$

$$\beta_{n',(2,p,l)}^{\{n,1\}}(r) = \left(\frac{P_{t,n}^{(1)}\kappa_{n'}^{(2,p,l)}}{P_{t,n'}^{(2)}\kappa_n^{(1)}} r^{-\alpha_n^{(1)}}\right)^{-1/\alpha_{n'}^{(2,p,l)}} \tag{3.23}$$

If the centric user is served by a BS of mmWave subtier $\{n,p,l\}$, the characteristic function of the aggregate interference conditioned on the service distance r is then given by

$$\phi_{I_{tot}}^{\{n,(2,p,l)\}}(t|r) = \left\{\prod_{n'=1}^{N_1} \phi_{I,n'}^{(1)}\left[t\middle|\beta_{n',1}^{\{n,(2,p,l)\}}(r)\right]\right\}\left\{\prod_{n'=1}^{N_2}\prod_{\substack{p'=\{I,o\}\\ l'=\{L,N\}}} \phi_{I,n'}^{(2,p',l')}\left[t\middle|\beta_{n',(2,p',l')}^{\{n,(2,p,l)\}}(r)\right]\right\} \tag{3.24}$$

where

$$\beta_{n',1}^{\{n,(2,p,l)\}}(r) = \left(\frac{P_{t,n}^{(2)}\kappa_{n'}^{(1)}}{P_{t,n'}^{(1)}\kappa_n^{(2,p,l)}} r^{-\alpha_n^{(2,p,l)}}\right)^{-1/\alpha_{n'}^{(1)}} \tag{3.25}$$

$$\beta_{n',(2,p',l')}^{\{n,(2,p,l)\}}(r) = \left(\frac{P_{t,n}^{(2)}\kappa_{n'}^{(2,p',l')}}{P_{t,n'}^{(2)}\kappa_n^{(2,p,l)}} r^{-\alpha_n^{(2,p,l)}}\right)^{-1/\alpha_{n'}^{(2,p',l)'}} \tag{3.26}$$

In these expressions, the individual CFs of the interference coming from each sub(tier) can be developed:

- *For sub-6 GHz tier n, the individual CF is given by*

$$\phi_{I,n}^{(1)}(t|z) = \exp\left[2\pi\lambda_n^{(1)}\Delta_{I,n}^{(1)}(t|z)\right] \tag{3.27}$$

where

$$\begin{aligned}\Delta_{I,n}^{(1)}(t|z) =& c_n^{(K,1)}\mathcal{Y}\left[z, R; P_{t,n}^{(1)}/\kappa_n^{(1)}, \alpha_n^{(1)}, M, 1\right]\mathbb{1}\left[d_n^{(K,1)} < z\right] \\ &+ a_n^{(K,1)}\mathcal{Y}\left[z, d_n^{(K,1)}; P_{t,n}^{(1)}/\kappa_n^{(1)}, \alpha_n^{(1)}, 1, 2\right]\mathbb{1}\left[z < d_n^{(K,1)} < R\right] \\ &+ b_n^{(K,1)}\mathcal{Y}\left[z, d_n^{(K,1)}; P_{t,n}^{(1)}/\kappa_n^{(1)}, \alpha_n^{(1)}, 1, 1\right]\mathbb{1}\left[z < d_n^{(K,1)} < R\right] \\ &+ c_n^{(K,1)}\mathcal{Y}\left[d_n^{(K,1)}, R; P_{t,n}^{(1)}/\kappa_n^{(1)}, \alpha_n^{(1)}, 1, 1\right]\mathbb{1}\left[z < d_n^{(K,1)} < R\right] \\ &+ a_n^{(K,1)}\mathcal{Y}\left[d_n^{(K,1)}, R; P_{t,n}^{(1)}/\kappa_n^{(1)}, \alpha_n^{(1)}, 1, 2\right]\mathbb{1}\left[d_n^{(K,1)} > R\right] \\ &+ b_n^{(K,1)}\mathcal{Y}\left[d_n^{(K,1)}, R; P_{t,n}^{(1)}/\kappa_n^{(1)}, \alpha_n^{(1)}, 1, 1\right]\mathbb{1}\left[d_n^{(K,1)} > R\right]\end{aligned} \tag{3.28}$$

In the above developments, the following function have been introduced:

$$\mathcal{Y}[L_1, L_2; u, v, p, q] = \int_{L_1}^{L_2}\left[1 - \left(1 - ux^{-v}/p\right)^{-p}\right]r^q dr \tag{3.29}$$

$$\begin{aligned}&= \frac{L_1^{q+1}}{q+1}\left\{{}_2F_1\left[p, -(q+1/v), 1-(q+1/v), uL_1^{-v}\right] - 1\right\} \\ &\quad - \frac{L_2^{q+1}}{q+1}\left\{{}_2F_1\left[p, -(q+1/v), 1-(q+1/v), uL_2^{-v}\right] - 1\right\}\end{aligned} \tag{3.30}$$

In the above definition, ${}_2F_1(\cdot,\cdot,\cdot,\cdot)$ represents Gauss hypergeometric function.

- *For mmWave subtier $\{n, p = I, l\}$ located inside the LOS ball, the individual CF of the interference is given by*

$$\phi_{I,n}^{(2,I,l)}(t|z) = \exp\left[2\pi\lambda_n^{(2,I,l)}\Delta_{I,n}^{(2,I,l)}(t|z)\mathbb{1}(z < D_n)\right] \tag{3.31}$$

where

$$\begin{aligned}\Delta_{I,n}^{(2,I,l)}(t|z) =& c_n^{(K,2)}\mathcal{Y}\Big[z, D_n; P_{t,n}^{(2)}/\kappa_n^{(2,I,l)}M_n, \alpha_n^{(2,o,l)}, M_n, 1\Big]\mathbb{1}\Big[d_n^{(K,2)} < z\Big] \\ &+ a_n^{(K,2)}\mathcal{Y}\Big[z, d_n^{(K,2)}; P_{t,n}^{(2)}/\kappa_n^{(2,I,l)}M_n, \alpha_n^{(2,o,l)}, M_n, 2\Big]\mathbb{1}\Big[z < d_n^{(K,2)} < D_n\Big] \\ &+ b_n^{(K,2)}\mathcal{Y}\Big[z, d_n^{(K,2)}; P_{t,n}^{(2)}/\kappa_n^{(2,I,l)}M_n, \alpha_n^{(2,o,l)}, M_n, 1\Big]\mathbb{1}\Big[z < d_n^{(K,2)} < D_n\Big] \\ &+ c_n^{(K,2)}\mathcal{Y}\Big[d_n^{(K,2)}, D_n; P_{t,n}^{(2)}/\kappa_n^{(2,I,l)}M_n, \alpha_n^{(2,o,l)}, M_n, 1\Big]\mathbb{1}\Big[z < d_n^{(K,2)} < D_n\Big] \\ &+ a_n^{(K,2)}\mathcal{Y}\Big[d_n^{(K,2)}, D_n; P_{t,n}^{(2)}/\kappa_n^{(2,I,l)}M_n, \alpha_n^{(2,o,l)}, M_n, 2\Big]\mathbb{1}\Big[d_n^{(K,2)} > D_n\Big] \\ &+ b_n^{(K,2)}\mathcal{Y}\Big[d_n^{(K,2)}, D_n; P_{t,n}^{(2)}/\kappa_n^{(2,I,l)}M_n, \alpha_n^{(2,o,l)}, M_n, 1\Big]\mathbb{1}\Big[d_n^{(K,2)} > D_n\Big]\end{aligned} \tag{3.32}$$

- *For mmWave subtier $\{n, p = o, l\}$ located outside the LOS ball, the individual CF of the interference is given by*

$$\phi_{I,n}^{(2,o,l)}(t|z) = \exp\left[2\pi\lambda_n^{(2,o,l)}\Delta_{I,n}^{(2,o,l)}(t|z)\right] \tag{3.33}$$

where

$$\begin{aligned}&\Delta_{o,n}^{(2,o,l)}(t|z) \\ &= c_n^{(K,2)}\mathcal{Y}\Big[\max(z, D_n), R; P_{t,n}^{(2)}/\kappa_n^{(2,o,l)}M_n, \alpha_n^{(2,o,l)}, M_n, 1\Big]\mathbb{1}\Big[d_n^{(K,2)} < \max(z, D_n)\Big] \\ &+ a_n^{(K,2)}\mathcal{Y}\Big[\max(z, D_n), d_n^{(K,2)}; P_{t,n}^{(2)}/\kappa_n^{(2,o,l)}M_n, \alpha_n^{(2,o,l)}, M_n, 2\Big]\mathbb{1}\Big[\max(z, D_n) < d_n^{(K,2)} < R\Big] \\ &+ b_n^{(K,2)}\mathcal{Y}\Big[\max(z, D_n), d_n^{(K,2)}; P_{t,n}^{(2)}/\kappa_n^{(2,o,l)}M_n, \alpha_n^{(2,o,l)}, M_n, 1\Big]\mathbb{1}\Big[\max(z, D_n) < d_n^{(K,2)} < R\Big] \\ &+ c_n^{(K,2)}\mathcal{Y}\Big[d_n^{(K,2)}, R; P_{t,n}^{(2)}/\kappa_n^{(2,o,l)}M_n, \alpha_n^{(2,o,l)}, M_n, 1\Big]\mathbb{1}\Big[\max(z, D_n) < d_n^{(K,2)} < R\Big] \\ &+ a_n^{(K,2)}\mathcal{Y}\Big[d_n^{(K,2)}, R; P_{t,n}^{(2)}/\kappa_n^{(2,o,l)}M_n, \alpha_n^{(2,o,l)}, M_n, 2\Big]\mathbb{1}\Big[d_n^{(K,2)} > R\Big] \\ &+ b_n^{(K,2)}\mathcal{Y}\Big[d_n^{(K,2)}, R; P_{t,n}^{(2)}/\kappa_n^{(2,o,l)}M_n, \alpha_n^{(2,o,l)}, M_n, 1\Big]\mathbb{1}\Big[d_n^{(K,2)} > R\Big]\end{aligned} \tag{3.34}$$

Proof. This result is obtained by adapting the proof of Theorem I in [38].

3.3.6 Marginal distributions

Coverage distribution

Proposition 3.5. *The coverage probability is given by*

$$\mathcal{P}_{cov}(T) = \sum_{n=1}^{N_1}\mathcal{A}_n^{(1)}\mathcal{P}_{cov,n}^{(1)}(T) + \sum_{n=1}^{N_2}\mathcal{A}_n^{(2,p,l)}\sum_{\substack{p=\{I,o\}\\ l=\{L,N\}}}\mathcal{P}_{cov,n}^{(2,p,l)}(T) \tag{3.35}$$

where

$$\mathcal{P}^{(1)}_{cov,n}(T) = \frac{1}{2} + \frac{1}{\pi}\int_0^\infty Im\left[e^{-jP_N t}\int_0^\infty \phi^{(1)}_{S,n}(t|r)\phi^{\{n,1\}}_{I_{tot}}(-Tt|r)f^{(1)}_{S,n}(r)dr\right]t^{-1}dt$$

$$\mathcal{P}^{(2,p,l)}_{cov,n}(T) = \frac{1}{2} + \frac{1}{\pi}\int_0^\infty Im\left[e^{-jP_N t}\int_0^\infty \phi^{(2,p,l)}_{S,n}(t|r)\phi^{\{n,(2,p,l)\}}_{I_{tot}}(-Tt|r)f^{(2,p,l)}_{S,n}(r)\right]t^{-1}dt$$

Proof: this result is obtained via Gil-Pelaez theorem [21] and by applying the law of total probability.

Exposure distribution

Proposition 3.6. *The exposure CDF is given by*

$$\mathcal{P}_{IPD}(T') = \sum_{n=1}^{N_1}\mathcal{A}^{(1)}_n\mathcal{P}^{(1)}_{IPD,n}(T') + \sum_{n=1}^{N_2}\mathcal{A}^{(2,p,l)}_n\sum_{\substack{p=\{I,o\}\\ l=\{L,N\}}}\mathcal{P}^{(2,p,l)}_{IPD,n}(T') \tag{3.36}$$

where

$$\mathcal{P}^{(1)}_{IPD,n}(T') = \frac{1}{2} - \frac{1}{\pi}\int_0^\infty Im\left[e^{-jT't}\int_0^\infty \phi^{(1)}_{S,n}(t|r)\phi^{\{n,1\}}_{I_{tot}}(t|r)f^{(1)}_{S,n}(r)dr\right]t^{-1}dt$$

$$\mathcal{P}^{(2,p,l)}_{IPD,n}(T') = \frac{1}{2} - \frac{1}{\pi}\int_0^\infty Im\left[e^{-jT't}\int_0^\infty \phi^{(2,p,l)}_{S,n}(t|r)\phi^{\{n,(2,p,l)\}}_{I_{tot}}(t|r)f^{(2,p,l)}_{S,n}(r)\right]t^{-1}dt$$

Proof. The reasoning is similar to the proof of the coverage probability.

3.3.7 Joint coverage and exposure distribution

Proposition 3.7. *The joint coverage and exposure distribution is given by*

$$\begin{aligned}\mathcal{J}_{lim}(T,T') &= \mathbb{P}\Big[SINR > T, IPD < T'\Big] \\ &= \sum_{n=1}^{N_1}\mathcal{A}^{(1)}_n\mathcal{J}^{(1)}_{lim,n}(T,T') + \sum_{n=1}^{N_2}\mathcal{A}^{(2,p,l)}_n\sum_{\substack{p=\{I,o\}\\ l=\{L,N\}}}\mathcal{J}^{(2,p,l)}_{lim,n}(T,T')\end{aligned} \tag{3.37}$$

where

$$\mathcal{J}^{(1)}_{lim,n}(T,T') = \int_r \psi^{(1)}_n(T',r) f^{(1)}_{S,n}(r) dr - \frac{1}{\pi}\left[\int_r \int_0^\infty Im\left[\phi^{\{n,(1)\}}_{I_{tot}}(t|r)\ \zeta^{(1)}_n(q,T,T',r)\right]\ q^{-1} dq\right] f^{(1)}_{S,n}(r) dr$$

$$\mathcal{J}^{(2,p,l)}_{lim,n}(T,T') = \int_r \psi^{(2,p,l)}_n(T',r) f^{(2,p,l)}_{S,n}(r) dr - \frac{1}{\pi}\left[\int_r \int_0^\infty Im\left[\phi^{\{n,(2,p,l)\}}_{I_{tot}}(t|r)\ \zeta^{(2,p,l)}_n(q,T,T',r)\right]\ q^{-1} dq\right] f^{(2,p,l)}_{S,n}(r) dr$$

$$\psi^{(1)}_n(T',r) = \frac{1}{2}\left[1 - \exp\left(\frac{T'}{P^{(1)}_{t,n}\kappa^{(1)-1}_n r^{-\alpha^{(1)}_n}}\right)\right]$$

$$\psi^{(2,p,l)}_n(T',r) = \frac{1}{2\Gamma(M_n)}\ \gamma\left[M_n, M_n \frac{T'}{P^{(2,p,l)}_{t,n}\kappa^{(2,p,l)-1}_n r^{-\alpha^{(2,p,l)}_n}}\right]$$

$$\zeta^{(1)}_n(q,T,T',r) = e^{jqP_N}\left(\exp\left(\frac{-T''\left(1+jqP^{(1)}_{t,n}\kappa^{(1)-1}_n r^{-\alpha^{(1)}_n} T^{-1}\right)}{P^{(1)}_{t,n}\kappa^{(1)-1}_n r^{-\alpha^{(1)}_n}}\right) - 1\right)\left(1+jqP^{(1)}_{t,n}\kappa^{(1)-1}_n r^{-\alpha^{(1)}_n} T^{-1}\right)$$
$$+ e^{-jqT'}\exp\left(\frac{T''\left(-1+jqP^{(1)}_{t,n}\kappa^{(1)-1}_n r^{-\alpha^{(1)}_n}\right)}{P^{(1)}_{t,n}\kappa^{(1)-1}_n r^{-\alpha^{(1)}_n}}\right)\left(-1+jqP^{(1)}_{t,n}\kappa^{(1)-1}_n r^{-\alpha^{(1)}_n}\right)$$
$$- e^{-jqT'}\exp\left(\frac{T'\left(-1+jqP^{(1)}_{t,n}\kappa^{(1)-1}_n r^{-\alpha^{(1)}_n}\right)}{P^{(1)}_{t,n}\kappa^{(1)-1}_n r^{-\alpha^{(1)}_n}}\right)\left(-1+jqP^{(1)}_{t,n}\kappa^{(1)-1}_n r^{-\alpha^{(1)}_n}\right)$$

$$\zeta^{(2,p,l)}_n(q,T,T',r) = e^{jqP_N}\mathcal{V}\left(M_n, 0, \frac{T''}{P^{(2,p,l)}_{t,n}\kappa^{(2,p,l)-1}_n r^{-\alpha^{(2,p,l)}_n}}, \frac{P^{(2,p,l)}_{t,n}\kappa^{(2,p,l)-1}_n r^{-\alpha^{(2,p,l)}_n}}{T}\right)$$
$$+ e^{-jqT'}\mathcal{V}\left(M_n, \frac{T''}{P^{(2,p,l)}_{t,n}\kappa^{(2,p,l)-1}_n r^{-\alpha^{(2,p,l)}_n}}, \frac{T'}{P^{(2,p,l)}_{t,n}\kappa^{(2,p,l)-1}_n r^{-\alpha^{(2,p,l)}_n}}, P^{(2,p,l)}_{t,n}\kappa^{(2,p,l)-1}_n r^{-\alpha^{(2,p,l)}_n}\right)$$

$$\mathcal{V}(M,a,b,c) = \frac{M^M}{\Gamma(M)}\left\{a^M E_{1-M}\left[(M+cj)\right] - b^M E_{1-M}\left[(M+cj)\right]\right\}$$

In the above developments, $\Gamma(\cdot)$ denotes the Gamma function, $\gamma(\cdot,\cdot)$ represents the lower incomplete Gamma function, $E_n(\cdot)$ is the exponential integral and $T'' = T(T'+P_N)/(1+T)$.

Proof. This result is derived by adapting Appendix C of this dissertation and by applying the law of total probability.

3.4 Numerical results

The IDT approach is used in this section to fit five empirical datasets of several operators in Paris. These datasets contain the locations of BS employing different technologies: GSM, UMTS, LTE, and 5G. The IDT parameters associated to each dataset are provided in Table 3.2. These parameters $\{a_F, b_F, c_F\}$ and $\{a_K, b_K, c_K\}$ are obtained via the fitting methods presented in [38]. On the basis of this data, Figure 3.2 (page 65) illustrates the joint coverage-exposure distribution $\mathcal{J}_{\text{lim}}(T, T')$ for a fixed value of T'. This metric is computed via three methods:

- empirically, by using the BS locations of the dataset and considering a user randomly positioned within the network area;
- via equation (3.37), using the IDT approach;
- using a HPPP approximation (with the density parameters given in Table 3.2).

The accuracy of the IDT approach can be observed compared to the HPPP approximation.

	IDT Density $\lambda(/\text{km}^2)$	Radius R (km)	$\{a_F, b_F, c_F\}$	$\{a_K, b_K, c_K\}$
BUYG 2600 LTE	8.12	2	{1.86e-3,1.00,1.46}	{1.00,0.90,0.91}
Free 700 5G	6.76	2	{3.56e-3,1.00,3.31}	{0.92,0.91,0.94}
Orange 900 GSM	4.93	2	{2.61e-3,1.00,2.69}	{0.99,0.90,0.98}
Orange 900 UMTS	8.28	2	{1.63e-3,1.00,2.03}	{0.74,0.90,0.95}
SFR 800 LTE	5.09	2.5	{9.94e-4,1.00,1.64}	{0.74,0.90,0.91}

Table 3.2 Table of parameters for urban Paris case.

3.5 Conclusions of the chapter

3.5.1 Summary

This chapter proposes a general model for analyzing the exposure in cellular networks. Several modern aspects are considered: presence of multiple tiers, co-existence of sub-6 GHz with mmWave bands, etc. Each tier is

modelled via two IPPPs, in accordance with the IDT methodology. Capitalizing on this framework, the obtained results enable to analyze topologies reproducing real world deployments.

3.5.2 Further research directions

Three direct extensions are considered for this chapter:

- Adapting the developed framework to model the absence of fading. The resulting analysis would enable to study the average statistics of the exposure measured during long[3] intervals.
- Generalizing the system by including base stations with multiple antennas. The notion of beamforming would therefore be incorporated within the model. Let us note that the resulting scenario would be *cellular massive MIMO*, which differs from the *cell-free MIMO* systems presented in the next chapter: the former architecture considers antennas collocated onto base stations defining Voronoi cells, while the latter consists in antennas distributed within the network without notion of cell.
- As previously mentioned, the IDT approach also enables to study categories of PPs for which the derivation of tractable results is difficult. The model developed in this chapter could therefore be employed to analyze the joint statistics of the exposure and coverage in other PPs without deriving the analytical distributions specific to these PPs. This approach could bring answers to questions such as:

  "Considering a point process characterized by a set of spatial parameters[4]*, which values of these parameters enable to maximize the probability of satisfying given coverage and exposure requirements?"*

[3] compared to the small-scale fading coherence time.
[4] density, attraction, repulsion or thinning parameter, etc.

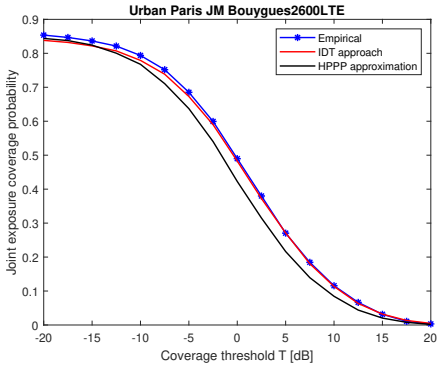

(a) Urban Paris JM Bouygues2600LTE.

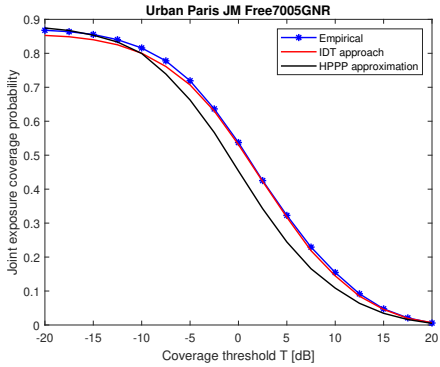

(b) Urban Paris JM Free7005GNR.

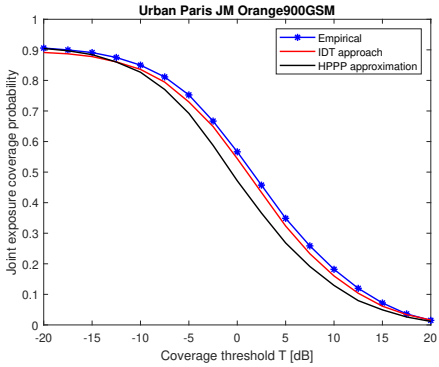

(c) Urban Paris JM Orange900GSM.

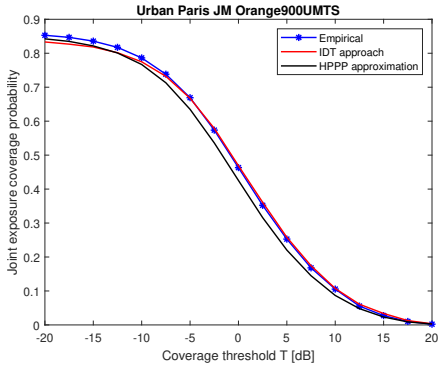

(d) Urban Paris JM Orange900UMTS.

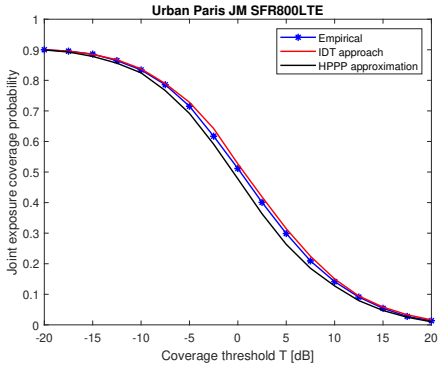

(e) Urban Paris JMSFR800 LTE

Fig. 3.2 Illustration of the IDT results obtained for several French operators in Paris. These graphs depict the joint probability $\mathcal{J}_{\text{lim}}(T, T')$ with a fixed exposure threshold $T' = -50dBm$. In addition to the IDT variables of table 3.2, the following parameters have been selected for each graph: $N_1 = 1$, $N_2 = 0$, $\alpha = 4$, $f = 2.1GHz$, $P_t = 1W$.

4

Analysis of cell-free networks

4.1 Introduction

During the past decade, cell-free (CF) networks have progressively been subject to numerous publications in the telecommunication literature. Several benefits of this architecture can be highlighted when comparing it with traditional cellular networks: improved interference management capabilities, increased SNR values (thanks to coherent transmissions), and a more uniform coverage [40]. Thanks to these assets, this network paradigm is considered as a promising solution for beyond 5G mobile communications [63].

In addition to the original CF structure, one will note the existence of a *user-centric* version [64]. In the first works considering the original CF architecture [65], each user is simultaneously served by all radio heads (Figure 4.1a). By contrast, user-centric cell-free networks (UCCFNs) restrict the serving access points to spatial subsets defined around every user (Figure 4.1b). In the rest of this work, these subsets will be named *cooperative clusters*. Such cluster structure is motivated by the scalability and reduced complexity obtained thanks to the access point selection [66]. In both cases, the signal transmitted by each radio head is composed of a superposition of precoded signals intended for the UEs served by this radio head. In the original CF architecture, this superposition hence includes all UEs in the

network. For UCCFNs, it can include one or more users if the radio head is selected to be part of several clusters [40], which explains the overlaps in Figure 4.1b. The system model of this study focuses on this user-centric adaptation.

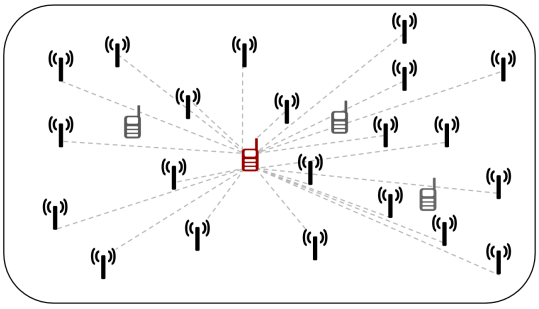

(a) Original CF network where each user can be served by any radio head.

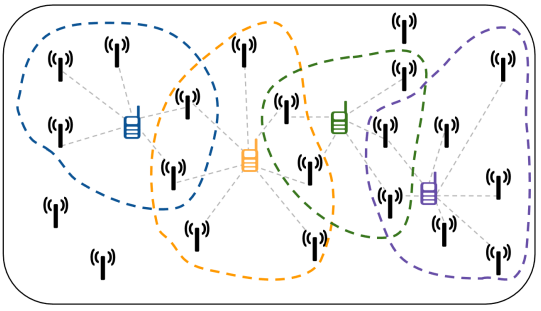

(b) UCCFN where clusters are defined around every user.

Fig. 4.1 Cell-free versus user-centric cell-free networks.

Most existing works related to CF networks have proposed a performance analysis relying on data-related metrics: coverage probability, spectral efficiency, etc. However, few publications have studied the statistics of the incident power density (IPD) affecting mobile users within this architecture. Power density analyses in existing CF-WPT works are partial: either no statistics are derived, or only the first moments of the incident power are computed. This chapter aims at bridging the resulting gap by deriving the individual and joint distributions of the IPD and rate in CF networks.

4.1.1 Related works

This section summarizes the studies analyzing CF networks by means of SG theory only. The analysis in [67] describes a CF network generated via a Poisson point process (PPP). The spectral efficiency of a typical user equipment (UE) is derived. The authors of [68] establish conditions for channel hardening in CF systems. In [69], an optimization problem is formulated to maximize the energy efficiency of a CF network as function of the node densities and pilot reuse factor. Another optimization problem is proposed in [70], aiming at minimizing the total transmit power of a CF network. The presented model considers coherent and non-coherent transmissions, as well as spatially correlated channels. The authors of [71] investigate the impact of fronthaul links of finite capacity on the performance. It is shown that the node deployment should be more distributed when the quality of the channel state information decreases. The model in [72] considers a time division duplexing CF system, whose frame length is optimized to limit Doppler shift effects. The framework of [73] analyzes a CF network featuring mobile edge computing functionalities: multiple user types are introduced, each category performing computing tasks with a given time requirement. The authors of [74] investigate optimality conditions for the interference to be approximated as noise in CF networks. [75] investigates the performance of CF systems with millimeter wave fronthaul. At the time of writing this paper, the analyses published in [76] and [77] constitute the only SG work studying SWIPT in a CF architecture. The authors of this study derive the mean and the variance of the energy harvested by the UE and characterize the steady-state probability of the UE battery to be charged.

4.1.2 Contributions

On the basis of the aforementioned works, the main findings of this chapter can be summarized as follows:

1. *Performance metrics:* this chapter provides a comprehensive analysis of the rate and IPD statistics in user-centric cell-free networks (UC-CFNs). To this purpose, our analytical framework enables to derive the following metrics:
    - the first moments of the total IPD measured at the UE;
    - the marginal distributions of the data rate and of the IPD;

- lower and upper bounds on the joint distributions of the rate and IPD.

To the best author's knowledge, this work is the first analysis introducing the IPD distribution, as well as the joint metrics for UCCFNs.

2. *System modeling:* this study includes system features related to UCCFNs which, to our best knowledge, have not been included so far in SG models:

   - the power allocation is based on collective channel statistics: given cluster serving a UE, the knowledge of the channels associated to all the RRHs of that cluster is employed to perform the allocation. The distribution guarantees a fixed transmit power budget per UE. This budget is then distributed among the remote radio heads (RRHs) serving the UE. The fraction of power allocated to each of these RRHs is computed based on their relative channel gains.
   - a new mathematical framework is provided to take into account the cluster overlaps (Figure 4.1b) in the case of distance-based association policies. The correlations between the useful and interfering signals resulting from these overlaps are captured in our mathematical developments. The impact of these correlations on the performance is then quantified by our numerical simulations.

3. *Performance analysis:* On the basis of the developed framework, the numerical results of this study enable to illustrate:

   - the achievable trade-offs in the rate and IPD requirements;
   - for the considered system, the existence of an optimal node density maximizing the joint data rate and IPD distributions.

4.2 System Model

4.2.1 Network topology

We consider the downlink of a UCCFN, as represented in Figure 4.1b. The RRH locations are modelled by means of a homogeneous PPP $\Psi_R \subset \mathbb{R}^2$

of intensity λ_R. Given one realization of this point process, we denote $\mathbf{x}_i$, the Cartesian coordinates of RRH $i \in \Psi_R$. All RRHs are equipped with M antennas and are connected via fronthaul links to a baseband processing unit (BBU). Users equipments (UEs) are distributed using a second homogeneous PPP Ψ_U, of intensity λ_U[2]. This point process is deployed over an area $\mathcal{A} \subset \mathbb{R}^2$ conditioned on the prior realization of Ψ_R. This area takes into account small exclusion zones around each RRH and is defined as

$$\mathcal{A} = \mathbb{R}^2 \setminus \left(\cup_{i \in \Psi_R} \mathcal{D}(\mathbf{x}_i, r_0) \right) \tag{4.1}$$

where $r_0 = 1$ m is an exclusion radius enabling to avoid singularities in the path loss (see next subsection). Each UE is equipped with a single antenna.

4.2.2 Channel model

The channel vector $\mathbf{g}_{iu} \in \mathbb{C}^{M \times 1}$ between RRH i and user equipment u is given by

$$\mathbf{g}_{iu} = \mathbf{h}_{iu} \kappa^{-1/2} r_{iu}^{-\alpha/2}. \tag{4.2}$$

In this definition, the following elements have been introduced:

- $\mathbf{h}_{iu} \in \mathbb{C}^{M \times 1}$, a vector containing the fading coefficients h_{iuk} (with $k = 1, \ldots, M$). These coefficients are assumed to be independently distributed. We consider Rayleigh fading, therefore $|\mathbf{h}_{iuk}|^2 \sim \exp(1)$.
- κr_{iu}^{α} is the path loss where
  - $\kappa = (4\pi f / c)^2$, is the reference path loss at a distance of 1 meter, where f is the carrier frequency and c the speed of light;
  - $\alpha > 2$ is the path loss exponent;
  - r_{iu} is the Euclidean distance between i and u. Since Ψ_U is defined over the area given by (4.1), potential singularities in (4.2) are circumvented.

For the sake of mathematical tractability, shadowing effects are not modelled here.

[2] In the case of a cell-free network, we will usually consider that $\lambda_U \ll \lambda_R$ [40].

4.2.3 Association policy

The cooperative clusters of the UCCFN are here distance based: every UE u is served by the RRHs located in the disk of radius r_1 centered around its position. We denote this set of RRHs by $\mathcal{C}_u$. All these RRHs are assumed to perfectly estimate their downlink channels before transmitting. The estimated channel values are systematically sent to the BBU.

Due to the random node locations, cooperative clusters may overlap (Figure 4.2). A given RRH might thus be associated to several UEs. As mentioned in Section I, such RRH simultaneously transmits a superposition of signals intended to distinct users. In that case, each of these UEs receives both useful information and interference from the same node. In terms of notations, we define $\mathcal{C}_u$ the set of RRHs serving user u and $\mathcal{B}_i$, the set of UEs served by RRH i.

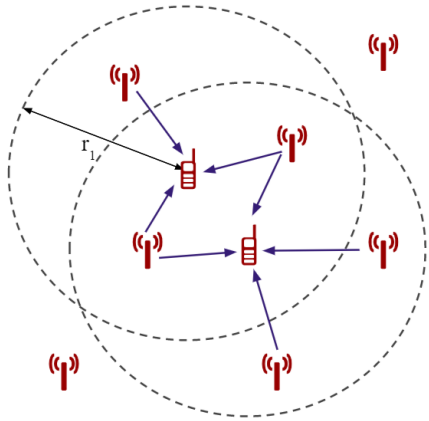

Fig. 4.2 Illustration of the cluster overlaps with distance-based clusters.

4.2.4 Downlink signal model

Without loss of generality, the network performance is evaluated for a centric UE u^* located at $\mathbf{o} = (0, 0)$, in accordance with Slivnyak-Mecke theorem (theorem 1.2.4). In the rest of this study, the set $\mathcal{C}_{u^*}$ of RRHs serving this user will be named *centric cluster*. The baseband signal received at that UE is given by

$$y_{u^*} = \sum_{i \in \mathcal{C}_{u^*}} \sqrt{P_t} \mathbf{w}_{iu^*} \mathbf{h}_{iu^*} \kappa^{-1/2} r_{iu^*}^{-\alpha/2} s_{u^*} + \sum_{u \in \Psi_U \setminus \{u^*\}} \left(\sum_{i \in \mathcal{C}_u} \sqrt{P_t} \mathbf{w}_{iu} \mathbf{h}_{iu^*} \kappa^{-1/2} r_{iu^*}^{-\alpha/2} \right) s_u + n_{u^*} \tag{4.3}$$

where the following notations have been introduced:

- P_t, a constant transmit power;
- $\mathbf{w}_{iu} \in \mathbb{C}^{1 \times M}$, the beamforming vector associated to transmission from i to u;
- s_u, the unit energy symbol intended for user u;
- n_u, the additive thermal noise of constant power density P_N.

Assuming coherent joint transmission, the corresponding received power is given by

$$P_{u^*} = \underbrace{\left| \sum_{i \in \mathcal{C}_{u^*}} \sqrt{P_t} \mathbf{w}_{iu^*} \mathbf{h}_{iu^*} \kappa^{-1/2} r_{iu^*}^{-\alpha/2} \right|^2}_{P_S} + \underbrace{\sum_{u \in \Psi_U \setminus \{u^*\}} \left| \sum_{i \in \mathcal{C}_u} \sqrt{P_t} \mathbf{w}_{iu} \mathbf{h}_{iu^*} \kappa^{-1/2} r_{iu^*}^{-\alpha/2} \right|^2}_{P_I} + P_N \tag{4.4}$$

where P_S is the useful information power and P_I the aggregate interference.

4.2.5 Beamforming strategy and power allocation

For the sake of mathematical tractability, we consider maximum ratio transmission as beamforming strategy. Therefore,

$$\mathbf{w}_{iu} = \frac{\mathbf{g}_{iu}^H}{\gamma_{iu}} \tag{4.5}$$

where γ_{iu} is a normalization factor that can be chosen in several manners. In the framework of this paper, this coefficient is defined as $\gamma_{iu} =$

$|\mathbf{g}_u|$, with $\mathbf{g}_u = [\mathbf{g}_{iu}]_{i \in \mathcal{C}_u}$ being the concatenation of the channel vectors of RRHs serving u. This normalization benefits from the following properties:

- the effective transmit power allocated to RRH i to serve user u is proportional to the relative channel gain of this RRH with respect to the channel coefficients of all RRHs of $\mathcal{C}_u$. This power can indeed be expressed as

$$P_t^{(u,i)} = P_t |\mathbf{w}_{iu} s_u|^2 = P_t \frac{|\mathbf{g}_{iu}|^2}{|\mathbf{g}_u|^2} = P_t \frac{|\mathbf{g}_{iu}|^2}{\sum_{i' \in \mathcal{C}_u} |\mathbf{g}_{i'u}|^2}$$

- the total power budget allocated to the RRHs of C_u to serve u is constant and given by

$$\begin{aligned} P_t^{(u)} &= \sum_{i \in \mathcal{C}_u} P_t^{(u,i)} \\ &= \sum_{i \in \mathcal{C}_u} \left| \sqrt{P_t} \mathbf{w}_{iu} s_u \right|^2 \\ &= P_t \frac{1}{|\mathbf{g}_u|^2} \sum_{i \in \mathcal{C}_u} |\mathbf{w}_{iu}|^2 \\ &= P_t \frac{1}{|\mathbf{g}_u|^2} \sum_{i \in \mathcal{C}_u} |\mathbf{g}_{iu}|^2 \\ &= P_t. \end{aligned} \tag{4.6}$$

From these properties, the power normalization can be interpreted as follows: each UE is granted the same global power P_t by the BBU. This power budget is shared among all RRHs serving this user. Among these RRHs, those experiencing better channel conditions are granted a greater fraction of P_t since their transmitted signals are less attenuated. Other normalization strategies might also be relevant for this scenario and are left for future work.

4.3 Performance Analysis

The structure of this section is illustrated in Figure 4.3. A preliminary assumption on the model is provided in Subsection 4.3.1. The incident powers coming from RRHs of the centric cluster and from the other RRHs are

studied in Subsections 4.3.2 and 4.3.3. Finally, the global performance metrics (main results of this paper) are developed in Subsection 4.3.3.

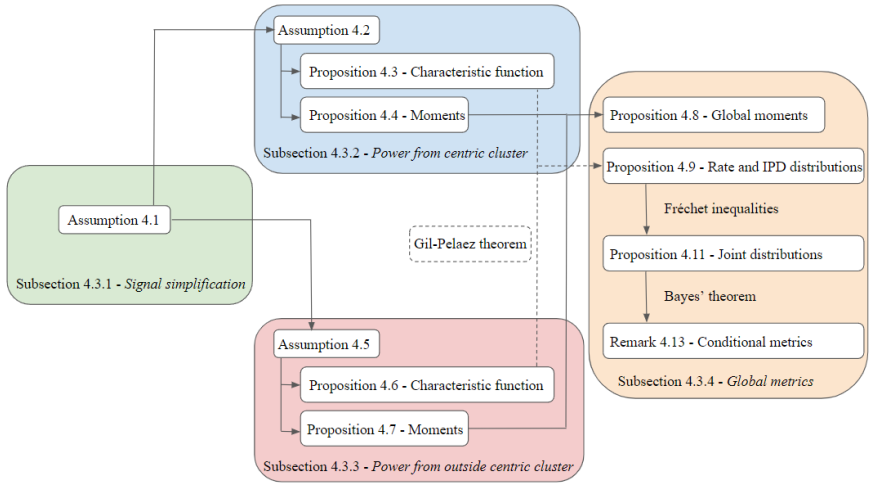

Fig. 4.3 Structure of Section 4.3.

4.3.1 Signal model simplification

The objective of this first proposition is to simplify the interference term in (4.4) to obtain more adequate expressions for a tractable SG analysis.

Assumption 4.1. *One possible approximation for the aggregate interference P_I is given by*

$$P_I' = \underbrace{\sum_{i\in\mathcal{C}_{u^*}} \sum_{\substack{u\in\mathcal{B}_i \\ u\neq u^*}} P_t Z_{|\mathcal{C}_u|}^{(i,u)} \kappa^{-1} r_{iu^*}^{-\alpha}}_{P_{I_1}} + \underbrace{\sum_{i\in\Psi_R\setminus\mathcal{C}_{u^*}} \sum_{u\in\mathcal{B}_i} P_t Z_{|\mathcal{C}_u|}^{(i,u)} \kappa^{-1} r_{iu^*}^{-\alpha}}_{P_{I_2}}. \tag{4.7}$$

where $\mathcal{B}_i$ denotes the set of UEs served by RRH i. The coefficients $Z_{|\mathcal{C}_u|}^{(i,u)}$ are random variables following a Gamma distribution of shape and scale parameters given by

$$k_{|\mathcal{C}_u|} = \begin{cases} 1 & \text{if } |\mathcal{C}_u| = M = 1 \\ \frac{|\mathcal{C}_u|M}{3|\mathcal{C}_u|-1} & \text{otherwise} \end{cases}$$

$$s_{|\mathcal{C}_u|} = \begin{cases} 1 & \text{if } |\mathcal{C}_u| = M = 1 \\ \frac{3|\mathcal{C}_u|-1}{|\mathcal{C}_u|^2 M} & \text{otherwise} \end{cases} \tag{4.8}$$

Proof. cfr. Appendix G.

In (4.7), the interference P_I' has been separated into two terms:

- P_{I_1}, corresponding to the interference power coming from the RRHs of the centric cluster. As explained in section 4.2.3, these RRHs can potentially interfere if they serve other adjacent UEs (cfr. Figure 4.2). This quantity could therefore be described as *intra-cluster interference*;
- P_{I_2}, representing the total interference coming from RRHs located outside the centric cluster. This power could hence be described as *inter-cluster interference.*

The objective of the next subsections is to compute the statistics of these two powers. These statistics include their first moments, as well as their characteristic functions (CFs). As illustrated in Figure 4.3, these quantities will be employed to derive the global network metrics, including the total IPD moments, as well as the rate and IPD distributions (obtained from the CFs via Gil-Pelaez inversion theorem [21]).

4.3.2 Statistics of the incident power coming from the centric cluster

The interference term P_{I_1} is statistically correlated to the useful received power P_S. Both powers share indeed common variables in their definitions, including the number of RRHs in the centric cluster and their locations. Numerical simulations show that deriving the distributions of P_S and P_{I_1} independently leads to a loss of accuracy owing to this correlation (cfr. Subsection 4.4.1). For this reason, the next proposition provides the characteristic function of the linear combination $P_{S_\eta} \triangleq P_S + \eta P_{I_1}$, taking into account the joint statistics of both variables. In order to introduce this proposition, the following elements are defined:

- $n_R \triangleq |\mathcal{C}_{u^*}|$, the number of RRHs in the centric cluster (Figure 4.5). This variable follows a Poisson distribution of parameter $\lambda_R \pi(r_1^2 - r_0^2)$. The corresponding probability mass function (PMF) is denoted by $p_R(n_R)$;

- n_U, the number of UEs different from u^* located in the disk $\mathcal{D}(\mathbf{o}, r_1)$ (Figure 4.4). This random variable also follows a Poisson distribution, of parameter $\lambda_U \pi r_1^2$ and PMF $p_U(n_U)$[2].

Considering an arbitrary RRH i of the centric cluster (in yellow in Figs. 4.4 and 4.5), we also define

- $n'_U = |\mathcal{B}_i|$, the number of UEs different from u^* served by this RRH (Figure 4.4);
- n'_R, the number of RRHs serving one arbitrary UE u among these n'_U UEs (Figure 4.5).

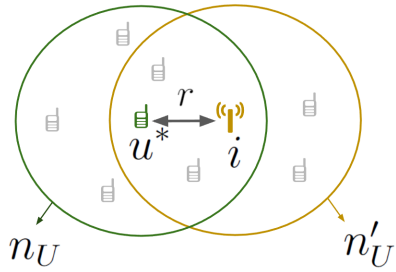

Fig. 4.4 Geometrical representation of the quantities n_U and n'_U, corresponding to the number of grey UEs contained in the green and yellow sets. All the disk are characterized by a radius of value r_1.

Let us still consider RRH i in Figure 4.5. The interference on u^* coming from this RRH depends on the number of users it serves (variable n'_U) and on the effective transmit powers it employs to cover each of these n'_U users. Because of the beamforming policy, these transmit powers are themselves function of the number of RRHs serving each of these n'_U users. In Figure 4.5, this number of RRHs corresponds to n'_R in the case of user u (in blue). Furthermore, one can observe from Figures 4.4 and 4.5 that n'_U and n'_R are respectively correlated with n_U and n_R. To take into account these dependencies, the statistics derived in this section are first conditioned on

[2]Although n_R and n_U are defined with respect to the centric cluster area, one will observe that their PMFs $p_R(\cdot)$ and $p_U(\cdot)$ can be interpreted with a more global point of view. In all generality, $p_R(\cdot)$ can be defined as the PMF of the number of RRHs serving *any* user in the network. Likewise, for $r_1 \gg r_0$, $p_U(\cdot)$ is also the PMF of the number of users served by *any* RRH of Ψ_R. In the rest of this paper, these distributions will also be employed with this more general interpretation.

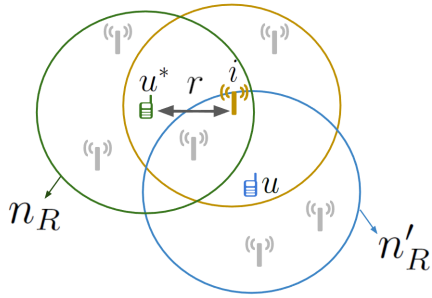

Fig. 4.5 Geometrical representation of the quantities n_R and n'_R, corresponding to the number of RRHs contained in the green and blue sets. All the disk are characterized by a radius of value r_1.

n_U, n'_U, n_R and n'_R, then progressively averaged: first over n'_U and n'_R, and then over n_U and n_R. In order to perform such averaging, the next assumption defines conditional probabilities linking these four variables.

Assumption 4.2. *Conditioned on n_U, n_R and distance r (from RRH i to the u^* in Fig. 4.5), the PMFs of n'_U and n'_R are approximated by $p(n'_U|n_U, r)$ and $p(n'_R|n_R, r)$ given in Appendix H.*

Proof. cfr. Appendix H.

Proposition 4.3. *Under the previous assumptions, the characteristic function of P_{S_η} is given by*

$$\phi_{P_{S_\eta}}(t) = \sum_{n_U=0}^{\infty} \sum_{n_R=0}^{\infty} p_R(n_R) p_U(n_U) \phi_{P_{S_\eta}}(t|n_R, n_U) \tag{4.9}$$

where

$$\phi_{P_{S_\eta}}(t|n_R, n_U) = \left[\int_{r_0}^{r_1} \phi_T(t|n_R, n_U, r) \phi_V(\eta t|n_R, n_U, r) \frac{2r}{r_1^2 - r_0^2} dr \right]^{n_R} \tag{4.10}$$

$$\phi_T(t|n_R, n_U, r) = \left(1 - jtP_t \kappa^{-1} r^{-\alpha}\right)^{-M} \tag{4.11}$$

$$\phi_V(t|n_R, n_U, r) = \sum_{n'_U=0}^{\infty} p(n'_U|n_U, r) X(n'_U, r) \tag{4.12}$$

$$X(n'_U, r) = \left[\sum_{n'_R=1}^{\infty} p(n'_R|n_R, r) \left(1 - jtP_t\kappa^{-1}r^{-\alpha}s_{n'_R}\right)^{-k_{n'_R}} \right]^{n'_U} \tag{4.13}$$

Proof. cfr. Appendix I.

Proposition 4.4. *The mean and the variance of $P_S + P_{I_1}$ are given by*

$$m_{P_S+P_{I_1}} = P_t\kappa^{-1} \sum_{n_U=0}^{\infty} \sum_{n_R=0}^{\infty} p_R(n_R)p_U(n_U)n_R L(n_U, n_R) \tag{4.14}$$

$$\sigma^2_{P_S+P_{I_1}} = P_t^2\kappa^{-2} \sum_{n_U=0}^{\infty} \sum_{n_R=0}^{\infty} p_R(n_R)p_U(n_U)n_R R(n_U, n_R) - m^2_{P_S+P_{I_1}} \tag{4.15}$$

where the following auxiliary functions are introduced:

$$L(n_U, n_R) = \int_{r_0}^{r_1} L'(r, n_U, n_R) \frac{2r^{1-\alpha}}{r_1^2 - r_0^2} dr$$

$$L'(r, n_U, n_R) = \left[(M + \sum_{n'_U=0}^{\infty} p(n'_U|n_U, r)n'_U \sum_{n'_R=0}^{\infty} p(n'_R|n_R, r)n'^{-1}_R \right]$$

$$R(n_U, n_R) = \int_{r_0}^{r_1} \left[\sum_{n=1}^{3} Y_i(r, n_U, n_R) \right] \frac{2r^{-2\alpha+1}}{r_1^2 - r_0^2} dr + Z(n_U, n_R)$$

$$Y_1(r, n_U, n_R) = M(M+1) + 2M \sum_{n'_U=0}^{\infty} p(n'_U|n_U, r)n'_U \sum_{n'_R=0}^{\infty} p(n'_R|n_R, r)n'^{-1}_R$$

$$Y_2(r, n_U, n_R) = \sum_{n'_U=0}^{\infty} p(n'_U|n_U, r)n'_U \sum_{n'_R=0}^{\infty} p(n'_R|n_R, r)s^2_{n'_R} \frac{\Gamma(2 + k_{n'_R})}{\Gamma(k_{n'_R})}$$

$$Y_3(r, n_U, n_R) = \sum_{n'_U=0}^{\infty} p(n'_U|n_U, r)n'_U(n'_U - 1) \left(\sum_{n'_R=0}^{\infty} p(n'_R|n_R, r)n'^{-1}_R \right)^2$$

$$Z(n_U, n_R) = (n_R - 1) \left(\int_{r_0}^{r_1} Z'(r, n_U, n_R) \frac{2r^{-\alpha+1}}{r_1^2 - r_0^2} dr \right)^2$$

$$Z'(n_U, n_R, r) = \left[M + \sum_{n'_U=0}^{\infty} p(n'_U|n_U, r)n'_U \sum_{n'_R=0}^{\infty} p(n'_R|n_R, r)n'^{-1}_R \right]$$

Proof. cfr. Appendix J.

4.3.3 Statistics of the power coming from outside the centric cluster

In order to derive the statistics of P_{I_2}, a third assumption is introduced, enabling to perform a spatial decomposition of the interferring RRHs.

Assumption 4.5. *Let $\tilde{\Psi}_R = \Psi_R \setminus \mathcal{C}_{u^*}$ be the set of RRHs generating P_{I_2}. This set can be decomposed as*

$$\tilde{\Psi}_R = \bigcup_{n=0}^{\infty} \tilde{\Psi}_{R,n} \tag{4.16}$$

where $\tilde{\Psi}_{R,n}$ is the set of RRHs serving exactly n users. Using the displacement theorem [16], each $\tilde{\Psi}_{R,n}$ can be approximated as a HPPP of reduced intensity $\lambda_{R,n} = \lambda_R \; p_U(n)$ with $p_U(n)$, the probability for an arbitrary RRH to serve n users.

Proposition 4.6. *Using the above decomposition, the CF of P_{I_2} can be written as*

$$\phi_{P_{I_2}}(t) = \prod_{n=1}^{\infty} \; \exp\left\{ -2\pi\lambda_{R,n} \int_{r_1}^{\infty} \left[1-\gamma(n)\right] r dr \right\} \tag{4.17}$$

where

$$\gamma(n) = \left[\sum_{m=1}^{\infty} \tilde{p}_R(m)(1 - jtP_t\kappa^{-1}r^{-\alpha}s_m)^{k_m} \right]^n \tag{4.18}$$

$$\tilde{p}_R(m) = \frac{\left[\lambda_R \pi (r_1^2 - r_0^2)\right]^m}{m!} \frac{e^{-\lambda_R \pi (r_1^2 - r_0^2)}}{1 - e^{-\lambda_R \pi (r_1^2 - r_0^2)}}. \tag{4.19}$$

Proof. See Appendix K.

Proposition 4.7. *The mean and the variance of P_{I_2} are given by*

$$m_{P_{I_2}} = 2\pi^2 P_t \kappa^{-1} r_1^{(2-\alpha)} (\alpha - 2)^{-1} \lambda_R \lambda_U (r_1^2 - r_0^2) \left(\sum_{m=1}^{\infty} p_R(m) m^{-1} \right) \tag{4.20}$$

$$\sigma^2_{P_{I_2}} = 2\pi P_t^2 \kappa^{-2} r_1^{(2-2\alpha)} (2\alpha - 2)^{-1} \lambda_R (\beta_1 + \beta_2) \tag{4.21}$$

with

$$\beta_1 = \pi \lambda_U (r_1^2 - r_0^2) \left(\sum_{m=1}^{\infty} p_R(m) \rho_m \right) \tag{4.22}$$

$$\beta_2 = \left(\sum_{n=1}^{\infty} p_U(n) n(n-1) \right) \left(\sum_{m=1}^{\infty} p_R(m) m^{-1} \right)$$
$$\rho_m = s_m^2 \Gamma(2 + k_m) / \Gamma(k_m) \tag{4.23}$$

Proof. The proof consist in applying Campbell theorem 1.2.5 as well as the second-order product density of the PPP [18].

4.3.4 Global metrics

On the basis of the previous results, the total exposure and data rate distribution can now be fully characterized.

Proposition 4.8. *The mean and the variance of the total IPD are given by*

$$m_{P_S + P_{I_1} + P_{I_2}} = m_{P_S + P_{I_1}} + m_{P_{I_2}} \tag{4.24}$$
$$\sigma^2_{P_S + P_{I_1} + P_{I_2}} = \sigma^2_{P_S + P_{I_1}} + \sigma^2_{P_{I_2}} \tag{4.25}$$

Proof. the proof follows from Propositions 4.4 and 4.7, and from the assumed independence between $P_S + P_{I_1}$ and P_{I_2}.

Proposition 4.9. *The distribution of the spectral efficiency is given by*

$$\begin{aligned} \mathcal{P}_{cov}(T) &\triangleq \mathbb{P}\left[\log_2 \left(1 + \frac{P_S}{P_I' + P_N} \right) > T \right] \\ &= \frac{1}{2} + \frac{1}{\pi} \int_0^{\infty} \mathrm{Im} \left\{ \phi_{P_{S_{\eta=-\tilde{T}}}}(t | n_R, n_U) \phi_{P_{I_2}}(-\tilde{T}t) e^{-jt\tilde{T}P_N} \right\} t^{-1} dt \end{aligned} \tag{4.26}$$

with $\tilde{T} = 2^T - 1$. *The expression of the IPD distribution is similar:*

$$\mathcal{P}_{IPD}(T) \triangleq \mathbb{P}\left[P_S + P_I' < T' \right] \tag{4.27}$$
$$= \frac{1}{2} - \frac{1}{\pi} \int_0^{\infty} \mathrm{Im} \left\{ \phi_{P_{S_{\eta=+1}}}(t | n_R, n_U) \phi_{P_{I_2}}(t) e^{-jtT'} \right\} t^{-1} dt \tag{4.28}$$

Proof. See Appendix L.

Remark 4.10. the coverage probability is trivially derived from (4.26) by interchanging $\tilde{T}$ and T.

On the basis of the above marginals, bounds on the joint rate-IPD distributions can now be established. As a reminder these distributions are given be:

$$\mathcal{J}_{\text{SWIPT}}(T,T') = \mathbb{P}\Big[\log_2\left(1+P_S/\left[P_I+P_N\right]\right) > T, P_S+P_I > T'\Big] \tag{4.29}$$

$$\mathcal{J}_{\text{lim}}(T,T') = \mathbb{P}\Big[\log_2\left(1+P_S/\left[P_I+P_N\right]\right) > T, P_S+P_I < T'\Big] \tag{4.30}$$

where (4.29) and (4.30) can respectively be employed scenarios of WPT and EMF monitoring for safety.

Proposition 4.11. *As mentioned in Remark 2.2, the joint rate-IPD distributions are bounded by the following expressions:*

$$\max\Big(0, \mathcal{P}_{cov}(T) - \mathcal{P}_{IPD}(T')\Big) \leq \mathcal{J}_{SWIPT}(T,T') \leq \min\Big(\mathcal{P}_{cov}(T), 1-\mathcal{P}_{IPD}(T')\Big) \tag{4.31}$$

$$\max\Big(0, \mathcal{P}_{cov}(T) + \mathcal{P}_{IPD}(T') - 1\Big) \leq \mathcal{J}_{lim}(T,T') \leq \min\Big(\mathcal{P}_{cov}(T), \mathcal{P}_{IPD}(T')\Big) \tag{4.32}$$

Remark 4.12. One will note that these bounds are defined with respect to the modified model of interference P'_I, employed to derive $\mathcal{P}_{\text{cov}}(T)$ and $\mathcal{P}_{\text{IPD}}(T')$. As a reminder, this modified model takes into account assumptions 4.1 to 4.5 compared to the original system model of Section 4.2.

4.4 Numerical Results

In this section, the following aspects are successively investigated: influence of the cluster overlaps, impact of the RRH density, rate-IPD tradeoffs, and optimal joint performance. For the sake of readability, the densities are here expressed in terms of average numbers of RRHs and UEs per cluster area (denoted by $n_{av,R}$ and $n_{av,U}$), instead of actual values λ_R and λ_U in m^{-2}. The relationships between these quantities are given by $n_{av,R} = \lambda_R \pi(r_1^2 - r_0^2)$ and $n_{av,U} = \lambda_U \pi r_1^2$.

4.4.1 Impact of the cluster overlaps

Figure 4.6 (page 84) illustrates the coverage obtained for the original system model of Section 4.2, along with three possible analytical adaptations:

- the full SG approach of this work detailed in Section 4.3;
- the model obtained if the intra-cluster interference (coming from RRHs serving the centric user) is not taken into account. This particular case is obtained from our results by setting η to 0 instead of $-\tilde{T}$ in (4.26), which enables to virtually set P_{I_1} to zero;
- a third case assuming that the intra-cluster interference is not neglected, but considered as a random variable independent of the useful power P_S. One possibility for this scenario can be obtained by modelling the intra-cluster interference in the same manner as the inter-cluster interference P_{I_2}. To this purpose, two modifications must be applied to the developments of section 4.3: P_{I_1} must be set to zero (as in the previous case) and the spatial zone associated to P_{I_2} must be extended to include the disk of radius r_1 around the centric user. This second modification is trivially obtained by replacing r_1 by r_0 in (4.17).

One will note the loss of accuracy obtained when the overlaps are not properly modelled. The curve derived when the intra-cluster interference is neglected naturally leads to higher coverage values compared to the other models. In addition, one can note that treating P_{I_1} independently of P_S produces a distribution centered around the same values as the original model, but with a different variance. Finally, one will note a slight gap remaining between the original system model of section II and the SG results of section III due to Assumptions 1 to 3.

4.4.2 Marginal distributions and RRH density

In Figure 4.7 (page 87), the cumulative distributions of the IPD and coverage are displayed for different RRH densities. Several elements can be observed from these graphs:

- The coverage and IPD tend to take higher values as the number of serving RRHs increases. These tendencies can be explained by the power allocation: as a reminder, each user is granted a constant power budget distributed among its serving RRHs. Among these RRHs, more power is allocated to those in good propagation conditions. Increasing the number of serving nodes results in obtaining candidates closer and closer to the user. These candidates are likely to benefit from better channel conditions (with a lower path loss), and are

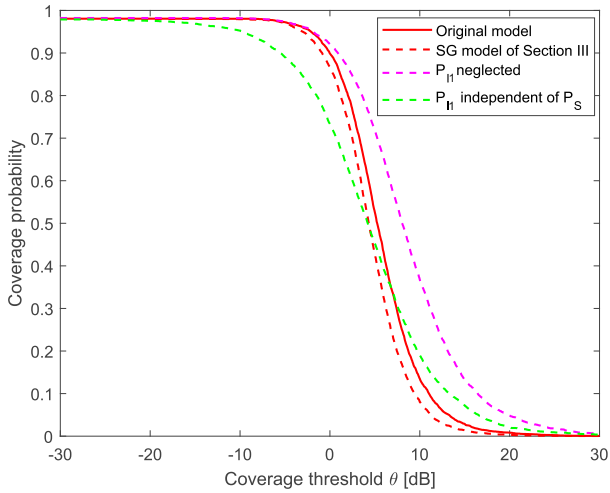

Fig. 4.6 Impact of the cluster overlaps. $P_t = 100\ mW$, $f = 3\ GHz$, $r_0 = 1\ m$, $r_1 = 100\ m$, $n_{av,R} = 4$, $n_{av,U} = 2.5$, $\alpha = 2.5$, $P_N = 0$ and $M = 4$.

therefore granted a larger share of the power budget. This increases the useful received power, and subsequently the SINR and exposure values.

- This increase tends to slow for higher RRH numbers (e.g. 18 and 28). In terms of interpretation, one can conclude that as the number of RRHs increases, a given improvement in SINR requires more and more additional nodes to obtain new candidates in better conditions.

4.4.3 Rate-IPD trade-offs

Figure 4.8a (page 88) shows isocurves observable when computing the joint metric $\mathcal{J}_{\text{lim}}(T, T')$. These curves illustrate the trade-offs limiting the coverage and IPD performance. The existence of such compromise is easily explained by considering the useful power P_S, which is likely to be high for users experiencing a good coverage. Since this useful power is generated by the RRHs which are the closest to the user, it is also dominant in the total exposure in a large number of cases. The probability of simultaneously experiencing a low exposure and a good coverage therefore decreases as

the requirements on (T, T') become more demanding. The same explanation also justifies the behaviour of $\mathcal{J}_{\text{lim}}(T, T')$ for fixed coverage thresholds (Figure 4.8b).

4.4.4 Existence of an optimal node density

Figures 4.9 (page 89) depicts $\mathcal{J}_{\text{lim}}(T, T')$ as function of both T and T', for increasing RRH densities. For a low density (Figure 4.9a), high probability values are located in the left zone of the graph, characterized by low coverage values. For increasing RRH densities (Figures 4.9b and 4.9c), this yellow zone of high probabilities evolves to eventually lie in an area characterized by a wider interval of coverage thresholds reachable, but with a narrower interval of exposure requirements satisfied. This tendency can be explained using the arguments mentioned in Subsection 4.4.3. In addition, this evolution suggests the existence of an optimal RRH density, different for every thresholds combination (T, T'). Figure 4.10 (page 90) confirms this hypothesis with two examples of threshold requirements.

Remark 4.13. As mentioned in Remark 4.12, the lower and upper bounds are computed from the SG model relying on Assumptions 4.1 to 4.5. Owing to these assumptions, the upper bound in Figure 4.10b goes slightly below the curve of the original model for low densities. Despite this observation, the two bounds enable to find optimal densities that are relatively accurate compared to the original model.

Remark 4.14. For the sake of space limitations, the analysis of this subsection has been focused on metric $\mathcal{J}_{\text{lim}}(T, T')$ for which an optimal RRH was highlighted. In a dual manner, this discussion could be transposed to the other metric $\mathcal{J}_{\text{SWIPT}}(T, T')$, in which case an optimal UE density can be studied. The existence of such optimum can be explained by considering the aggregate interference: bringing additional users in the network has the effect of increasing this interference, which simultaneously decreases the coverage, but increases the total IPD. From the perspective of a network operator, these optima can provide indications on how many RRHs to deploy (resp. users to schedule in a time slot) to maximize the number of UEs satisfying the threshold requirements related to $\mathcal{J}_{\text{lim}}(T, T')$ (resp. $\mathcal{J}_{\text{SWIPT}}(T, T')$).

4.5 Conclusions of the chapter

4.5.1 Summary

This study proposes a comprehensive framework to jointly analyze the rate and IPD in UCCFNs. The complete statistics of these quantities have been derived: moments, marginal, joint and conditional distributions. The provided expressions take into account the important features in the analysis of UCCFNs (cluster intercorrelation, beamforming strategy, etc), some of them being new in SG models.

4.5.2 Further research directions

Possible direct extensions for this work are listed below:

- The model proposed in this chapter considers independent HPPPs for both UEs and RRHs. In practical scenarios, these nodes are not always distributed in an independent and homogeneous manner. Including other point processes (e.g. PCPs) might therefore be relevant for future work.

- Regarding the beamforming, other precoding strategies could be studied and compared with this work.

- UCCFNs are assumed to be much denser than cellular networks. As a result, the distance between the centric UE and its serving RRHs is in average much shorter. As a result, the fading distribution on useful links might in practice be Ricean instead or Rayleigh. During the writing of this chapter, Ricean and Nakagami fading were incorporated in the SG framework: the resulting loss of accuracy in the final results was however much more significant than with Rayleigh fading. For this reason these two distributions were finally not included here. One could however consider an upper bound corresponding to the absence of fading on all communications on a distance lower than the cluster radius.

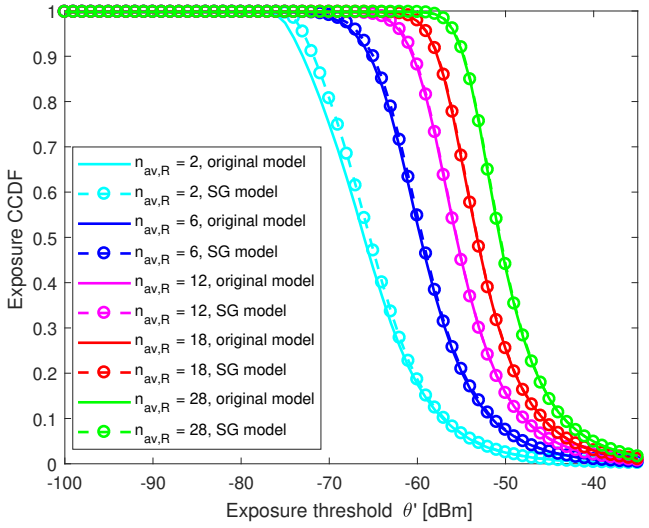

(a) Exposure distribution.

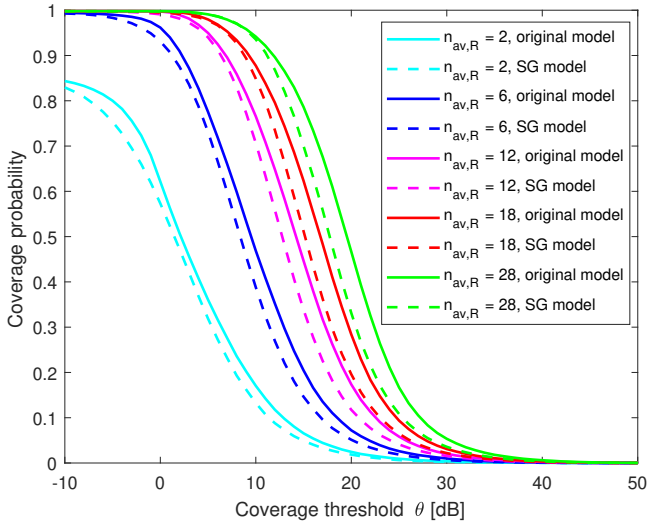

(b) Coverage probability.

Fig. 4.7 Coverage and exposure cumulative distributions for several RRH densities, and for $P_t = 100\ mW$, $f = 4\ GHz$, $r_0 = 1\ m$, $r_1 = 100\ m$, $n_{av,U} = 0.5$, $\alpha = 2.5$, $P_N = 0$ and $M = 1$.

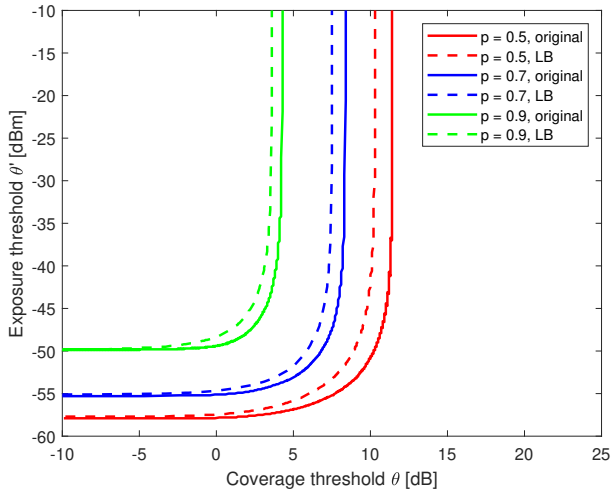

(a) Isocurves of the distribution $\mathcal{J}_{\text{lim}}(T, T')$ shown for different isovalues p. Both curves associated to the original system model and the lower bound are shown.

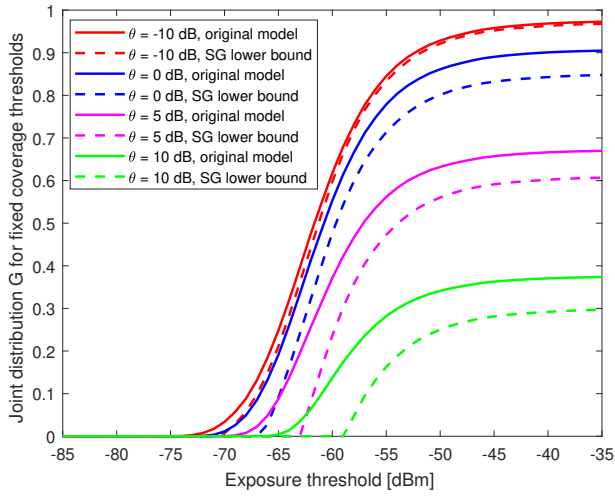

(b) Joint distribution $\mathcal{J}_{\text{lim}}(T, T')$ as function of the exposure threshold T', for fixed SIR thresholds ranging from -10 to 10 dB.

Fig. 4.8 Rate-IPD trade-offs. Parameters: $P_t = 100\ mW$, $f = 4\ GHz$, $r_0 = 1\ m$, $r_1 = 100\ m$, $n_{av,U} = 0.5$, $\alpha = 2.5$, $P_N = 0$ and $M = 1$ $n_{av,R} = 8$ for (a) and $n_{av,R} = 4$ for (b).

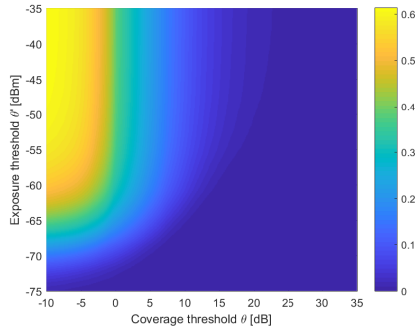

(a) $n_{av,R} = 1$

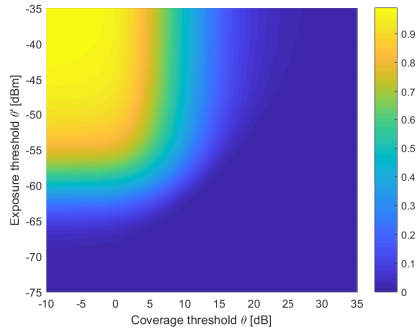

(b) $n_{av,R} = 6$

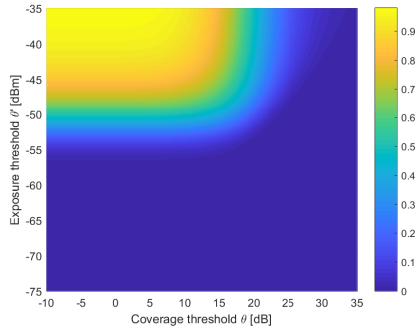

(c) $n_{av,R} = 30$

Fig. 4.9 Evolution of the metric $\mathcal{J}_{\lim}(T, T')$ as function of the average number of RRHs per cluster. The system parameters are here given by $P_t = 100\ mW$, $f = 4\ GHz$, $r_0 = 1\ m$, $r_1 = 100\ m$, $n_{av,U} = 0.5$, $\alpha = 2.5$, $P_N = 0$ and $M = 1$.

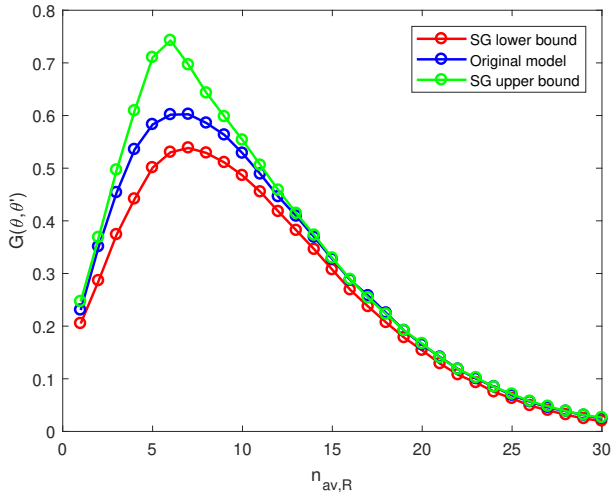

(a) $(T, T') = (5\ dB, -55\ dBm)$

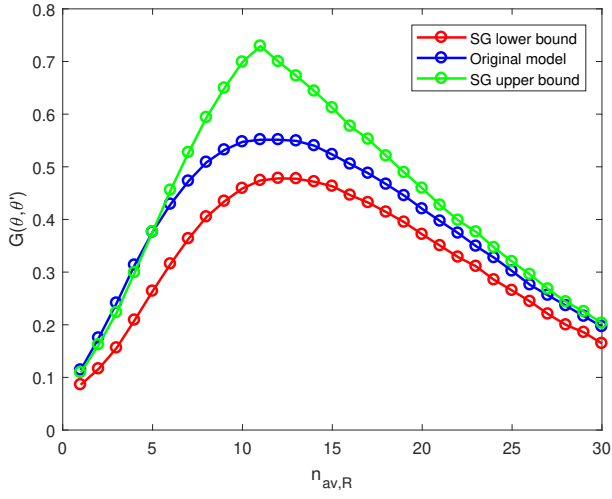

(b) $(T, T') = (10\ dB, -52\ dBm)$

Fig. 4.10 Illustration of the optimal RRH densities maximizing $\mathcal{J}_{\text{lim}}(T, T')$. The system parameters are here given by $P_t = 100\ mW$, $f = 4\ GHz$, $r_0 = 1\ m$, $r_1 = 100\ m$, $n_{av,U} = 0.5$, $\alpha = 2.5$, $P_N = 0$ and $M = 1$.

5

Constrained minimization of the EMF exposure

5.1 Introduction

The objective of this chapter is to propose an optimization problem including both the notions of coverage and EMF exposure. The analysis is here restricted to cellular networks only. In order to study this architecture, multiple models are possible in the literature (other than the scenario presented in Chapter 3). The framework developed in [52] has the advantage of providing linear expressions and is employed here for this reason. As detailed later in this chapter, these linear expressions enable to obtain closed-form solutions for the proposed optimization problem. The associated system model and analytical results are presented in sections 5.2 and 5.3. The considered problem as well as its solutions are then detailed in sections 5.4 and 5.5.

Three possible categories of optimization problems can be distinguished when jointly considering the coverage and EMF exposure:

1. *Maximizing the joint probability* of these two quantities (eq. (2.22)). An attempt to solve such problems is proposed in [41].
2. *Maximizing the coverage probability with a constraint on the EMF expo-*

sure. This case can be trivially deduced from the work of [78]. In that reference, optimization problem P0 proposes the maximization of the coverage based in the same system model as [52]. One of the constraints of the problem consists in imposing a useful received power high enough for detection. This constraint is mathematically expressed as

$$\mathbb{P}\left[S_0 < \delta\right] < \epsilon \tag{5.1}$$

where S_0 is the received useful power. This condition guarantees that S_0 remains below a fixed threshold δ with a probability lower than ϵ. In the context of that problem:

- the threshold δ can be fixed according to the noise level;
- ϵ is supposed to be a low value since the event $S_0 < \delta$ should happen with a low probability.

This constraint can be adapted in our case by considering instead

$$\mathbb{P}\left[S_0 > \delta'\right] < \epsilon' \tag{5.2}$$

$$\Leftrightarrow\ 1 - \mathbb{P}\left[S_0 < \delta'\right] < \epsilon' \tag{5.3}$$

$$\Leftrightarrow\ \mathbb{P}\left[S_0 < \delta'\right] > \underbrace{1 - \epsilon'}_{\epsilon''} \tag{5.4}$$

where the threshold δ' is fixed by the exposure regulations of the operator. The incorporation of (5.4) in the problem P0 of [78] is relatively straightforward and will not be covered here for this reason.

3. *Minimizing the EMF exposure with a constraint of the coverage*. This third option is explored in this chapter.

To the best author's knowledge, no publication including an exposure-aware optimization has been produced based on SG. A few studies optimizing the exposure via other frameworks are available: [79] proposes an exposure minimization in indoor environments based on ray-tracing and genetics algorithms. [80, 81] also consider indoor scenarios and respectively introduce heuristic and multi-objective algorithms. The studies detailed in [82–84] propose resource allocation algorithm to minimize the exposure in multi-carrier systems. Finally, the authors of [85, 86] present methods to reduce minimize the uplink EMF exposure via convex optimization and unsupervised learning in non-orthogonal multiple access networks.

5.2 System model

We consider a K-tier network deployed in $\mathbb{R}^2$. Each tier i is generated by means of an independent HPPP Ψ_i. The triplet (λ_i, T_i, P_i) is employed to denote the density, the targeted[1] SINR, as well as the BS transmit power associated to each tier. Regarding the propagation model:

- Rayleigh fading is assumed on all links;
- The path loss model is given by $l(r) = r^{-\alpha}$ where r and $\alpha > 2$ denote the BS-receiver distance as well as the path loss exponent.

A closed access scenario is here considered: a subset $\mathcal{B} \in \{1, \ldots, K\}$ of the tiers is available to the centric user. The other tiers are assumed to belong to other operators and act as interferers. Regarding the association policy, the centric user connects to its strongest instantaneous BS, i.e. the BS offering the highest receive SIR. This user is therefore in coverage if the following condition is satisfied:

$$\max_{x \in \Psi_i} \text{SIR}(x) > T_i \tag{5.5}$$

for at least one $i \in \mathcal{B}$. Assuming that BS x_j belonging to tier $j \in \mathcal{B}$ is serving the user, this SIR can be expressed as

$$\text{SIR}(x) = \frac{P_j |h_{x_j}|^2 |x_j|^{-\alpha}}{\sum_{k=1}^{K} \sum_{y \in \Psi_k \setminus x_j} P_k |h_y|^2 |y|^{-\alpha}} \tag{5.6}$$

where $|h_y|^2$ are the fading coefficients. In order to obtain simple analytical results, two additional assumptions are made:

- The network is assumed to be interference-limited: the background noise is hence ignored.
- The analysis is restricted to networks operating at thresholds $T_i > 1$ (0 dB).

[1] One will note that in Chapter 3, the same SINR threshold T is required for each tier to operate. In order to be consistent with [52], we introduce multiple thresholds T_i as an additional degree of freedom. This generalization can be justified by the fact that each tier may belong to different operators, and therefore operate in different conditions (with different desired data rates, coding or antenna gains, etc). The impact of this degree of freedom on our optimization problems will be discussed in section 5.4. One will also note that the case of a universal target SINR can also be recovered from our model by setting $T_i = T \; \forall i$.

5.3 Analytical framework

The results presented in this section have been derived in [52] and [78] and are reused later in this chapter within the optimization problem.

Lemma 5.1. *Given the association policy of section 5.2, at most one base station among the set* $\cup_{i=1}^{K} \Psi_i$ *is able to satisfy the coverage requirement of equation (5.5) for* $T_i > 1$, $i \in \mathcal{B}$.

Proof. see Appendix A of [52].

Proposition 5.2. *The coverage probability can be expressed as*

$$\mathcal{P}_{cov}\left[\{T_i\}_{i\in\mathcal{B}}\right] = \mathbb{P}\left[\bigcup_{i\in\mathbb{B}} \max_{x\in\Psi_i} SIR(x) > T_i\right] \tag{5.7}$$

$$= \gamma(\alpha)\frac{\sum_{i\in\mathcal{B}} \lambda_i P_i^{2/\alpha} T_i^{-2/\alpha}}{\sum_{i=1}^{K} \lambda_i P_i^{2/\alpha}}, \quad T_i > 1 \tag{5.8}$$

where $\gamma(\alpha) = \alpha \sin(2\pi/\alpha)/(2\pi)$.

Proof. see Appendix B of [52].

Proposition 5.3. *The cumulative CDF of the useful received power is given by*

$$\mathcal{P}_{P_S}(T') = \mathbb{P}\left[P_S < T'\right] = \exp\left[-\frac{2\pi}{\alpha}\Gamma\left(\frac{2}{\alpha}\right) T'^{-2/\alpha} \sum_{k\in\mathcal{B}} \lambda_k P_k^{2/\alpha}\right] \tag{5.9}$$

Proof. see Appendix A of [78].

Proposition 5.4. *The fraction load*[2] *of tier* $i \in \mathcal{B}$ *is given by*

$$\eta_i = \frac{P_i^{2/\alpha} T_i^{-2/\alpha} \lambda_i}{\sum_{k\in\mathcal{B}} P_k^{2/\alpha} T_k^{-2/\alpha} \lambda_k} \tag{5.10}$$

Proof. see Appendix C of [52].

[2] fraction of the time during which the typical user connects to the tier.

5.4 Formulation of the optimization problem

This proposed optimization problem considers a scenario of *tier addition*: a mobile operator wishes to deploy two tiers of BS in an environment where a number N_c of other tiers are already deployed by other companies. The considered problem is characterized by the following specifications:

- The centric user is allowed to connect to one of the two tiers of the new operator. The N_c other tiers act as interferers.
- The probability for the useful power[3] received by the user to be below a given threshold T' should be maximized.
- *Constraint c*1: despite this minimization, the coverage probability should remain above a specified value p.
- *Constraints c*2*a and c*2*b*: the fraction loads of the two new tiers should remain above two given values θ_1 and θ_2
- *Constraint c*3*a and c*3*b*: the densities should be non-negative.

The parameters associated to the two new tiers are denoted by (λ_1, T_1, P_1) and (λ_2, T_2, P_2). By contrast, variables $(\tilde{\lambda}_i, \tilde{P}_i)$, $i = 1 \ldots, N_c$ are used to represent quantities associated to the interfering tiers.

On the basis of the framework of sections 5.2 and 5.3, the optimization problem describing the above requirements can be formulated as

$$\begin{array}{lll} \max\limits_{(\lambda_1,\lambda_2)} & \mathcal{P}_{P_S}(\lambda_1,\lambda_2) & \\ \text{s.t.} & \mathcal{P}_{\text{cov}} > p & (c1) \\ & \eta_i \geq \theta_i \;\; i = 1,2 & (c2a, c2b) \\ & \lambda_i \geq 0 \;\; i = 1,2 & (c3a, c3b) \end{array} \tag{5.11}$$

where $\mathcal{P}_{P_S}(\lambda_1, \lambda_2)$ represents the CDF of the useful received power.

[3] which dominant in the total IPD at high SNR

5.5 Solutions of the optimization problem

By inspection of (5.9) and by developing the constraints, problem (5.11) can be reformulated as

$$\begin{aligned} \min_{(\lambda_1,\lambda_2)} \quad & P_1^{2/\alpha}\lambda_1 + P_2^{2/\alpha}\lambda_2 & \\ \text{s.t.} \quad & a\lambda_1 + b\lambda_2 \geq c & (c1) \\ & \lambda_2 \leq d\lambda_1 & (c2a) \\ & \lambda_2 \geq e\lambda_1 & (c2b) \\ & \lambda_i \geq 0 \;\; i = 1,2 & (c3a, c3b) \end{aligned} \tag{5.12}$$

where

$$a = P_1^{2/\alpha}\left[T_1^{-2/\alpha} - \frac{p}{\gamma(\alpha)}\right] \tag{5.13}$$

$$b = P_2^{2/\alpha}\left[T_2^{-2/\alpha} - \frac{p}{\gamma(\alpha)}\right] \tag{5.14}$$

$$c = \frac{p}{\gamma(\alpha)}\sum_{i=1}^{N_c}\tilde{\lambda}_i\tilde{P}_i^{2/\alpha} \tag{5.15}$$

$$d = \left[\frac{\theta_1}{(1-\theta_1)}\left(\frac{P_2T_1}{P_1T_2}\right)^{2/\alpha}\right]^{-1} \tag{5.16}$$

$$e = \frac{\theta_2}{(1-\theta_2)}\left(\frac{P_1T_2}{P_2T_1}\right)^{2/\alpha} \tag{5.17}$$

This new problem can be solved via graphical method by following the same line-of-thought as in [78]. The probability $\mathcal{P}_{P_S}(\lambda_1, \lambda_2)$ is illustrated in Figure 5.1 next page. One will note that the isocurves of this graph evolve according to the gradient of objective function (5.12), given by $[P_1^{2/\alpha}\ P_2^{2/\alpha}]^T$. This objective function shown in the first quadrant of $\mathbb{R}^2$ but its domain is more restricted due to the constraints. Capitalizing on optimization theory [87], it is well established that the solutions of this linear problem will be located at the boundaries of this domain. The objective of the next pages is therefore to identify the possible shapes taken by the domain of (5.12) in $\mathbb{R}^2$. For each of the cases detailed here below, the identification of the

optimal solution is trivially deduced (given the behaviour of the gradient) once the domain is delimited.

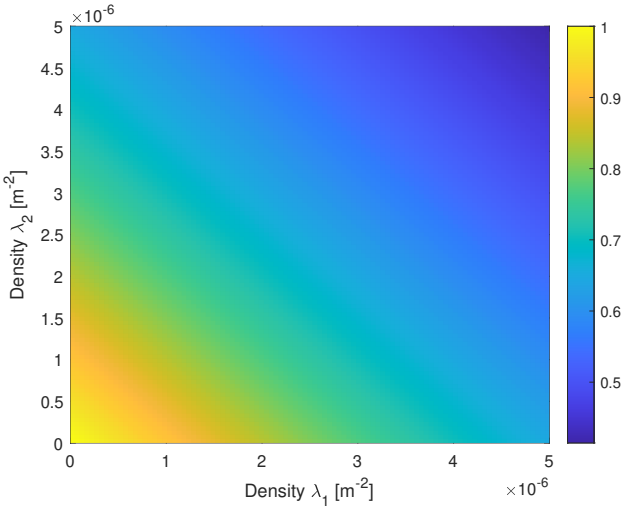

Fig. 5.1 Illustration of useful received power CDF $\mathcal{P}_{P_S}(\lambda_1, \lambda_2)$ as function of λ_1 and λ_2. The following parameters were selected: $N_c = 1$, $P_1 = P_2 = \tilde{P}_1 = 0.1W$, $\tilde{\lambda_1} = 10^{-6}m^{-2}$, $\alpha = 4$, $T' = -70dBm$.

Inequalities $(c2a)$ and $(c2b)$ are depicted in Figure 5.2 below.

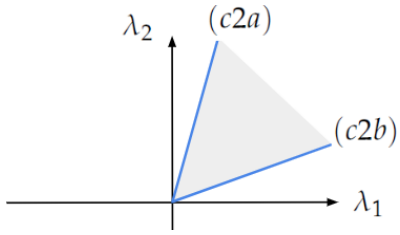

Fig. 5.2 Representation of the constraints $c2a$ and $c2b$.

For the area defined by these inequalities to be non-empty, one must have $\theta_1 + \theta_2 \leq 1$. A first trivial case can be defined in this manner:

- *Case 0 - $\theta_1 + \theta_2 > 1$*

  The domain is empty: the problem admits no solution.

The actual domain of (5.12) can take different shapes depending on the signs of a and b in $(c1)$. One will first note that

$$\begin{aligned} a > 0 \quad &\Rightarrow \quad p < \gamma(\alpha) T_1^{-2/\alpha}, \\ b > 0 \quad &\Rightarrow \quad p < \gamma(\alpha) T_2^{-2/\alpha}. \end{aligned}$$

Four general cases can be distinguished based on the four combinations of the signs of these two coefficients.

- *Case I* - $\theta_1 + \theta_2 \leq 1$, $p < \gamma(\alpha) T_1^{-2/\alpha}$, $p < \gamma(\alpha) T_2^{-2/\alpha}$
  This scenario is depicted in Figure 5.3a (page 105). Three different subcases can be discussed:
  - *Case Ia* - $T_1 = T_2$
    The isocurves of the objective function are parallel to constraint $(c1)$. The problem admits an interval of solutions, delimited by the intersections of $(c1)$ with $(c2a)$ and $(c2b)$. This interval is represented by the purple line in 5.3a.
  - *Case Ib* - $T_1 > T_2$
    The isocurves of the objective function are no longer parallel to $(c1)$. The unique solution is in that case given by the intersection of $(c1)$ with $(c2a)$ (blue dot in Figure 5.3a).
  - *Case Ic* - $T_1 < T_2$
    The isocurves of the objective function are no longer parallel to $(c1)$. The unique solution is in that case given by the intersection of $(c1)$ with $(c2b)$ (green dot in Figure 5.3a).
- *Case II* - $\theta_1 + \theta_2 \leq 1$, $p > \gamma(\alpha) T_1^{-2/\alpha}$, $p > \gamma(\alpha) T_2^{-2/\alpha}$
  This scenario is illustrated in Figure 5.3b. Two subcases can be mentioned:
  - *Case IIa* - $\sum_{i=1}^{N_c} \tilde{\lambda}_i \tilde{P}_i^{2/\alpha} = 0$
    The problem admits the unique trivial solution $(\lambda_1, \lambda_2) = (0, 0)$.
  - *Case IIb* - $\sum_{i=1}^{N_c} \tilde{\lambda}_i \tilde{P}_i^{2/\alpha} > 0$
    The problem admits no solution since its domain is empty.
- *Case III* - $\theta_1 + \theta_2 \leq 1$, $p > \gamma(\alpha) T_1^{-2/\alpha}$, $p < \gamma(\alpha) T_2^{-2/\alpha}$

  - *Case IIIa* - $(-a/b) < d$
    The problem admits one unique solution given by the intersection of constraints $(c1)$ and $(c2a)$ (see Figure 5.3c).
  - *Case IIIb* - $(-a/b) > d$
    The problem admits no solution since its domain is empty (see Figure 5.3d).

- *Case IV* - $\theta_1 + \theta_2 \leq 1$, $p < \gamma(\alpha) T_1^{-2/\alpha}$, $p > \gamma(\alpha) T_2^{-2/\alpha}$

  - *Case IVa* - $(-a/b) > e$
    The problem admits one unique solution given by the intersection of constraints $(c1)$ and $(c2b)$ (see Figure 5.3e).
  - *Case IVb* - $(-a/b) < e$
    The problem admits no solution since its domain is empty (see Figure 5.3f).

Five particular cases must then be mentioned to include scenarios where a and/or b might be equal to zero.

- *Case V* - $\theta_1 + \theta_2 \leq 1$, $p = \gamma(\alpha) T_1^{-2/\alpha}$, $p = \gamma(\alpha) T_2^{-2/\alpha}$

  - *Case Va* - $\sum_{i=1}^{N_c} \tilde{\lambda}_i \tilde{P}_i^{2/\alpha} = 0$
    Constraint $(c1)$ reduces to the trivial equality $0 = 0$ and therefore disappears from the optimization problem. The domain is then only delimited by $(c2a)$ and $(c2b)$ (Figure 5.2). As a result, the optimal solution trivially given by $(\lambda_1, \lambda_2) = (0, 0)$.
  - *Case Vb* - $\sum_{i=1}^{N_c} \tilde{\lambda}_i \tilde{P}_i^{2/\alpha} > 0$
    Constraint $c1$ is in that case never satisfied. The domain is therefore empty and the problem admits no solution.

- *Case VI* - $\theta_1 + \theta_2 \leq 1$, $p = \gamma(\alpha) T_1^{-2/\alpha}$, $p < \gamma(\alpha) T_2^{-2/\alpha}$
  This scenario is illustrated in Figure 5.4a. The solution is unique and given by the orange intersection of constraints (c1) and (c2a).

- *Case VII* - $\theta_1 + \theta_2 \leq 1$, $p = \gamma(\alpha) T_1^{-2/\alpha}$, $p > \gamma(\alpha) T_2^{-2/\alpha}$
  In this case, one will note that constraints (c1) is never fulfilled given the sign of the coefficients. The problem admits no solution.

- *Case VIII - $\theta_1 + \theta_2 \leq 1$, $p < \gamma(\alpha) T_1^{-2/\alpha}$, $p = \gamma(\alpha) T_2^{-2/\alpha}$*

  This scenario is illustrated in Figure 5.4a. The solution is unique and given by the cyan intersection of constraints (c1) and (c2b).

- *Case IX - $\theta_1 + \theta_2 \leq 1$, $p > \gamma(\alpha) T_1^{-2/\alpha}$, $p = \gamma(\alpha) T_2^{-2/\alpha}$*

  In this case, one will note that constraints (c1) is never fulfilled given the sign of the coefficients. The problem admits no solution.

All these cases are summarized in Table 5.1 next page. In this table, the following notations are employed:

- $\left(\lambda_1^{(c1,c2a)}, \lambda_2^{(c1,c2a)}\right)$ denote the intersection of (c1) and (c2a), with

$$\lambda_1^{(c1,c2a)} = \frac{\frac{p}{\gamma(\alpha)} \sum_{i=1}^{N_c} \tilde{\lambda}_i \tilde{P}_i^{2/\alpha}}{P_2^{2/\alpha} \left[T_2^{-2/\alpha} - \frac{p}{\gamma(\alpha)}\right] \left[\frac{\theta_1}{(1-\theta_1)} \left(\frac{P_2 T_1}{P_1 T_2}\right)^{2/\alpha}\right]^{-1} + P_1^{2/\alpha} \left[T_1^{-2/\alpha} - \frac{p}{\gamma(\alpha)}\right]}$$

$$\lambda_2^{(c1,c2a)} = \frac{\left[\frac{\theta_1}{(1-\theta_1)} \left(\frac{P_2 T_1}{P_1 T_2}\right)^{2/\alpha}\right]^{-1} \frac{p}{\gamma(\alpha)} \sum_{i=1}^{N_c} \tilde{\lambda}_i \tilde{P}_i^{2/\alpha}}{P_2^{2/\alpha} \left[T_2^{-2/\alpha} - \frac{p}{\gamma(\alpha)}\right] \left[\frac{\theta_1}{(1-\theta_1)} \left(\frac{P_2 T_1}{P_1 T_2}\right)^{2/\alpha}\right]^{-1} + P_1^{2/\alpha} \left[T_1^{-2/\alpha} - \frac{p}{\gamma(\alpha)}\right]}$$

- $\left(\lambda_1^{(c1,c2b)}, \lambda_2^{(c1,c2b)}\right)$ denote the intersection of (c1) and (c2b), with

$$\lambda_1^{(c1,c2b)} = \frac{\frac{p}{\gamma(\alpha)} \sum_{i=1}^{N_c} \tilde{\lambda}_i \tilde{P}_i^{2/\alpha}}{P_2^{2/\alpha} \left[T_2^{-2/\alpha} - \frac{p}{\gamma(\alpha)}\right] \frac{\theta_2}{(1-\theta_2)} \left(\frac{P_1 T_2}{P_2 T_1}\right)^{2/\alpha} + P_1^{2/\alpha} \left[T_1^{-2/\alpha} - \frac{p}{\gamma(\alpha)}\right]}$$

$$\lambda_2^{(c1,c2b)} = \frac{\frac{\theta_2}{(1-\theta_2)} \left(\frac{P_1 T_2}{P_2 T_1}\right)^{2/\alpha} \frac{p}{\gamma(\alpha)} \sum_{i=1}^{N_c} \tilde{\lambda}_i \tilde{P}_i^{2/\alpha}}{P_2^{2/\alpha} \left[T_2^{-2/\alpha} - \frac{p}{\gamma(\alpha)}\right] \frac{\theta_2}{(1-\theta_2)} \left(\frac{P_1 T_2}{P_2 T_1}\right)^{2/\alpha} + P_1^{2/\alpha} \left[T_1^{-2/\alpha} - \frac{p}{\gamma(\alpha)}\right]}$$

- $\mathcal{I}$ denotes the closed segment between points $\left(\lambda_1^{(c1,c2a)}, \lambda_2^{(c1,c2a)}\right)$ and $\left(\lambda_1^{(c1,c2b)}, \lambda_2^{(c1,c2b)}\right)$ (if this segment exists).

$\theta_1+\theta_2>1$			$\mathcal{S}=\varnothing$	Case 0
$\theta_1+\theta_2\leq 1$	$p<\gamma(\alpha)T_1^{-2/\alpha}, p<\gamma(\alpha)T_2^{-2/\alpha}$	$T_1=T_2$	$\mathcal{S}=\{(\lambda_1,\lambda_2)\|(\lambda_1,\lambda_2)\in\mathcal{I}\}$	Case Ia
		$T_1>T_2$	$\mathcal{S}=\left(\lambda_1^{(c1,c2a)},\lambda_2^{(c1,c2a)}\right)$	Case Ib
		$T_1<T_2$	$\mathcal{S}=\left(\lambda_1^{(c1,c2b)},\lambda_2^{(c1,c2b)}\right)$	Case Ic
	$p>\gamma(\alpha)T_1^{-2/\alpha}, p>\gamma(\alpha)T_2^{-2/\alpha}$	$\sum_{i=1}^{N_c}\tilde{\lambda}_i\tilde{P}_i^{2/\alpha}=0$	$\mathcal{S}=(0,0)$	Case IIa
		$\sum_{i=1}^{N_c}\tilde{\lambda}_i\tilde{P}_i^{2/\alpha}>0$	$\mathcal{S}=\varnothing$	Case IIb
	$p>\gamma(\alpha)T_1^{-2/\alpha}, p<\gamma(\alpha)T_2^{-2/\alpha}$	$(-a/b)<d$	$\mathcal{S}=\left(\lambda_1^{(c1,c2a)},\lambda_2^{(c1,c2a)}\right)$	Case IIIa
		$(-a/b)>d$	$\mathcal{S}=\varnothing$	Case IIIb
	$p<\gamma(\alpha)T_1^{-2/\alpha}, p>\gamma(\alpha)T_2^{-2/\alpha}$	$(-a/b)>e$	$\mathcal{S}=\left(\lambda_1^{(c1,c2b)},\lambda_2^{(c1,c2b)}\right)$	Case IVa
		$(-a/b)<e$	$\mathcal{S}=\varnothing$	Case IVb
	$p=\gamma(\alpha)T_1^{-2/\alpha}, p=\gamma(\alpha)T_2^{-2/\alpha}$	$\sum_{i=1}^{N_c}\tilde{\lambda}_i\tilde{P}_i^{2/\alpha}=0$	$\mathcal{S}=(0,0)$	Case Va
		$\sum_{i=1}^{N_c}\tilde{\lambda}_i\tilde{P}_i^{2/\alpha}>0$	$\mathcal{S}=\varnothing$	Case Vb
	$p=\gamma(\alpha)T_1^{-2/\alpha}, p<\gamma(\alpha)T_2^{-2/\alpha}$		$\mathcal{S}=\left(\lambda_1^{(c1,c2a)},\lambda_2^{(c1,c2a)}\right)$	Case VI
	$p=\gamma(\alpha)T_1^{-2/\alpha}, p>\gamma(\alpha)T_2^{-2/\alpha}$		$\mathcal{S}=\varnothing$	Case VII
	$p<\gamma(\alpha)T_1^{-2/\alpha}, p=\gamma(\alpha)T_2^{-2/\alpha}$		$\mathcal{S}=\left(\lambda_1^{(c1,c2b)},\lambda_2^{(c1,c2b)}\right)$	Case VIII
	$p>\gamma(\alpha)T_1^{-2/\alpha}, p=\gamma(\alpha)T_2^{-2/\alpha}$		$\mathcal{S}=\varnothing$	Case IX

Table 5.1 Summary of the solutions of (5.11)

5.6 Numerical results

The analysis of this section focuses on case Ia above. As a reminder, this case corresponds to the standard scenario for which all operators target the same coverage threshold T, and for which solutions to problem (5.11) exist. Before proceeding to the performance analysis, it is also worth reminding that problem (5.11) aims at maximizing $\mathcal{P}_{P_S}(T')$, the probability for the received signal strength P_S to be below a specified threshold T'. The inspection of $\mathcal{P}_{P_S}(T')$ in equation (5.9) shows that the solution of (5.12) is actually optimal for any threshold T'. In other words, the optimal solution $(\lambda_1^*, \lambda_2^*)$ optimizes the whole distribution.

Figure 5.5 (page 106) depicts the optimal CDF $\mathcal{P}^*_{P_S}(T')$ obtained for given coverage constraints $\mathcal{P}_{\text{cov}}(T) > p$. This figure confirms that more demanding[4] coverage constraints lead to higher values of the useful received power.

Figures 5.6 to 5.8 (pages 107-108) propose another way to illustrate the exposure and coverage trade-offs. In these three figures, the optimal achievable CDF $\mathcal{P}^*_{P_S}(T')$ (with fixed T') is shown for each pair (p, T) constituting the coverage requirement. The blank zones of the figures correspond to coverage requirements which are not achievable. The boundary delimiting this zone is given by the relationship $p = \gamma(\alpha)T^{-2/\alpha}$. In the area where a solution exists, each point provides the information *"if a user must achieve a SIR above T with probability p, this user can at best experience a received signal strength below T' with probability $\mathcal{P}^*_{P_S}(T')$"*. By comparing the three figures, it is also possible to note the global increase in the values of $\mathcal{P}^*_{P_S}(T')$ when increasing the exposure threshold: the requirement associated to the received signal strength becomes less and less demanding, and can be achieved with a higher probability.

Figures 5.9 and 5.10 (pages 108-109) illustrate the influence of the propagation model on the performance via the path loss exponent. Figure 5.9 (for which $\alpha = 4.5$) must be compared with Figure 5.7 (generated with the same parameters, except $\alpha = 3.75$). The graphs show an increase in per-

[4] One can note that the values of p and T in Figure 5.5 are relatively low compared to the specifications of current mobile networks. These values can be explained by the low coverage performance achievable for HPPP and heterogeneous networks (see [51] and [52]). Including an antenna gain in the useful received power can be a possible manner to improve this coverage performance.

formance for environments featuring more attenuation (i.e. with higher α). This behaviour is naturally explained by the relative distances of the BSs providing the useful signal and the interference. In the case of higher path loss exponents, the interference is proportionally more strongly attenuated. As a consequence, one can afford a lower useful signal strength to achieve the same SIR values as α increases.

As a final remark, it is possible to observe that for the considered case Ia, the objective function and constraint $c1$ can be rewritten as

$$\begin{aligned} \min_{(x_1,x_2)} \quad & x_1 + x_2 \\ \text{s.t.} \quad & (x_1 + x_2) \geq c' \end{aligned} \tag{5.18}$$

where $x_1 = \lambda_1 P_1^{2/\alpha}$, $x_2 = \lambda_2 P_2^{2/\alpha}$ and $c' = c[T^{-2/\alpha} - p/\gamma(\alpha)]^{-1}$. The inspection of the above equations shows that the transmit powers and densities of each tier can be grouped into global variables x_1 and x_2. From the expressions of these two variables, it is possible to conclude that a pair of solutions (x_1^*, x_2^*), corresponds to continuous set of values (P_1, λ_1) and (P_2, λ_2) equally minimizing P_S. By rewriting $\lambda_1^* = x_1^*/P_1^{*2/\alpha}$ and $\lambda_2^* = x_2^*/P_2^{*2/\alpha}$, one can note that the optimal density of each tier must be inversely proportional to the associated transmit power. As a consequence, both macrocells and microcells are possible options to minimize the signal strength while meeting the coverage constraint.

5.7 Conclusions of the chapter

5.7.1 Summary

This chapter capitalizes on the works of [78] and [52] to develop an exposure minimization problem. This problem is established for a scenario of tier addition in the presence of a coverage constraint. After deriving tractable solutions, a number of analyses are proposed as function of the parameters of the model. These analyses highlight the inherent trade-offs between the coverage and exposure performance as well as the influence of the propagation environment.

5.7.2 Further research directions

The particular framework of [52] (on which this chapter is based) has the remarkable advantage of providing linear expressions. These expressions enabled to propose a problem admitting closed form solutions. Such an outcome is not possible in all generality: optimization problems leading to analytical solutions are often difficult to develop when using SG models. In the case of this dissertation, most of the results derived in other chapters involve non-linear expressions with multiple integrals. Taking this observation into consideration, one would recommend using advanced optimization methods to solve the non-linear problems potentially associated to these results. The objective of such an approach would be to solve the problems numerically rather than analytically.

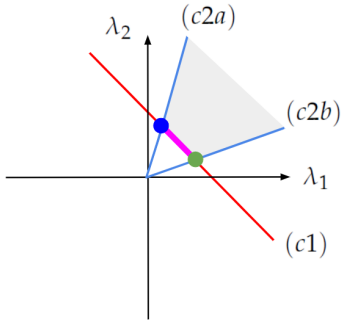

(a) Case I

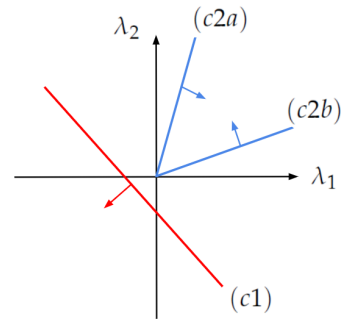

(b) Case II

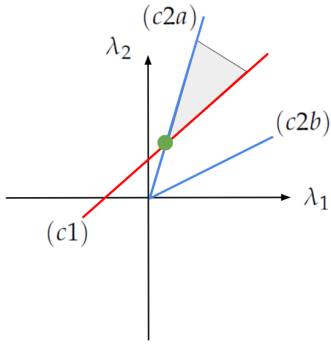

(c) Case IIIa

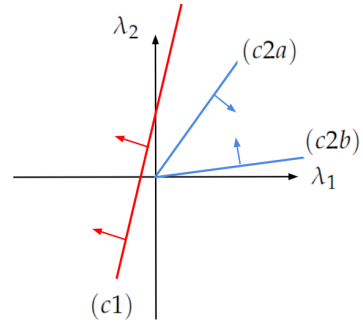

(d) Case IIIb

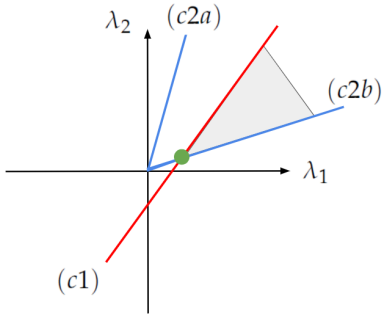

(e) Case IVa

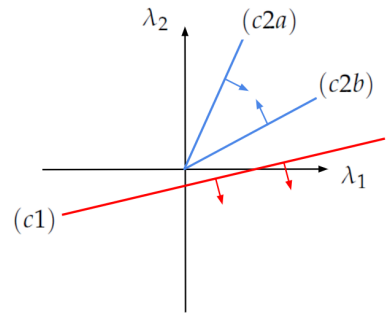

(f) Case IVb

Fig. 5.3 Representation of domains associated to cases I to IV.

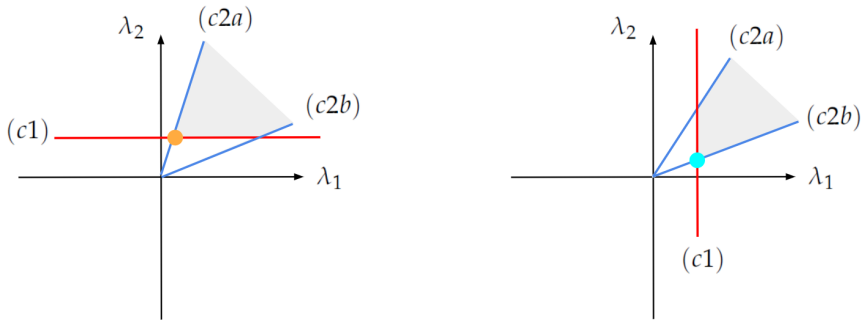

(a) Case VI **(b)** Case VIII

Fig. 5.4 Representation of domains associated to cases VI and VIII

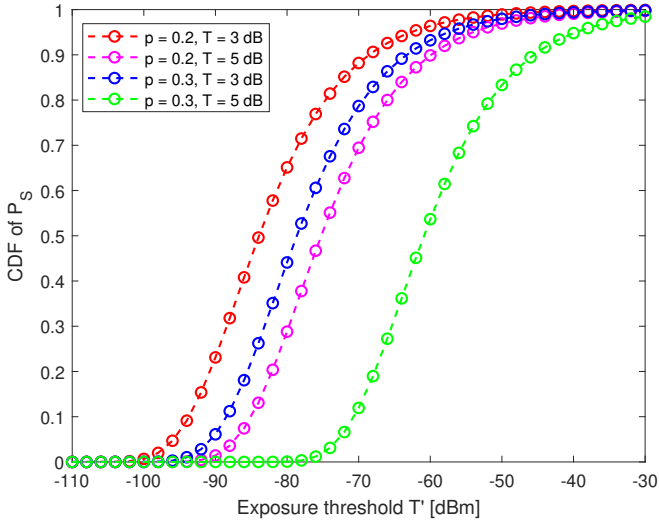

Fig. 5.5 Optimal CDF $\mathcal{P}^*_{P_S}(T')$ of the useful received power illustrated for several coverage constraints. The following parameters have been selected: $N_c = 1$, $P_1 = P_2 = \tilde{P}_1 = 0.1W$, $\tilde{\lambda_1} = 10^{-6}m^{-2}$, $\alpha = 3.75$.

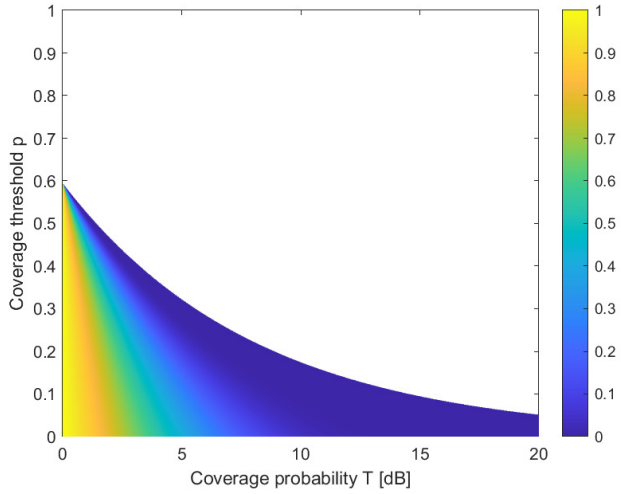

Fig. 5.6 Optimal CDF of the useful received power $\mathcal{P}^*_{P_S}(T' = -85dBm)$ as function of the coverage constraint (p, T). The following parameters have been selected: $N_c = 1$, $P_1 = P_2 = \tilde{P}_1 = 0.1W$, $\tilde{\lambda_1} = 10^{-6}m^{-2}$, $\alpha = 3.75$

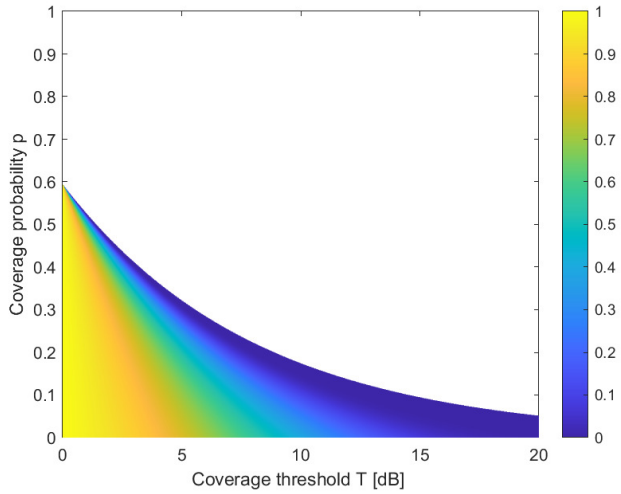

Fig. 5.7 Optimal CDF of the useful received power $\mathcal{P}^*_{P_S}(T' = -75dBm)$ as function of the coverage constraint (p, T). The following parameters have been selected: $N_c = 1$, $P_1 = P_2 = \tilde{P}_1 = 0.1W$, $\tilde{\lambda_1} = 10^{-6}m^{-2}$, $\alpha = 3.75$.

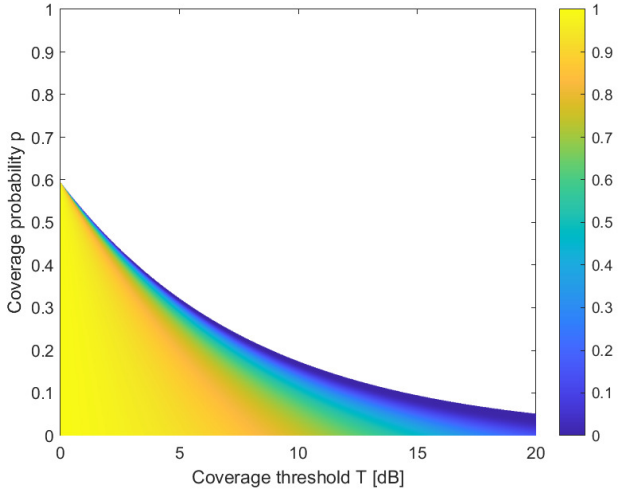

Fig. 5.8 Optimal CDF of the useful received power $\mathcal{P}^*_{P_S}(T' = -65dBm)$ as function of the coverage constraint (p, T). The following parameters have been selected: $N_c = 1$, $P_1 = P_2 = \tilde{P}_1 = 0.1W$, $\tilde{\lambda_1} = 10^{-6}m^{-2}$, $\alpha = 3.75$.

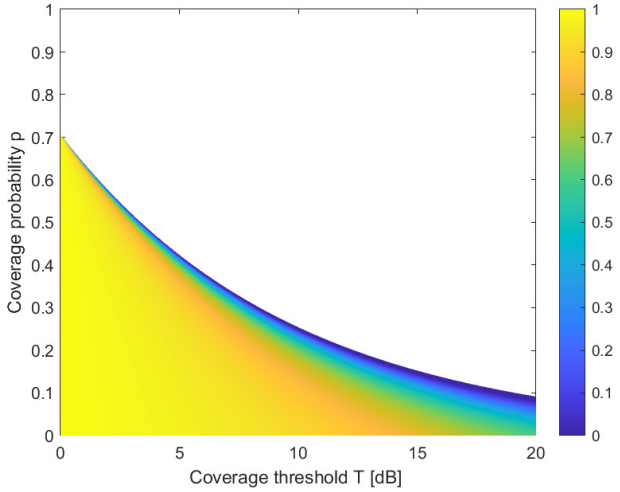

Fig. 5.9 Optimal CDF of the useful received power $\mathcal{P}^*_{P_S}(T' = -75dBm)$ with $\alpha = 4.5$. The following parameters have been selected: $N_c = 1$, $P_1 = P_2 = \tilde{P}_1 = 0.1W$, $\tilde{\lambda_1} = 10^{-6}m^{-2}$.

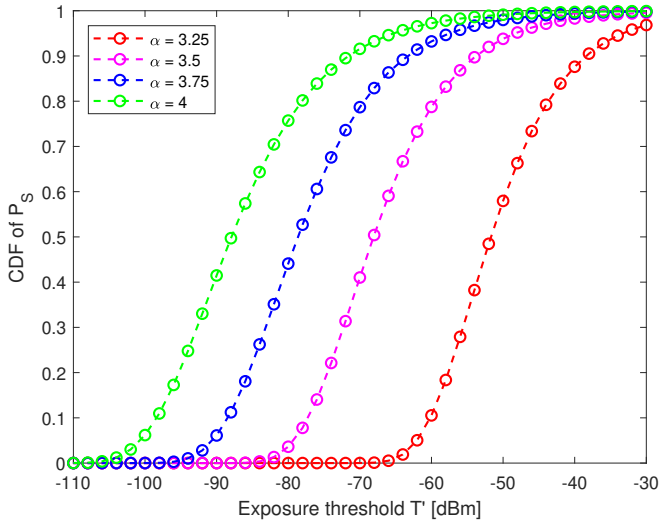

Fig. 5.10 Influence of the path loss exponent α on the optimal $\mathcal{P}^*_{P_S}(T')$. The following parameters have been selected: $N_c = 1$, $P_1 = P_2 = \tilde{P}_1 = 0.1W$, $\tilde{\lambda_1} = 10^{-6}m^{-2}$, $p = 0.3$, $T = 3dB$.

6

Conclusions

6.1 Summary of the thesis

The objective of this dissertation is to jointly study the coverage and the EMF exposure in random wireless networks. To this purpose, this manuscript is structured into the three successive successive parts detailed here below.

The first part (*Chapter 2*) is dedicated to the **design** of novel performance metrics: a new coverage-exposure distribution, meta distributions, joint spatial metrics, and efficiency ratios are developed. These metrics are specifically created to answer questions of mobile operators in practical scenarios (network deployment, monitoring, etc). Closed-form expressions are derived for each of these metrics using stochastic geometry theory.

Capitalizing on part of these metrics, the second major outcome of this treatise consists in the **analysis** of two known wireless architectures: cellular and cell-free networks, respectively covered in *Chapters 3 and 4*. Various results are established from the study of these two topologies. In addition to illustrating rate-exposure trade-offs, the framework proposed in *Chapters 3* is employed to reproduce deployments of real-world networks in France. Regarding cell-free networks, the study of optimal access point densities maximizing the joint performance is provided as well.

The third and last part of the thesis proposes a first attempt to incorporate the developed concepts within an **optimization** problem (*Chapter 5*). The proposed problem consists in minimizing the EMF exposure in a multi-tier network while satisfying coverage constraints.

6.2 Future work

In addition to the possible improvements mentioned at the end of each chapter, this section covers longer term research directions associated to this thesis. These directions are grouped into three categories: extensions directly based on the developed models, ideas based on a critical view of the stochastic geometry tool, as well as potential works beyond the scope of this manuscript.

6.2.1 Extensions of the current models

- After reading this manuscript, one will note that all the metrics introduced in Chapter 2 have not been evaluated for the cellular and cell-free networks of Chapters 3 and 4. The analysis performed in these two chapters was indeed relying on the joint distribution of the SIR and exposure, as well as on their marginals exclusively. A direct extension of this work could therefore consist in deriving in a more systematic manner every new metric for each of the two topologies.

- Cell-free networks are presented in the literature as potential successor of the current cellular systems [88]. Evaluating the relevance of such a technology requires a comprehensive comparison between the two paradigms, which was not developed in this dissertation. Following this line of thought, comparing the models individually analyzed in Chapters 3 and 4 makes perfect sense. Such a comparison was already performed in [40] for coverage metrics only. The extension of this approach should however be written in a coherent manner: the propagation models, transmit powers, and densities of the two networks should be selected to be consistent with the reality.

6.2.2 About stochastic geometry

- The stochastic geometry framework employed in this work has the advantage of providing analytical expressions characterizing the proposed models. One original advantage of this mathematical theory was the competitive runtime required to evaluate these expressions compared to Monte-Carlo simulations. This observation was verified in pioneering works for which the derived expressions were relatively compact. By contrast, more recent publications consider more advanced models, resulting in heavier and often less tractable forms. The benefit in terms of runtime in therefore no longer observed for these new works (see Appendix B). In the particular case of this manuscript, the main ingredient causing large computation times for the mathematical results is the oscillatory integral associated to Gil-Pelaez theorem [21]. This observation was also made for the other works supervised by the author at UCLouvain (see section 1.4). In addition, the integrands involved here with this theorem are often characterized by the same structure (typically PGFLs, see equation (1.19)). Given the recurrence of this problem, more interest could be dedicated to the development of numerical toolboxes and software providing a faster evaluation of such categories of integral.

6.2.3 Further research directions

- The system model of Chapter 3 was featuring two different categories of tiers, respectively operating in sub-6 GHz and mmWave bands. More diversity could however be exploited by exploring other propagation models. On the one hand, future technologies envisioned for beyond 5G are expected to employ terahertz bands [89]. Propagation models associated to these bands significantly differ from sub-6 GHz or mmWaves [90]. On the other hand, the fading, path-loss and shadowing effects depend on the carrier frequency in a continuous manner. Developing a general framework with a frequency-dependent propagation model might therefore be a promising direction. To the best of the author's knowledge, no such global analysis (valid for any band) has been established under a SG umbrella. Investigating this direction would enable to perform joint space-frequency analyses, enabling to answer questions such as: *'Given a frequency band, what should be the density and spatial distribution of the base stations op-*

erating in this band in order to maximize the probability of satisfying given coverage and exposure requirements?'

- Apart from the line-of-sight model employed in Chapter 3, no notion of blockage was present in this dissertation. Shadowing effects nonetheless have a considerable impact on the propagation and induce correlations in the measured signals. A novel user-centric analysis was recently introduced in [91] to model such correlations. This work derives the Laplace transform of the interference in an iterative manner which explicitly takes into account common blockages obstructing adjacent base stations. Capitalizing on this Laplace transform, the metrics of Chapter 1 could be rederived using our methodology and enable to study the effect of correlated shadowing on the exposure statistics. In particular, analyzing the impact of correlations on meta distributions would be of particular interest: to the best of the author's knowledge, such a study has never been considered in existing publications.

- The notion of sleep strategy was first introduced in a SG model in [92]. This technique consists in muting base stations in low mobile traffic conditions to reduce the amount of multi-user interference. Sleep control was so far mostly studied for energy savings purposes. Another benefit of this paradigm is the resulting reduction in EMF exposure. Following this line of thought, the joint coverage-exposure distribution introduced in this thesis could be derived for the system model of [92]. The results of such an analysis would enable to determine the optimal sleep strategies maximizing the joint probability for a given pair of coverage and exposure requirements.

- The philosophy of joint distributions can be extended to statistical quantities different from coverage and exposure. The visions proposed for beyond 5G in the literature consider a plethora of metrics. On top of the elements highlighted in Fig. 6.1, one can mention the energy efficiency, as well as all the metrics associated to physical layer security (e.g. secrecy rate). Future projects in SG might therefore consider joint distributions for two (or more) of these quantities, aiming at illustrating potential trade-offs or developing multi-objective optimization problems.

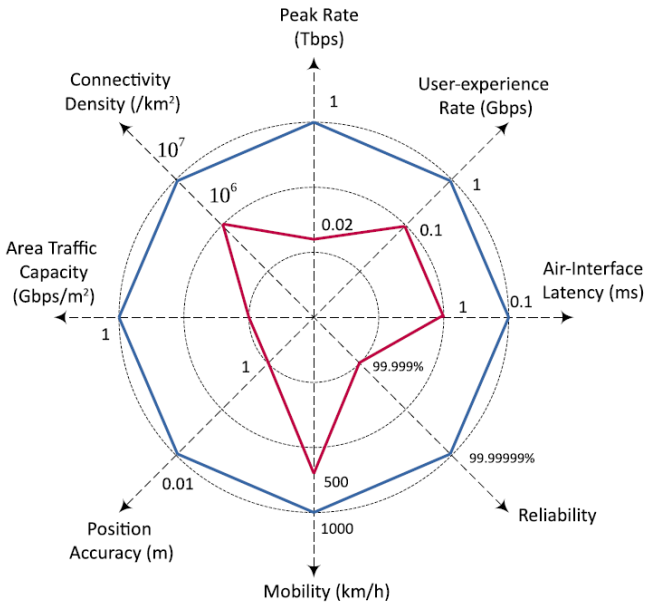

Fig. 6.1 From [89]: examples of metrics considered in the deployment of future mobile generations. The purple and blue curves respectively correspond to potential objectives associated to 5G and 6G.

Appendices

A On the units of the EMF exposure

The user downlink exposure is in general characterized by

$$\mathcal{P} = \sum_{i \in \Psi} P_t \, |h_i|^2 \, l_i \tag{1}$$

where

- Ψ is the PP of BS present in the network;
- P_t is the equivalent isotropic radiated power coming from each BS;
- $|h_i|^2$ and l_i are the path loss and fading coefficient associated to BS i;

This variable can be converted to W/m² [37]:

$$\mathcal{S}_{[\mathrm{W/m^2}]} = \frac{\mathcal{P}}{\mathcal{A}_e} \tag{2}$$

where $\mathcal{A}_e = \frac{(c/f)^2}{4\pi} G_u$ is the effective antenna area of the user with antenna gain G_u and carrier frequency f. The conversion into an electric field amplitude (in V/m) is also possible:

$$E_{[\mathrm{V/m}]} = \sqrt{Z_0 \mathcal{S}}. \tag{3}$$

where $Z_0 = 120\pi$ is the impedance of free space. In the framework of this thesis, the exposure is quantified by means of (1), expressed in dBm. The interested reader can readily convert the provided values by means of (2) and (3).

B On the computational complexity of SG results

Table 1 compares the computational times required to evaluate some of the performance metrics using Monte Carlo (MC) simulations and stochastic geometry. All the computations were performance via the sofware `Matlab R2021a` on a computer equipped with the processor Intel Core I5. Two examples are here considered:

- *Case 1*, evaluating the coverage probability of Chapter 5, given by equation (5.7). This equation is the quotient of two expressions which are linear in the density parameters, and feature no integral. The following parameters have been selected: $\alpha = 4$, $P_1 = P_2 = \tilde{P}_1 = 0.1W$, $\lambda_1 = 3.10^{-6}m^{-2}$, $\lambda_2 = 2.10^{-6}m^{-2}$, $\tilde{\lambda}_1 = 10^{-6}m^{-2}$, Network radius $R = 5km$, 10^5 iterations.
- *Case 2*, related to the second moment of the conditional exposure CDF provided in Chapter 2 and given by (2.37). The following parameters were selected: $\lambda = 2.10^{-6}m^{-2}$, $\alpha = 4$, $P_t = 1W$, $f = 3GHz$, $T' = -130dBm$, Network radius $R = 5km$, 10^4 spatial iterations, 2.10^3 realizations of the fading coefficients per spatial iteration.

	SG expression	MC simulation
Case 1 - Chapter 5	$2.77.10^{-7}$ s	47s
Case 2 - Chapter 2	154s	728s

Table 1 Comparison of the runtimes required to evaluate equations (5.7) and (2.37) via MC simulations and SG.

In order to perform an objective comparison, the following elements should be mentioned:

- the time values indicated for the SG method in the table correspond to the evaluation of one point (i.e. for one threshold T'). By contrast, the MC simulation enables to evaluate any point and has to be run only once. This observation must be taken into account since generating an accurate CDF curve requires a certain number of points.
- the notion of precision should be considered as well. In the case of the MC simulations, the number of iterations corresponding to the

runtime of Table 1 enable to obtain a fair precision (1-2 % of relative error for the majority of the points). Regarding the SG results, the values of eq. (5.7) have the advantage of being produced with the precision of the software[1] thanks to the linearity of the expression. By contrast, the integral expression of eq. (2.37) has a variable precision. Depending on the selected parameters, the tolerance parameters of the different integrals must be adapted in order to obtain a correct result.

In the light of the above arguments, the benefit of SG in terms of computational time is therefore observable in case 1 (linear expression) but not in case 2 (integral expression). Most of the results derived this thesis are similar to this second case. For this reason, a number of figures of this text have been generated using pure MC simulations due to computational constraints. The validation of the corresponding analytical expressions had to be completed via alternative methods:

- by using a set of parameters which was less realistic but leading to a faster convergence of the numerical integrals.
- by slightly modifying the system model, fixing one of the random quantities to avoid the evaluation of one supplementary integral (over a distance or an angle).
- when the convergence of Gil-Pelaez theorem was too slow, by only validating the integrands of the oscillatory integral (i.e. the CFs of both useful signal and interference).

[1] 16 digits by default.

C Proof of Proposition 2.3

The joint metric can be expressed as

$$\begin{aligned}\mathcal{J}_{\lim}(T,T') &\triangleq \mathbb{P}\left[\frac{P_S}{P_I+P_N} > T, P_S + P_I < T'\right] \\ &= \mathbb{P}\left[P_I < \frac{P_S}{T} - P_N, P_I < T' - P_S\right] \\ &= \begin{cases} \mathbb{P}\left[P_I < \frac{P_S}{T} - P_N\right] & \text{if } \frac{P_S}{T} - P_N < T' - P_S \\ \mathbb{P}\left[P_I < T' - P_S\right] & \text{if } T' - P_S < \frac{P_S}{T} - P_N \end{cases}\end{aligned}$$

(Rewriting the inequalities, and remembering that P_I is a positive random variable)

$$= \begin{cases} \mathbb{P}\left[P_I < \frac{P_S}{T} - P_N\right] & \text{if } P_S < \underbrace{\frac{T(T'+P_N)}{1+T}}_{T''} \\ \mathbb{P}\left[P_I < T' - P_S\right] & \text{if } T'' < P_S < T' \\ 0 & \text{if } P_S > T' \end{cases}$$

Let us define

- $F_{P_I}(y|r_0)$, the interference CDF conditioned on the serving distance
- $X = |h|^2$, the channel fading gain

Using the definition of P_S, the last equality can be rewritten as

$$\begin{aligned}\mathcal{J}_{\lim}(T,T') = \mathbb{E}_{r_0}\Bigg[&\int_0^{\frac{T''r_0^\alpha}{P_t\kappa^{-1}}} F_{P_I}\left(\frac{xP_t\kappa^{-1}}{Tr_0^\alpha} - P_N \,\middle|\, r_0\right) f_X(x)dx \\ &+ \int_{\frac{T''r_0^\alpha}{P_t\kappa^{-1}}}^{\frac{T'r_0^\alpha}{P_t\kappa^{-1}}} F_{P_I}\left(T' - \frac{xP_t\kappa^{-1}}{r_0^\alpha} \,\middle|\, r_0\right) f_X(x)dx\Bigg]\end{aligned}$$

By linearity, this expression becomes

$$\mathcal{J}_{\lim}(T,T') = \underbrace{\mathbb{E}_{r_0}\left[\int_0^{\frac{T''r_0^{\alpha}}{P_t\kappa^{-1}}} F_{P_I}\left(\frac{xP_t\kappa^{-1}}{Tr_0^{\alpha}} - P_N \,\middle|\, r_0\right) f_X(x)dx\right]}_{T_1} + \underbrace{\mathbb{E}_{r_0}\left[\int_{\frac{T''r_0^{\alpha}}{P_t\kappa^{-1}}}^{\frac{T'r_0^{\alpha}}{P_t\kappa^{-1}}} F_{P_I}\left(T' - \frac{xP_t\kappa^{-1}}{r_0^{\alpha}} \,\middle|\, r_0\right) f_X(x)dx\right]}_{T_2}$$

Let us develop the first term T_1. The following elements can be replaced in the last expression:

- $f_X(x) = \exp(-x)u(x)$ where $u(x)$ is the step function.
- $F_{P_I}(y) = \frac{1}{2} - \frac{1}{\pi}\int_0^{\infty} Im\left[\phi_I(q)e^{-jqy}\right] q^{-1}dq$ (using Gil-Pelaez theorem)

By injecting these elements, we obtain by linearity

$$T_1 = \mathbb{E}_{r_0}\left[\frac{1}{2}\int_0^{\frac{T''}{P_t\kappa^{-1}r_0^{-\alpha}}} e^{-x}dx - \frac{1}{\pi}\int_0^{\frac{T''}{P_t\kappa^{-1}r_0^{-\alpha}}}\int_0^{\infty} Im\left[\phi_I(q|r_0)\exp\left(-jq\frac{xP_t\kappa^{-1}r_0^{-\alpha}}{T}\right)e^{jqP_N}\right] q^{-1}dq\, e^{-x}dx\right]$$

By swapping the integrals, and remembering the definition of the CDF:

$$T_1 = \mathbb{E}_{r_0}\left[\frac{1}{2}F_X\left(\frac{T''}{P_t\kappa^{-1}r_0^{-\alpha}}\right) - \frac{1}{\pi}\int_0^{\infty}\int_0^{\frac{T''}{P_t\kappa^{-1}r_0^{-\alpha}}} Im\left[\phi_I(q|r_0)\exp\left(-jq\frac{xP_t\kappa^{-1}r_0^{-\alpha}}{T}\right)e^{jqP_N}\right] e^{-x}dx\, q^{-1}dq\right]$$

By swapping the integral over the real number x with the imaginary part

$$T_1 = \mathbb{E}_{r_0}\left[\frac{1}{2}F_X\left(\frac{T''}{P_t\kappa^{-1}r_0^{-\alpha}}\right) - \frac{1}{\pi}\int_0^{\infty} Im\left[\phi_I(q|r_0)\int_0^{\frac{T''}{P_t\kappa^{-1}r_0^{-\alpha}}}\exp\left(-jq\frac{xP_t\kappa^{-1}r_0^{-\alpha}}{T}\right)e^{jqP_N}e^{-x}dx\right] q^{-1}dq\right]$$

The integral inside the imaginary part is of the form

$$\int_a^b e^{-(1+jc)x}dx = \frac{1}{1+jc}\left(e^{-a(1+jc)} - e^{-b(1+jc)}\right)$$

By evaluating this integral, we obtain

$$T_1 = \mathbb{E}_{r_0}\left[\frac{1}{2}F_X\left(\frac{T''}{P_t\kappa^{-1}r_0^{-\alpha}}\right) - \frac{1}{\pi}\int_0^\infty Im\left[\phi_I(q|r_0)\frac{1-\exp\left(\frac{-T''}{P_t\kappa^{-1}r_0^{-\alpha}}\left(1+j\frac{qP_t\kappa^{-1}r_0^{-\alpha}}{T}\right)\right)}{1+j\frac{qP_t\kappa^{-1}r_0^{-\alpha}}{T}}e^{jqP_N}\right]q^{-1}dq\right]$$

By integrating over r_0:

$$T_1 = \frac{1}{2}\int_{r_0}F_X\left(\frac{T''r_0^\alpha}{P_t\kappa^{-1}}\right)f_{R_0}(r_0)dr_0 - \frac{1}{\pi}\int_{r_0}\int_0^\infty Im\left[\phi_I(q|r_0)\frac{1-\exp\left(\frac{-T''r_0^\alpha}{P_t\kappa^{-1}}\left(1+j\frac{qP_t\kappa^{-1}}{Tr_0^\alpha}\right)\right)}{1+j\frac{qP_t\kappa^{-1}}{Tr_0^\alpha}}e^{jqP_N}\right]q^{-1}dqf_{R_0}(r_0)dr_0$$

By applying the same steps for term T_2, one obtains:

$$T_2 = \frac{1}{2}\int_{r_0}F_X\left(\frac{T'}{P_t\kappa^{-1}r_0^{-\alpha}}\right)f_{R_0}(r_0)dr_0 - \frac{1}{2}\int_{r_0}F_X\left(\frac{T''}{P_t\kappa^{-1}r_0^{-\alpha}}\right)f_{R_0}(r_0)dr_0 - \frac{1}{\pi}\int_0^\infty\int_{r_0}Im\left[\phi_I(q|r_0)e^{-jqT'}\frac{\exp\left(\frac{T'r_0^\alpha}{P_t\kappa^{-1}}\left(-1+\frac{jqP_t\kappa^{-1}}{r_0^\alpha}\right)\right)}{-1+jqP_t\kappa^{-1}r_0^{-\alpha}}\right]q^{-1}dqf_{R_0}(r_0)dr_0 + \frac{1}{\pi}\int_0^\infty\int_{r_0}Im\left[\phi_I(q|r_0)e^{-jqT'}\frac{\exp\left(\frac{T''r_0^\alpha}{P_t\kappa^{-1}}\left(-1+\frac{jqP_t\kappa^{-1}}{r_0^\alpha}\right)\right)}{-1+jqP_t\kappa^{-1}r_0^{-\alpha}}\right]q^{-1}dqf_{R_0}(r_0)dr_0$$

The final result is obtained by grouping the two terms.

D Proof of Proposition 2.6

The second order moment of the conditional IPD distribution is given by

$$\mathcal{M}_{\mathcal{P}_{IPD}}(2,T') = \mathbb{E}_\Psi\left[\left(\mathbb{P}_{\{h_i\}_{i\in\Psi}}\left[\text{IPD} < T'|\Psi\right]\right)^2\right] \tag{4}$$

$$= \mathbb{E}_\Psi\left[\left(\frac{1}{2} - \frac{1}{\pi}\int_0^\infty \text{Im}\left[\phi_{\text{IPD}}(t|\Psi)e^{-jT't}\right]t^{-1}dt\right)^2\right] \tag{5}$$

$$= \mathbb{E}_\Psi\left[\frac{1}{4} - \frac{1}{\pi}\int_0^\infty \text{Im}\left[\phi_{\text{IPD}}(t|\Psi)e^{-jT't}\right]t^{-1}dt\right. \tag{6}$$

$$\left. + \frac{1}{\pi^2}\left(\int_0^\infty \text{Im}\left[\phi_{\text{IPD}}(t|\Psi)e^{-jT't}\right]t^{-1}dt\right)^2\right] \tag{7}$$

$$= \underbrace{\frac{1}{4} - \mathbb{E}_\Psi\left[\frac{1}{\pi}\int_0^\infty \text{Im}\left[\phi_{\text{IPD}}(t|\Psi)e^{-jT't}\right]t^{-1}dt\right]}_{\beta(T')} \tag{8}$$

$$+ \frac{1}{\pi^2}\underbrace{\mathbb{E}_\Psi\left[\left(\int_0^\infty \text{Im}\left[\phi_{\text{IPD}}(t|\Psi)e^{-jT't}\right]t^{-1}dt\right)^2\right]}_{\Omega(T')} \tag{9}$$

By swapping the expectation with the integral and the imaginary part, $\beta(T')$ becomes

$$\beta(T') = \frac{1}{4} - \frac{1}{\pi}\int_0^\infty \text{Im}\left[\mathbb{E}_\Psi\left[\phi_{\text{IPD}}(t|\Psi)\right]e^{-jT't}\right]t^{-1}dt \tag{10}$$

$$= \frac{1}{4} - \frac{1}{\pi}\int_0^\infty \text{Im}\left[\phi_{\text{IPD}}(t)e^{-jT't}\right]t^{-1}dt \tag{11}$$

$$= \frac{-1}{4} + \mathcal{P}_{IPD}(T') \tag{12}$$

The second term can be developed in the following manner:

$$\Omega(T') = \mathbb{E}_\Psi\left[\left(\int_0^\infty \text{Im}\left[\phi_{\text{IPD}}(t|\Psi)e^{-jT't}\right]t^{-1}dt\right)\left(\int_0^\infty \text{Im}\left[\phi_{\text{IPD}}(t'|\Psi)e^{-jT't'}\right]t'^{-1}dt'\right)\right] \tag{13}$$

$$= \int_0^\infty\int_0^\infty \underbrace{\mathbb{E}_\Psi\left[\text{Im}\left[\phi_{\text{IPD}}(t|\Psi)e^{-jT't}\right]\text{Im}\left[\phi_{\text{IPD}}(t'|\Psi)e^{-jT't'}\right]\right]}_{\Delta(T',t,t')} t^{-1}t'^{-1}dtdt' \tag{14}$$

Using the following property:

$$\mathrm{Im}(z_1 z_2) = \mathrm{Re}(z_1)\mathrm{Im}(z_2) + \mathrm{Re}(z_2)\mathrm{Im}(z_1), \tag{15}$$

the term $\Delta(T', t, t')$ can be further expanded:

$$\Delta(T', t, t') = \mathbb{E}_\Psi \Big[\Big(\mathrm{Re}\big[\phi_{\mathrm{IPD}}(t|\Psi)\big] \sin(-tT') + \mathrm{Im}\big[\phi_{\mathrm{IPD}}(t|\Psi)\big] \cos(tT') \Big) \tag{16}$$

$$\times \Big(\mathrm{Re}\big[\phi_{\mathrm{IPD}}(t'|\Psi)\big] \sin(-t'T') + \mathrm{Im}\big[\phi_{\mathrm{IPD}}(t'|\Psi)\big] \cos(t'T') \Big) \Big] \tag{17}$$

$$= \mathbb{E}_\Psi \Big[\mathrm{Re}\big[\phi_{\mathrm{IPD}}(t|\Psi)\big] \mathrm{Re}\big[\phi_{\mathrm{IPD}}(t'|\Psi)\big] \Big] \sin(tT') \sin(t'T') \tag{18}$$

$$- \mathbb{E}_\Psi \Big[\mathrm{Re}\big[\phi_{\mathrm{IPD}}(t|\Psi)\big] \mathrm{Im}\big[\phi_{\mathrm{IPD}}(t'|\Psi)\big] \Big] \sin(tT') \cos(t'T') \tag{19}$$

$$- \mathbb{E}_\Psi \Big[\mathrm{Im}\big[\phi_{\mathrm{IPD}}(t|\Psi)\big] \mathrm{Re}\big[\phi_{\mathrm{IPD}}(t'|\Psi)\big] \Big] \cos(tT') \sin(t'T') \tag{20}$$

$$+ \mathbb{E}_\Psi \Big[\mathrm{Im}\big[\phi_{\mathrm{IPD}}(t|\Psi)\big] \mathrm{Im}\big[\phi_{\mathrm{IPD}}(t'|\Psi)\big] \Big] \cos(tT') \cos(t'T') \tag{21}$$

In order to further develop the above expression, the following definitions are introduced:

$$\phi_{\mathrm{IPD}}(t|\Psi) = \prod_{\underline{x}_i \in \Psi} \frac{1}{1 - jtP_t l(r_i)} \cdot \frac{1 + jtP_t l(r_i)}{1 + jtP_t l(r_i)} \tag{22}$$

$$= \prod_{\underline{x}_i \in \Psi} \underbrace{\left(\frac{1}{1 + t^2 P_t^2 l^2(r_i)} + j \frac{tP_t l(r_i)}{1 + t^2 P_t^2 l^2(r_i)} \right)}_{\eta_i} \tag{23}$$

The norm and the phase of each element η_i are given by

$$R_i(t) = \sqrt{\frac{1}{\Big[1 + t^2 P_t^2 l^2(r_i)\Big]^2} + \frac{t^2 P_t^2 l^2(r_i)}{\Big[1 + t^2 P_t^2 l^2(r_i)\Big]^2}} = \Big[1 + t^2 P_t^2 l^2(r)\Big]^{-1/2} \tag{24}$$

$$\theta_i(t) = \mathrm{atan}\Big[tP_t l(r_i)\Big] \tag{25}$$

The norm and the phase of $\phi_{\text{IPD}}(t|\Psi)$ are hence given by

$$R_\phi(t) = \prod_{i\in\Psi} R_i(t) = \prod_{i\in\Psi} \left[1 + t^2 P_t^2 l^2(r)\right]^{-1/2} \tag{26}$$

$$\theta_\phi(t) = \sum_{i\in\Psi} \theta_i(t) = \sum_{i\in\Psi} \operatorname{atan}\left[tP_t l(r_i)\right] \tag{27}$$

Using these notations, one can rewrite

$$\Delta(T',t,t') = \mathbb{E}_\Psi\left[R_\phi(t)R_\phi(t')\cos\left(\theta_\phi(t)\right)\cos\left(\theta_\phi(t')\right)\right]\sin(tT')\sin(t'T') \tag{28}$$

$$- \mathbb{E}_\Psi\left[R_\phi(t)R_\phi(t')\cos\left(\theta_\phi(t)\right)\sin\left(\theta_\phi(t')\right)\right]\sin(tT')\cos(t'T') \tag{29}$$

$$- \mathbb{E}_\Psi\left[R_\phi(t)R_\phi(t')\sin\left(\theta_\phi(t)\right)\cos\left(\theta_\phi(t')\right)\right]\cos(tT')\sin(t'T') \tag{30}$$

$$+ \mathbb{E}_\Psi\left[R_\phi(t)R_\phi(t')\sin\left(\theta_\phi(t)\right)\sin\left(\theta_\phi(t')\right)\right]\cos(tT')\cos(t'T') \tag{31}$$

Using Simpson's formula, the last expression can be rewritten as

$$\Delta(T',t,t') = \underbrace{\frac{1}{2}\mathbb{E}_\Psi\left[R_\phi(t)R_\phi(t')\cos\left(\theta_\phi(t)+\theta_\phi(t')\right)\right]\sin(tT')\sin(t'T')}_{A} \tag{32}$$

$$+ \underbrace{\frac{1}{2}\mathbb{E}_\Psi\left[R_\phi(t)R_\phi(t')\cos\left(\theta_\phi(t)-\theta_\phi(t')\right)\right]\sin(tT')\sin(t'T')}_{B} \tag{33}$$

$$- \frac{1}{2}\mathbb{E}_\Psi\left[R_\phi(t)R_\phi(t')\sin\left(\theta_\phi(t)+\theta_\phi(t')\right)\right]\sin(tT')\cos(t'T') \tag{34}$$

$$+ \frac{1}{2}\mathbb{E}_\Psi\left[R_\phi(t)R_\phi(t')\sin\left(\theta_\phi(t)-\theta_\phi(t')\right)\right]\sin(tT')\cos(t'T') \tag{35}$$

$$- \frac{1}{2}\mathbb{E}_\Psi\left[R_\phi(t)R_\phi(t')\sin\left(\theta_\phi(t)+\theta_\phi(t')\right)\right]\cos(tT')\sin(t'T') \tag{36}$$

$$- \frac{1}{2}\mathbb{E}_\Psi\left[R_\phi(t)R_\phi(t')\sin\left(\theta_\phi(t)-\theta_\phi(t')\right)\right]\cos(tT')\sin(t'T') \tag{37}$$

$$+ \frac{1}{2}\mathbb{E}_\Psi\left[R_\phi(t)R_\phi(t')\cos\left(\theta_\phi(t)-\theta_\phi(t')\right)\right]\cos(tT')\cos(t'T') \tag{38}$$

$$- \frac{1}{2}\mathbb{E}_\Psi\left[R_\phi(t)R_\phi(t')\cos\left(\theta_\phi(t)+\theta_\phi(t')\right)\right]\cos(tT')\cos(t'T') \tag{39}$$

The first term of the last expression can be rewritten as

$$A = \frac{1}{2}\mathbb{E}_\Psi\left\{\operatorname{Re}\left[R_\phi(t)R_\phi(t')\exp\left(j\left[\theta_\phi(t)+\theta_\phi(t')\right]\right)\right]\right\}\sin(tT')\sin(t'T') \tag{40}$$

$$= \frac{1}{2}\operatorname{Re}\left[\mathbb{E}_\Psi\left\{R_\phi(t)R_\phi(t')\exp\left(j\left[\theta_\phi(t)+\theta_\phi(t')\right]\right)\right\}\right]\sin(tT')\sin(t'T') \tag{41}$$

By using the definitions of $R_\phi(t)$ and $\theta_\phi(t)$, the last line becomes

$$A = \frac{1}{2}\mathrm{Re}\left[\mathbb{E}_\Psi\left\{\prod_{i\in\Psi}\left(\underbrace{R_i(t)e^{j\theta_i(t)}}_{\frac{1}{1-jtP_tl(r_i)}}\ \underbrace{R_i(t')e^{j\theta_i(t')}}_{\frac{1}{1-jt'P_tl(r_i)}}\right)\right\}\right]\sin(tT')\sin(t'T') \tag{42}$$

Using the PGFL, the expectation becomes

$$A = \frac{1}{2}\mathrm{Re}\left[\underbrace{\exp\left\{-2\pi\lambda\int_0^\infty\left(1-\frac{1}{1-jtP_tl(r)}\frac{1}{1-jtP_tl(r)}\right)rdr\right\}}_{\Delta_+(t,t')}\right]\sin(tT')\sin(t'T') \tag{43}$$

In a similar manner, term B in (33) can be expressed as

$$B = \frac{1}{2}\mathbb{E}_\Psi\left\{\mathrm{Re}\left[R_\phi(t)R_\phi(t')\exp\left(j\left[\theta_\phi(t)-\theta_\phi(t')\right]\right)\right]\right\}\sin(tT')\sin(t'T') \tag{44}$$

$$= \frac{1}{2}\mathrm{Re}\left[\mathbb{E}_\Psi\left\{R_\phi(t)R_\phi(t')\exp\left(j\left[\theta_\phi(t)-\theta_\phi(t')\right]\right)\right\}\right]\sin(tT')\sin(t'T') \tag{45}$$

By using the definitions of $R_\phi(t)$ and $\theta_\phi(t)$, the last line becomes

$$B = \frac{1}{2}\mathrm{Re}\left[\mathbb{E}_\Psi\left\{\prod_{i\in\Psi}\left(\underbrace{R_i(t)e^{j\theta_i(t)}}_{\frac{1}{1-jtP_tl(r_i)}}\ \underbrace{R_i(t')e^{-j\theta_i(t')}}_{\frac{1}{1+jt'P_tl(r_i)}}\right)\right\}\right]\sin(tT')\sin(t'T') \tag{46}$$

Using the PGFL, the expectation becomes

$$B = \frac{1}{2}\mathrm{Re}\left[\underbrace{\exp\left\{-2\pi\lambda\int_0^\infty\left(1-\frac{1}{1-jtP_tl(r)}\frac{1}{1+jtP_tl(r)}\right)rdr\right\}}_{\Delta_-(t,t')}\right]\sin(tT')\sin(t'T') \tag{47}$$

Thanks to these simplifications, one obtains

$$\Delta(T',t,t') = \frac{1}{2}\Big[\mathrm{Re}\Big[\Delta_+(t,t')\Big]\sin(tT')\sin(t'T') + \mathrm{Re}\Big[\Delta_-(t,t')\Big]\sin(tT')\sin(t'T') \tag{48}$$

$$-\mathrm{Im}\Big[\Delta_+(t,t')\Big]\sin(tT')\cos(t'T') + \mathrm{Im}\Big[\Delta_-(t,t')\Big]\sin(tT')\cos(t'T') \tag{49}$$

$$-\mathrm{Im}\Big[\Delta_+(t,t')\Big]\cos(tT')\sin(t'T') - \mathrm{Im}\Big[\Delta_-(t,t')\Big]\cos(tT')\sin(t'T') \tag{50}$$

$$+\mathrm{Re}\Big[\Delta_-(t,t')\Big]\cos(tT')\cos(t'T') - \mathrm{Re}\Big[\Delta_+(t,t')\Big]\cos(tT')\cos(t'T')\Big] \tag{51}$$

By means of trigonometric simplifications, the last expression can be rewritten as

$$\Delta(T',t,t') = \frac{1}{2}\Bigg[\mathrm{Re}\Big[\Delta_-(t,t')\Big]\cos\Big[(t-t')T'\Big] + \mathrm{Im}\Big[\Delta_-(t,t')\Big]\sin\Big[(t-t')T'\Big] - \Bigg(\mathrm{Re}\Big[\Delta_+(t,t')\Big]\cos\Big[(t+t')T'\Big] + \mathrm{Im}\Big[\Delta_+(t,t')\Big]\sin\Big[(t+t')T'\Big]\Bigg)\Bigg]$$

Using the following property:

$$\mathrm{Re}(z_1\bar{z}_2) = \mathrm{Re}(z_1)\mathrm{Re}(z_2) + \mathrm{Im}(z_2)\mathrm{Im}(z_1), \tag{52}$$

the last result can be rewritten as

$$\begin{aligned}\Delta(T',t,t') &= \frac{1}{2}\left[\mathrm{Re}\Big[\Delta_-(t,t')e^{-j(t-t')T'}\Big] - \mathrm{Re}\Big[\Delta_+(t,t')e^{+j(t+t')T'}\Big]\right] \\ &= \frac{1}{2}\mathrm{Re}\Big[\Delta_-(t,t')e^{-j(t-t')T'} - \Delta_+(t,t')e^{-j(t+t')T'}\Big]\end{aligned}$$

E Proof of Proposition 2.12

The derivation of equation (2.59) follows the same steps as the proof of proposition 2.6. One major difference between these two proofs is the expression of the path loss attenuation associated to the second user located. Given a base station i of located at (r, β) in polar coordinates, this path loss can be expressed as

$$\tilde{l}(r; d, \beta) = \min\left[1, \kappa^{-1} p^{-\alpha}\right] \tag{53}$$

where $p = \sqrt{r^2 + d^2 - 2rd\cos(\beta)}$ is obtained via trigonometry (see Fig. 2)

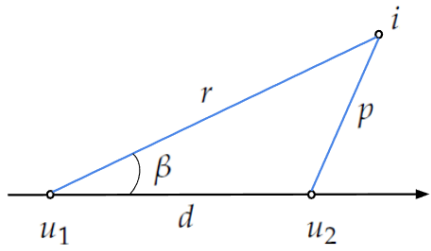

Fig. 2 Illustration of the distances with two users.

F Proof of Proposition 2.14

An upper bound for χ_1 is given by

$$\bar{\chi}_1 = \mathbb{E}\left[\frac{\log\left(1+\frac{P_S}{P_I+P_N}\right)}{P_S}\right] \tag{54}$$

where the interference power has been neglected at the denominator. This bound can be developed using Lemma 1 in [93]:

$$\bar{\chi}_1 = \mathbf{E}_{P_S}\left[\frac{1}{P_S}\mathbf{E}_{P_I}\left[\log\left(1+\frac{P_S}{P_I+P_N}\right)\right]\right] \tag{55}$$

$$= \mathbf{E}_{P_S}\left[\frac{1}{P_S}\int_0^\infty \frac{1}{s}(1-e^{-sP_S})\mathcal{L}_I(s|r)e^{-sP_N}ds\right] \tag{56}$$

where $\mathcal{L}_I(s|r)$ is the Laplace transform[2] of the interference:

$$\mathcal{L}_I(s|r) = \exp\left\{-2\pi\lambda\int_r^\infty\left(1-\frac{1}{1+sP_t l(r')}r'dr'\right)\right\}. \tag{57}$$

The end of the proof consists in applying the expectation over P_S in (56) by integrating over both the fading and the path loss.

[2] one can observe that the expression of (57) is identical to the characteristic function (2.20) via the change of variable $s = -jt$

G Proof of Assumption 4.1

By injecting (4.5) in (4.4), and developing the squared norm, one obtains

$$P_I = P_t \kappa^{-1} \sum_{u \in \Psi_U \setminus \{u^*\}} \frac{1}{|\mathbf{g}_u|^2} \sum_{i \in \mathcal{C}_u} \left| \mathbf{h}_{iu}^H \mathbf{h}_{iu^*} r_{iu}^{-\alpha/2} r_{iu^*}^{-\alpha/2} \right|^2 \tag{58}$$

$$+ P_t \kappa^{-1} \sum_{u \in \Psi_U \setminus \{u^*\}} \frac{1}{|\mathbf{g}_u|^2} \sum_{i \in \mathcal{C}_u} \sum_{i' \in \mathcal{C}_u, i' \neq i} \underbrace{\mathbf{h}_{iu}^H \mathbf{h}_{iu^*} r_{iu}^{-\alpha/2} r_{iu^*}^{-\alpha/2} \mathbf{h}_{i'u^*}^H \mathbf{h}_{i'u} r_{i'u}^{-\alpha/2} r_{i'u^*}^{-\alpha/2}}_{\text{cross terms}}. \tag{59}$$

Since the fading is Rayleigh, all the cross terms in the above expression are zero mean. As a result, these terms only impact higher order moments of the aggregate interference. Numerical simulations (see Section 4.4) show that neglecting these terms has a low impact on the accuracy of the results. These terms are therefore neglected, which enables to obtain a simpler expression:

$$P_I \approx P_t \kappa^{-1} \sum_{u \in \Psi_U \setminus \{u^*\}} \frac{1}{|\mathbf{g}_u|^2} \sum_{i \in \mathcal{C}_u} \left| \mathbf{h}_{iu}^H \mathbf{h}_{iu^*} r_{iu}^{-\alpha/2} r_{iu^*}^{-\alpha/2} \right|^2 \tag{60}$$

$$\approx P_t \kappa^{-1} \sum_{u \in \Psi_U \setminus \{u^*\}} \frac{1}{|\mathbf{g}_u|^2} \sum_{i \in \mathcal{C}_u} \left| \Big(\sum_{k=1}^{M} h_{iuk}^* h_{iu^*k} \Big) r_{iu}^{-\alpha/2} r_{iu^*}^{-\alpha/2} \right|^2. \tag{61}$$

By neglecting again the cross-terms coming from the norm of (61) and developing the normalization factor $|\mathbf{g}_u|^2$, the expression can be further simplified as

$$P_I \approx P_t \kappa^{-1} \sum_{u \in \Psi_U \setminus \{u^*\}} \sum_{i \in \mathcal{C}_u} \frac{\sum_{k=1}^{M} |h_{iuk}|^2 |h_{iu^*k}|^2 r_{iu}^{-\alpha}}{\sum_{i' \in \mathcal{C}_u} \sum_{k=1}^{M} |h_{i'uk}|^2 r_{i'u}^{-\alpha}} r_{iu^*}^{-\alpha}. \tag{62}$$

In the quotient in (62), the distances r_{iu} and $r_{i'u}$ represent the distances from two RRHs i and i' serving a UE $u \neq u^*$. A geometrical representation is proposed in Figure 4a (next page). By approximating these distances as

being equal for $u \neq u^*$ (cfr. Figure 4b), one obtains:

$$P_I \approx P_t \kappa^{-1} \sum_{u \in \Psi_U \setminus \{u^*\}} \sum_{i \in \mathcal{C}_u} \underbrace{\frac{\sum_{k=1}^{M} \left|h_{iuk}\right|^2 \left|h_{iu^*k}\right|^2}{\sum_{i' \in \mathcal{C}_u} \sum_{k=1}^{M} \left|h_{i'uk}\right|^2}}_{Z_{|\mathcal{C}_u|}^{(i,u)}} r_{iu^*}^{-\alpha} \tag{63}$$

The distribution of $Z_{|\mathcal{C}_u|}^{(i,u)}$ is then approximated by a Gamma distribution via moment matching. To compute the shape and scale parameters of this distribution, the moments of the quotient $Z_{|\mathcal{C}_u|}^{(i,u)}$ are approximated using the Taylor expansions presented in [94–96]. Equation (4.7) is finally obtained by rewriting the double summation as functions of sets Ψ_R and $\mathcal{B}_i$.

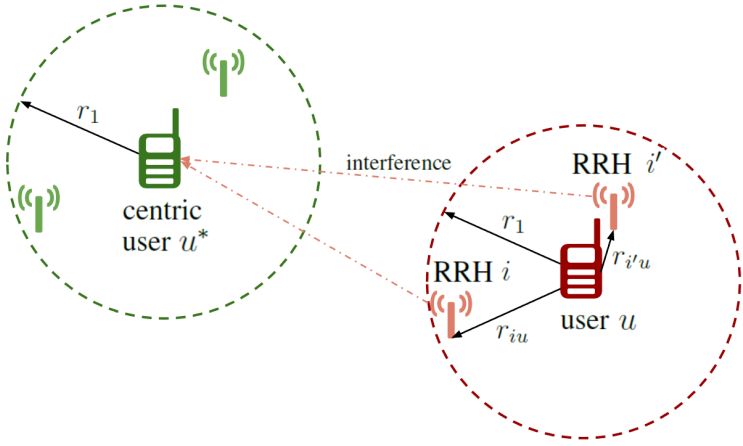

(a) Original topology with $r_{iu} \neq r_{i'u}$.

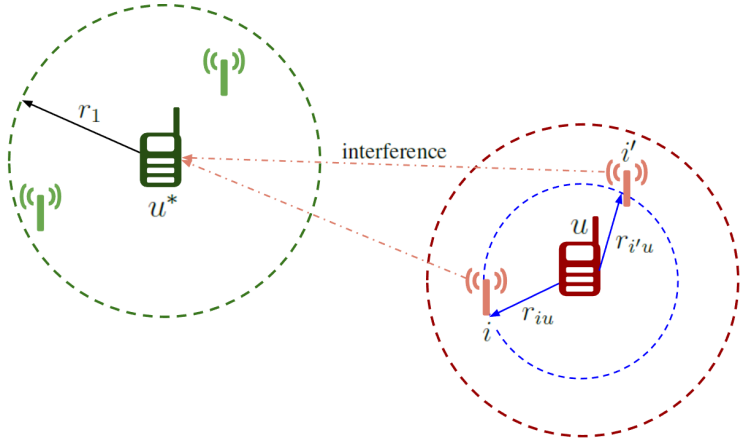

(b) Modified topology with assumption $r_{iu} = r_{i'u}$.

Fig. 3 Illustration of the approximation employed to obtain (63).

H Proof of Assumption 4.2

The probabilities $p(n'_U|n_U, r)$ and $p(n'_R|n_R)$ are defined as follows:

- $p(n'_U|n_U, r)$ is the probability for a RRH i belonging to the centric cluster to serve n'_U UEs different from u^*, given that n_U UEs different from u^* are in $\mathcal{D}(\mathbf{o}, r_1)$ (cfr. Figure 4a).
- Considering a UE $u \neq u^*$ served by a RRH i of the centric cluster, $p(n'_R|n_R, r)$ represents the probability for this UE to be served by n'_R RRHs, given n_R RRHs in the centric cluster (cfr. Figure 4b).

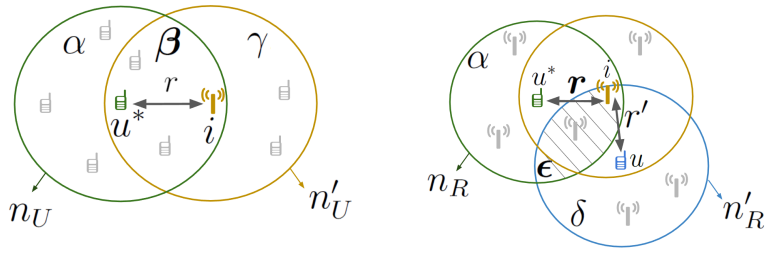

(a) Intersection for $p(n'_U|n_U, r)$. **(b)** Intersections for $p(n'_R|n_R, r)$

Fig. 4 Intersections considered to compute the conditional probabilities.

These two probabilities can be computed using a geometrical reasoning based on Figure 4. In Figure 4a, the intersection area β of the two disks around u^* and i is given by [97]:

$$\mathcal{A}(r) = 2r_1^2 \text{acos}\left(\frac{r}{2r_1}\right) - \frac{r}{2}\sqrt{4r_1^2 - r^2}. \tag{64}$$

Nb: in order to obtain simpler forms, this expression can also be replaced by its linearization around zero, without loss of significant accuracy:

$$\tilde{\mathcal{A}}(r) = \pi r_1^2 \left[1 - \frac{2r}{\pi r_1}\right]. \tag{65}$$

Since the users are distributed using a PPP, the number of nodes in the zones α, β and γ follow independent Poisson distributions. The condi-

tional probability of n'_U is hence given by

$$p(n'_U|n_U) = \frac{p\Big[\Big(n_U \text{ in } (\alpha \cup \beta)\Big) \cap \Big(n'_U \text{ in } (\beta \cup \gamma)\Big)\Big]}{p\Big[n_U \text{ in } (\alpha \cup \beta)\Big]} \tag{66}$$

$$= \frac{\sum_{k=0}^{\min(n_U, n'_U)} p\big[n_U - k \text{ in } \alpha\big]\, p\big[k \text{ in } \beta\big]\, p\big[n'_U - k \text{ in } \gamma\big]}{p\big[n_U \text{ in } (\alpha \cup \beta)\big]} \tag{67}$$

where

$$p\big[n_U - k \text{ in } \alpha\big] = \Big[\lambda_U\big(\pi r_1^2 - \mathcal{A}(r)\big)\Big]^{n_U - k} \exp\Big[-\lambda_U\big(\pi r_1^2 - \mathcal{A}(r)\big)\Big]\Big[(n_U - k)!\Big]^{-1}$$

$$p\big[k \text{ in } \beta\big] = \big[\lambda_U \mathcal{A}(r)\big]^k \exp\big[-\lambda_U \mathcal{A}(r)\big]\big[k!\big]^{-1}$$

$$p\big[n'_U - k \text{ in } \gamma\big] = \Big[\lambda_U\big(\pi r_1^2 - \mathcal{A}(r)\big)\Big]^{n'_U - k} \exp\Big[-\lambda_U\big(\pi r_1^2 - \mathcal{A}(r)\big)\Big]\Big[(n'_U - k)!\Big]^{-1}$$

$$p\big[n_U \text{ in } (\alpha \cup \beta)\big] = \big(\lambda_U \pi r_1^2\big)^{n_U} \exp\big(-\lambda_U \pi r_1^2\big)\big(n_U!\big)^{-1}.$$

Using the same reasoning, the probability of n'_R is hence given by

$$p(n'_R|n_R) = \frac{p\Big[\Big(n_R \text{ in } (\alpha \cup \epsilon)\Big) \cap \Big(n'_R \text{ in } (\epsilon \cup \delta)\Big)\Big]}{p\Big[n_R \text{ in } (\alpha \cup \epsilon)\Big]} \tag{68}$$

$$= \frac{\sum_{k=0}^{\min(n_R, n'_R)} p\big[n_R - k \text{ in } \alpha\big]\, p\big[k \text{ in } \epsilon\big]\, p\big[n'_R - k \text{ in } \delta\big]}{p\big[n_R \text{ in } (\alpha \cup \epsilon)\big]} \tag{69}$$

The probabilities involved in this last expression require to compute the area of the intersection ϵ in Figure 4b. This area depends on the distance between the green and blue circle, given by $r'' = \big(r^2 + r'^2 - 2rr' \cos(\angle rr')\big)^{1/2}$. The resulting intersection should be average over the distribution of r', which does not easily lead to tractable expressions. In order to work with a simple expression, an analytical expression $\mathcal{S}(r)$ only function of variable r. In addition, we consider a linear expression for the relative area of intersection: $\mathcal{S}(r)/(\pi r_1^2) = \chi + \zeta r$, whose coefficients are determined by considering the average case $r' = r_1/2$ and $\angle rr' = \pi/2$. The resulting values are given by

$$\chi = \left(2\text{acos}\Big(\frac{\sqrt{5}}{4}\Big) - \frac{5}{4}\sqrt{4 - \frac{1}{4}}\right) \tag{70}$$

$$\zeta = \frac{1}{r_1}\left(\chi - 2\text{acos}\left(\frac{1}{4}\right) + \frac{1}{4}\sqrt{4 - \frac{1}{4}}\right). \tag{71}$$

The probabilities present in (68) can in that case be expressed as

$$p\left[n_R - k \text{ in } \alpha\right] = \left[\lambda_R\left(\pi r_1^2 - \mathcal{S}(r)\right)\right]^{n_R - k} \exp\left[-\lambda_R\left(\pi r_1^2 - \mathcal{S}(r)\right)\right]\left[(n_R - k)!\right]^{-1}$$
$$p\left[k \text{ in } \epsilon\right] = \left[\lambda_R \mathcal{S}(r)\right]^{k} \exp\left[-\lambda_R \mathcal{S}(r)\right]\left[(k)!\right]^{-1}$$
$$p\left[n'_R - k \text{ in } \delta\right] = \left[\lambda_R\left(\pi r_1^2 - \mathcal{S}(r)\right)\right]^{n'_R - k} \exp\left[-\lambda_R\left(\pi r_1^2 - \mathcal{S}(r)\right)\right]\left[(n'_R - k)!\right]^{-1}$$
$$p\left[n_R \text{ in } (\alpha \cup \epsilon)\right] = \left(\lambda_U \pi r_1^2\right)^{n_R} \exp\left(-\lambda_R \pi r_1^2\right)\left(n_R!\right)^{-1}.$$

I Proof of Proposition 4.3

In this proof, (4.10), (4.11), (4.13) and (4.9) are successively derived.

Equation (4.10): conditioned on n_U and n_R, the characteristic function of P_{S_η} is given by

$$\begin{aligned}
\phi_{P_{S_\eta}}(t|n_R,n_U) &= \mathbb{E}\Big[\exp(jtP_{S_\eta})\Big] \\
&\overset{(a)}{=} \mathbb{E}\left[\exp\left\{jt\left(\sum_{i=1}^{n_R} P_{S,i} + \eta\sum_{i=1}^{n_R} P_{I_1,i}\right)\right\}\right] \\
&= \mathbb{E}\left[\prod_{i=1}^{n_R}\exp\left(jtP_{S,i}\right)\exp\left(jt\eta P_{I_1,i}\right)\right] \\
&\overset{(b)}{=} \left(\mathbb{E}\left[\exp\left(jtP_{S,i}\right)\exp\left(jt\eta P_{I_1,i}\right)\right]\right)^{n_R} \\
&\overset{(c)}{=} \left(\mathbb{E}_r\Big[\phi_T(t|n_R,n_U,r)\phi_V(\eta t|n_R,n_U,r)\Big]\right)^{n_R} \\
&\overset{(d)}{=} \left[\int_{r_0}^{r_1}\phi_T(t|n_R,n_U,r)\phi_V(\eta t|n_R,n_U,r)\frac{2r}{r_1^2-r_0^2}dr\right]^{n_R}.
\end{aligned}$$

In these developments, (a) is obtained by decomposing P_{S_η} into the useful and interference powers provided by each RRH $i \in \mathcal{C}_{u^*}$. (b) comes from the assumed independence between the different RRHs under conditioning on n_U and n_R. (c) is obtained by defining $\phi_T(\cdot)$ and $\phi_V(\cdot)$ as the characteristic functions of powers $P_{S,i}$ and $P_{I_1,i}$ coming from an arbitrary RRH i. (d) is derived by averaging over the pdf of the distance r_{iu^*} between the RRH and the user.

Equation (4.11): by replacing $\mathbf{w}_{iu^*}$ by its definition in (4.4), we obtain

$$P_{S,i} = P_t|\mathbf{h}_{iu^*}|^2\kappa^{-1}r_{iu^*}^{-\alpha}. \tag{72}$$

This right member of (72) follows a Gamma distribution of shape M and scale $P_t\kappa^{-1}r_{iu^*}^{-\alpha}$, which results in $\phi_T(\cdot)$ given by (4.11).

Equation (4.13): $\phi_V(\cdot)$ is the characteristic function of the interference power

coming from one RRH $i \in \mathcal{C}_{u^*}$. This interference power is given by

$$P_{I_1,i} = \sum_{\substack{u \in \mathcal{B}_i \\ u \neq u^*}} P_t Z^{(i,u)}_{|\mathcal{C}_u|} \kappa^{-1} r_{iu^*}^{-\alpha}$$

On the basis of this definition, one has

$$\phi_V(t|n_R, n_U, r) = \mathbb{E}\Big[\exp(jtP_{I_1,i})\Big] \tag{73}$$

$$= \mathbb{E}\left[\exp\left\{jt\left(\sum_{\substack{u \in \mathcal{B}_i \\ u \neq u^*}} P_t Z^{(i,u)}_{|\mathcal{C}_u|} \kappa^{-1} r_{iu^*}^{-\alpha}\right)\right\}\right] \tag{74}$$

$$\overset{(a)}{=} \sum_{n'_U=0}^{\infty} p(n'_U|n_U, r)\, \mathbb{E}\left[\exp\left\{jt\left(\sum_{u=1}^{n'_U} P_t Z^{(i,u)}_{|\mathcal{C}_u|} \kappa^{-1} r^{-\alpha}\right)\right\}\right] \tag{75}$$

$$\overset{(b)}{=} \sum_{n'_U=0}^{\infty} p(n'_U|n_U, r) \left(\mathbb{E}\left[\exp\left\{jtP_t Z^{(i,u)}_{|\mathcal{C}_u|} \kappa^{-1} r^{-\alpha}\right\}\right]\right)^{n'_U} \tag{76}$$

$$\overset{(c)}{=} \sum_{n'_U=0}^{\infty} p(n'_U|n_U, r) \left(\sum_{n'_R=1}^{\infty} p(n'_R|n_R, r)\, \mathbb{E}\left[e^{jtP_t Z^{(i,u)}_{n'_R} \kappa^{-1} r^{-\alpha}}\right]\right)^{n'_U} \tag{77}$$

$$\overset{(d)}{=} \sum_{n'_U=0}^{\infty} p(n'_U|n_U, r) \left[\sum_{n'_R=1}^{\infty} p(n'_R|n_R, r)\, \left(1 - jtP_t \kappa^{-1} r^{-\alpha} s_{n'_R}\right)^{-k_{n'_R}}\right]^{n'_U} \tag{78}$$

In these developments, (a) comes from the averaging over $n'_U = |\mathcal{B}_i| - 1$, the number of UEs different from u^* served by RRH i. (b) comes from the assumed independence between the interference terms associated to the n'_U users under conditioning on n_U and n_R. (c) is obtained via averaging over the n'_R RRHs serving an arbitrary u among the n'_U UEs. (d) is finally derived by definition of the characteristic function of the Gamma random variable $Z^{(i,u)}_{n'_R}$.

Equation (4.9): this final characteristic function is finally obtained by averaging over the (Poisson) distributions of n_R and n_U.

J Proof of Proposition 4.4

The proof consists in computing the expectation of P_{S_η} and $P_{S_\eta}^2$ for $\eta = 1$. The steps of the developments rely on the same hypotheses as the proof of Proposition 4.3. The mean can be expressed as follows:

$$m_{S+P_{I_1}} = \mathbb{E}\left[\sum_{i\in\mathcal{C}_{u^*}} P_t|\mathbf{h}_{iu^*}|^2\kappa^{-1}r_{iu^*}^{-\alpha} + \sum_{i\in\mathcal{C}_{u^*}}\sum_{\substack{u\in\mathcal{B}_i\\u\neq u^*}} P_t Z_{|\mathcal{C}_u|}^{(i,u)}\kappa^{-1}r_{iu^*}^{-\alpha}\right] \tag{79}$$

$$\overset{(a)}{=} P_t\kappa^{-1}\mathbb{E}\left[\sum_{i\in\mathcal{C}_{u^*}}\left(|\mathbf{h}_{iu^*}|^2 + \sum_{\substack{u\in\mathcal{B}_i\\u\neq u^*}} Z_{|\mathcal{C}_u|}^{(i,u)}\right)r_{iu^*}^{-\alpha}\right] \tag{80}$$

$$\overset{(b)}{=} P_t\kappa^{-1}\sum_{n_U=0}^{\infty}\sum_{n_R=0}^{\infty}\Bigg\{p_R(n_R)p_U(n_U) \tag{81}$$

$$\times \underbrace{\mathbb{E}\left[\sum_{i=1}^{n_R}\left(|\mathbf{h}_{iu^*}|^2 + \sum_{\substack{u\in\mathcal{B}_i\\u\neq u^*}} Z_{|\mathcal{C}_u|}^{(i,u)}\right)r_{iu^*}^{-\alpha}\middle| n_R, n_U\right]}_{L(n_U,n_R)}\Bigg\} \tag{82}$$

where (a) is obtained by grouping terms and (b) by conditioning on variables n_U and n_R, as performed in Appendix I. The term $L(n_U, n_R)$ can then be written as

$$L(n_U,n_R) \overset{(a)}{=} n_R\mathbb{E}\left[\left(|\mathbf{h}_{iu^*}|^2 + \sum_{\substack{u\in\mathcal{B}_i\\u\neq u^*}} Z_{|\mathcal{C}_u|}^{(i,u)}\right)r_{iu^*}^{-\alpha}\middle| n_R, n_U\right] \tag{83}$$

$$\overset{(b)}{=} n_R\int_{r_0}^{r_1}\mathbb{E}\left[\left(|\mathbf{h}_{iu^*}|^2 + \sum_{\substack{u\in\mathcal{B}_i\\u\neq u^*}} Z_{|\mathcal{C}_u|}^{(i,u)}\right)\middle| r, n_R, n_U\right]r^{-\alpha}f_R(r)dr \tag{84}$$

$$\overset{(c)}{=} n_R\int_{r_0}^{r_1}\Bigg(\underbrace{M + \mathbb{E}\left[\sum_{\substack{u\in\mathcal{B}_i\\u\neq u^*}} Z_{|\mathcal{C}_u|}^{(i,u)}\middle| r, n_R, n_U\right]}_{\xi}\Bigg)r^{-\alpha}f_R(r)dr \tag{85}$$

where (a) is obtained by linearity. The rest of the developments are hence performed for an arbitrary RRH i among the n_R RRHs serving u^*. (b) is obtained by developing the averaging with respect to the distance r_{iu^*}. We denote the probability density function of this distance by $f_R(r) = 2r/(r_1^2 - r_0^2)$. The remaining term ξ is then computed by expanding then averaging over variables n'_R and n'_U introduced in section **??**4.24.2his purpose, the conditional probabilities computed in Assumption 4.2 are employed. One obtains:

$$\xi \overset{(a)}{=} \sum_{n'_U=0}^{\infty} p(n'_U|n_U,r)\mathbb{E}\left[\sum_{u=1}^{n'_U} Z^{(i,u)}_{|\mathcal{C}_u|}\middle| r, n_R, n_U\right] \tag{86}$$

$$\overset{(b)}{=} \sum_{n'_U=0}^{\infty} p(n'_U|n_U,r)n'_U\mathbb{E}\left[Z^{(i,u)}_{|\mathcal{C}_u|}\middle| r, n_R, n_U, n'_U\right] \tag{87}$$

$$\overset{(c)}{=} \sum_{n'_U=0}^{\infty} p(n'_U|n_U,r)n'_U \sum_{n'_R=0}^{\infty} p(n'_R|n_R,r)\mathbb{E}\left[Z^{(i,u)}_{n'_R}\middle| r, n_R, n_U, n'_R\right] \tag{88}$$

$$\overset{(d)}{=} \sum_{n'_U=0}^{\infty} p(n'_U|n_U,r)n'_U \sum_{n'_R=0}^{\infty} p(n'_R|n_R,r)n'^{-1}_R \tag{89}$$

where (a) is obtained by expanding the averaging with respect to $n'_U \triangleq |\mathcal{B}_i|$. (b) is derived by linearity. The rest of the developments are hence performed for one unique term of the summation, associated to an arbitrary user u among the n'_U UEs served by i. (c) is derived by developing the averaging with respect to $n'_R \triangleq |\mathcal{C}_u|$. In order to compute the variance, the computation of $\mathbb{E}[P^2_{S_\eta}]$ follows the same reasoning and is here omitted due to space limitations.

K Proof of Proposition 4.6

On the basis of the proposed decomposition, the interference P_{I_2} can be expressed as

$$P_{I_2} = \sum_{n=1}^{\infty} \underbrace{\sum_{i\in\tilde{\Psi}_{R,n}} \sum_{u=1}^{n} P_t Z_{|\mathcal{C}_u|}^{(i,u)} \kappa^{-1} r_{iu^*}^{-\alpha}}_{P_{I_{2,n}}}. \tag{90}$$

where $P_{I_{2,n}}$ is the interference coming from $\tilde{\Psi}_{R,n}$. Since the subsets of the decomposition are independent, the characteristic function of P_{I_2} can is given by

$$\phi_{P_{I_2}}(t) = \prod_{n=1}^{\infty} \phi_{P_{I_{2,n}}}(t). \tag{91}$$

where $\phi_{P_{I_{2,n}}}(t)$ is the characteristic function of the interference coming from the set $\tilde{\Psi}_{R,n}$. This function is by definition given by

$$\phi_{P_{I_{2,n}}}(t) = \mathbb{E}\left\{ \prod_{i\in\tilde{\Psi}_{R,n}} \exp\left[jt \sum_{u=1}^{n} P_t Z_{|\mathcal{C}_u|}^{(i,u)} \kappa^{-1} r_{iu^*}^{-\alpha} \right] \right\} \tag{92}$$

Introducing the slack variable $Y_{i,n} = \sum_{u=1}^{n} Z_{|\mathcal{C}_u|}^{(i,j)}$, this expression can be rewritten as

$$\phi_{P_{I_{2,n}}}(t) = \mathbb{E}_{\tilde{\Psi}_{R,n}}\left\{ \prod_{i\in\tilde{\Psi}_{R,n}} \mathbb{E}_{Y_{i,n}}\left[\exp\left(jtP_t\kappa^{-1} r_{iu^*}^{-\alpha} Y_{i,n} \right) \right] \right\} \tag{93}$$

$$\overset{(a)}{=} \mathbb{E}_{\tilde{\Psi}_{R,n}}\left\{ \prod_{i\in\tilde{\Psi}_{R,n}} \phi_{Y_{i,n}}(P_t\kappa^{-1} r_{iu^*}^{-\alpha} t) \right\} \tag{94}$$

$$\overset{(b)}{=} \exp\left\{ -2\pi\lambda_{R,n} \int_{r_1}^{\infty} \left[1 - \phi_{Y_{i,n}}(P_t\kappa^{-1} r^{-\alpha} t) \right] r dr \right\} \tag{95}$$

where (a) comes from the definition of the characteristic function and (b) is obtained using the probability generating functional (cfr subsection 1.2.6) .

Finally, the characteristic function of $Y_{i,n}$ is given by

$$\phi_{Y_{i,n}}(t) = \mathbb{E}\left[\exp\left(jt\sum_{u=1}^{n} Z^{(i,u)}_{|\mathcal{C}_u|}\right)\right] \tag{96}$$

$$\overset{(a)}{=} \left(\mathbb{E}\left[\exp\left(jtZ^{(i,u)}_{|\mathcal{C}_u|}\right)\right]\right)^n \tag{97}$$

$$\overset{(b)}{=} \left(\mathbb{E}_{|\mathcal{C}_u|}\left[\mathbb{E}_{Z^{(i,u)}_{|\mathcal{C}_u|}}\left[\exp\left(jtZ^{(i,u)}_{|\mathcal{C}_u|}\right)\middle|\ |\mathcal{C}_u|\right]\right]\right)^n \tag{98}$$

$$\overset{(c)}{=} \left(\mathbb{E}_{|\mathcal{C}_u|}\left[\left(1-jts_{|\mathcal{C}_u|}\right)^{k_{|\mathcal{C}_u|}}\right]\right)^n \tag{99}$$

$$\overset{(d)}{=} \left(\sum_{m=1}^{\infty} \tilde{p}_R(m)(1-jts_m)^{k_m}\right)^n \tag{100}$$

where (a) comes from the fact that the variables $Z^{(i,j)}_{|\mathcal{C}_j|}$ are i.i.d. (b) is obtained by decomposing the expectation and (c) is derived using the characteristic function of the gamma random variable $Z^{(i,u)}_{|\mathcal{C}_u|}$ (cfr. Appendix G). (d) is obtained by averaging over the possible values of $|\mathcal{C}_u|$, whose pmf is given by $\tilde{p}(m)$. Note that the truncated Poisson distribution of (4.19) is here used since the each considered user is served at least by one RRH for $n > 1$.

L Proof of Proposition 4.9

The data rate distribution can be expressed as

$$\mathcal{P}_{\text{cov}}(T|n_U, n_R) \triangleq \mathbb{P}\left[\log_2\left(1 + P_S/(P_I + P_N)\right) > T\right] \tag{101}$$

$$= \mathbb{P}\left[P_S - \underbrace{(2^T - 1)}_{\tilde{T}} P_I - \underbrace{(2^T - 1)}_{\tilde{T}} P_N > 0\right] \tag{102}$$

$$= \mathbb{P}\left[\underbrace{P_S - \tilde{T}P_{I_1}}_{P_{S_{-\tilde{T}}}} - \tilde{T}P_{I_2}\tilde{T}P_N > 0\right] \tag{103}$$

where the last equality comes from the decomposition of the interference into P_{I_1} and P_{I_2}. The final result (4.26) is finally obtained by defining the auxiliary variable $P_{S_{-\tilde{T}}}$ (equal to P_{S_η} defined in section 4.2, for the particular case of $\eta = -\tilde{T}$) and by applying Gil-Pelaez theorem (cfr. Subsection 1.2.7). The reasoning employed to derive the IPD distribution is identical.

Bibliography

[1] J. A. Stratton, *Electromagnetic theory*. New York: McGraw-Hill, 1st edition ed., 1941.

[2] W. H. Organization, "Exposure limits for radio-frequency fields (public), data by country." available at https://apps.who.int/gho/data/view.main.EMFLIMITSPUBCRADIOFREQUENCYv.

[3] R. Wydaeghe, S. Shikhantsov, E. Tanghe, G. Vermeeren, L. Martens, P. Demeester, and W. Joseph, "Realistic human exposure at 3.5 ghz and 28 ghz for distributed and collocated mamimo in indoor environments using hybrid ray-tracing and fdtd," *IEEE Access*, vol. 10, pp. 130996–131004, 2022.

[4] X. Lu, P. Wang, D. Niyato, D. I. Kim, and Z. Han, "Wireless networks with rf energy harvesting: A contemporary survey," *IEEE Communications Surveys Tutorials*, vol. 17, no. 2, pp. 757–789, 2015.

[5] S. Bi, C. K. Ho, and R. Zhang, "Wireless powered communication: opportunities and challenges," *IEEE Communications Magazine*, vol. 53, no. 4, pp. 117–125, 2015.

[6] I. Krikidis, S. Timotheou, S. Nikolaou, G. Zheng, D. W. K. Ng, and R. Schober, "Simultaneous wireless information and power transfer in modern communication systems," *IEEE Communications Magazine*, vol. 52, no. 11, pp. 104–110, 2014.

[7] K. V. Mishra, B. Shankar M.R., and B. Ottersten, "Stochastic-geometry-based interference modeling in automotive radars using matérn hard-

core process," in *2020 IEEE Radar Conference (RadarConf20)*, pp. 1–5, 2020.

[8] Z. Fang, Z. Wei, X. Chen, H. Wu, and Z. Feng, "Stochastic geometry for automotive radar interference with rcs characteristics," *IEEE Wireless Communications Letters*, vol. 9, no. 11, pp. 1817–1820, 2020.

[9] S. Chen, F. Qin, B. Hu, X. Li, and Z. Chen, "User-centric ultra-dense networks for 5g: challenges, methodologies, and directions," *IEEE Wireless Communications*, vol. 23, no. 2, pp. 78–85, 2016.

[10] W. Saad, M. Bennis, and M. Chen, "A vision of 6g wireless systems: Applications, trends, technologies, and open research problems," *IEEE Network*, vol. 34, no. 3, pp. 134–142, 2020.

[11] P. Almers, E. Bonek, A. Burr, N. Czink, M. Debbah, V. Degli-Esposti, H. Hofstetter, P. Kyösti, D. Laurenson, G. Matz, *et al.*, "Survey of channel and radio propagation models for wireless mimo systems," *EURASIP Journal on Wireless Communications and Networking*, vol. 2007, pp. 1–19, 2007.

[12] W. S. K. J. M. Sung Nok Chiu, Dietrich Stoyan, *Stochastic Geometry and its Applications*. 2013.

[13] M. Haenggi, J. G. Andrews, F. Baccelli, O. Dousse, and M. Franceschetti, "Stochastic geometry and random graphs for the analysis and design of wireless networks," *IEEE Journal on Selected Areas in Communications*, vol. 27, no. 7, pp. 1029–1046, 2009.

[14] H. ElSawy, A. Sultan-Salem, M.-S. Alouini, and M. Z. Win, "Modeling and analysis of cellular networks using stochastic geometry: A tutorial," *IEEE Communications Surveys Tutorials*, vol. 19, no. 1, pp. 167–203, 2017.

[15] Y. Hmamouche, M. Benjillali, S. Saoudi, H. Yanikomeroglu, and M. D. Renzo, "New trends in stochastic geometry for wireless networks: A tutorial and survey," *Proceedings of the IEEE*, vol. 109, no. 7, pp. 1200–1252, 2021.

[16] F. Baccelli and B. Blaszczyszyn, *Stochastic Geometry and Wireless Networks: Volume I Theory*. 2010.

[17] F. Baccelli and B. Blaszczyszyn, *Stochastic Geometry and Wireless Networks: Volume II Applications*. 2010.

[18] M. Haenggi, *Stochastic Geometry for Wireless Networks*. Cambridge university press, 2012.

[19] W. Lu and M. D. Renzo, "Stochastic geometry modeling of cellular networks: Analysis, simulation and experimental validation," 2015.

[20] J. G. Andrews, A. K. Gupta, and H. S. Dhillon, "A primer on cellular network analysis using stochastic geometry," 2016.

[21] J. Gil-Pelaez, "Note on the inversion theorem," *Biometrika*, vol. 38, pp. 481–482, 1951.

[22] S. Lee, R. Zhang, and K. Huang, "Opportunistic wireless energy harvesting in cognitive radio networks," *IEEE Transactions on Wireless Communications*, vol. 12, no. 9, pp. 4788–4799, 2013.

[23] M. Di Renzo and W. Lu, "System-level analysis and optimization of cellular networks with simultaneous wireless information and power transfer: Stochastic geometry modeling," *IEEE Transactions on Vehicular Technology*, vol. 66, no. 3, pp. 2251–2275, 2017.

[24] T. Tu Lam, M. Di Renzo, and J. P. Coon, "System-level analysis of swipt mimo cellular networks," *IEEE Communications Letters*, vol. 20, no. 10, pp. 2011–2014, 2016.

[25] X. Zhou, J. Guo, S. Durrani, and I. Krikidis, "Performance of maximum ratio transmission in ad hoc networks with swipt," *IEEE Wireless Communications Letters*, vol. 4, no. 5, pp. 529–532, 2015.

[26] S. Akbar, Y. Deng, A. Nallanathan, M. Elkashlan, and A.-H. Aghvami, "Simultaneous wireless information and power transfer in k-tier heterogeneous cellular networks," *IEEE Transactions on Wireless Communications*, vol. 15, no. 8, pp. 5804–5818, 2016.

[27] Y. Liu, Z. Ding, M. Elkashlan, and H. V. Poor, "Cooperative nonorthogonal multiple access with simultaneous wireless information and power transfer," *IEEE Journal on Selected Areas in Communications*, vol. 34, no. 4, pp. 938–953, 2016.

[28] J. Park, B. Clerckx, C. Song, and Y. Wu, "An analysis of the optimum node density for simultaneous wireless information and power transfer in ad hoc networks," *IEEE Transactions on Vehicular Technology*, vol. 67, no. 3, pp. 2713–2726, 2018.

[29] A. I. Akin, I. Stupia, and L. Vandendorpe, "On the effect of blockage objects in dense mimo swipt networks," *IEEE Transactions on Communications*, vol. 67, no. 2, pp. 1059–1069, 2019.

[30] I. Krikidis, "Relay selection in wireless powered cooperative networks with energy storage," *IEEE Journal on Selected Areas in Communications*, vol. 33, no. 12, pp. 2596–2610, 2015.

[31] Q. Gontier, L. Petrillo, F. Rottenberg, F. Horlin, J. Wiart, C. Oestges, and P. De Doncker, "A stochastic geometry approach to emf exposure modeling," *IEEE Access*, vol. 9, pp. 91777–91787, 2021.

[32] C. Wiame, S. Demey, L. Vandendorpe, P. De Doncker, and C. Oestges, "Joint data rate and emf exposure analysis in manhattan environments: stochastic geometry and ray tracing approaches," 2023.

[33] Q. Gontier, C. Wiame, S. Wang, M. Di Renzo, J. Wiart, F. Horlin, C. Tsigros, C. Oestges, and P. De Doncker, "Joint metrics for exposure and coverage in real-world homogeneous and inhomogeneous cellular networks." available at https://drive.google.com/file/d/1jat1LI75rhkApVqWoigOmGCojltPVXXj/view?usp=sharing, 2023.

[34] M. A. Hajj, S. Wang, P. d. Doncker, C. Oestges, and J. Wiart, "A statistical estimation of 5g massive mimo's exposure using stochastic geometry," in *2020 XXXIIIrd General Assembly and Scientific Symposium of the International Union of Radio Science*, pp. 1–3, 2020.

[35] M. A. Hajj, S. Wang, and J. Wiart, "Characterization of emf exposure in massive mimo antenna networks with max-min fairness power control," in *2022 16th European Conference on Antennas and Propagation (EuCAP)*, pp. 1–5, 2022.

[36] L. Chen, A. Elzanaty, M. A. Kishk, L. Chiaraviglio, and M.-S. Alouini, "Joint uplink and downlink emf exposure: Performance analysis and design insights," *IEEE Transactions on Wireless Communications*, pp. 1–1, 2023.

[37] N. A. Muhammad, N. Seman, N. I. A. Apandi, C. T. Han, Y. Li, and O. Elijah, "Stochastic geometry analysis of electromagnetic field exposure in coexisting sub-6 ghz and millimeter wave networks," *IEEE Access*, vol. 9, pp. 112780–112791, 2021.

[38] M. Di Renzo, S. Wang, and X. Xi, "Inhomogeneous double thinning—modeling and analysis of cellular networks by using inhomogeneous poisson point processes," *IEEE Transactions on Wireless Communications*, vol. 17, no. 8, pp. 5162–5182, 2018.

[39] Q. Gontier, C. Wiame, S. Wang, M. D. Renzo, J. Wiart, F. Horlin, C. Tsigros, C. Oestges, and P. D. Doncker, "Joint metrics for emf exposure and coverage in real-world homogeneous and inhomogeneous cellular networks," 2023.

[40] T. Demir, E. Björnson, and L. Sanguinetti, *Foundations of User-Centric Cell-Free Massive MIMO*. 2021.

[41] J. Pirard, "Stochastic geometry based optimization of coverage and exposure in wireless networks," Master's thesis, UCLouvain, 2020.

[42] X. Lu, M. Salehi, M. Haenggi, E. Hossain, and H. Jiang, "Stochastic geometry analysis of spatial-temporal performance in wireless networks: A tutorial," *IEEE Communications Surveys Tutorials*, vol. 23, no. 4, pp. 2753–2801, 2021.

[43] M. Haenggi, "Meta distributions—part 1: Definition and examples," *IEEE Communications Letters*, vol. 25, no. 7, pp. 2089–2093, 2021.

[44] M. Haenggi, "Meta distributions—part 2: Properties and interpretations," *IEEE Communications Letters*, vol. 25, no. 7, pp. 2094–2098, 2021.

[45] W. Lu, M. Di Renzo, and T. Q. Duong, "On stochastic geometry analysis and optimization of wireless-powered cellular networks," in *2015 IEEE Global Communications Conference (GLOBECOM)*, pp. 1–7, 2015.

[46] N. Deng and M. Haenggi, "The energy correlation coefficient and its key role in wirelessly powered networks," *IEEE Transactions on Wireless Communications*, vol. 20, no. 12, pp. 8233–8247, 2021.

[47] X. Zhang and J. G. Andrews, "Downlink cellular network analysis with multi-slope path loss models," *IEEE Transactions on Communications*, vol. 63, no. 5, pp. 1881–1894, 2015.

[48] M. Fréchet, "Sur les tableaux dont les marges et des bornes sont données," *Revue de l'Institut International de Statistique*, vol. 28, no. 1/2, pp. 10–32, 1960.

[49] M. Haenggi, "The meta distribution of the sir in poisson bipolar and cellular networks," *IEEE Transactions on Wireless Communications*, vol. 15, no. 4, pp. 2577–2589, 2016.

[50] D.-T. P. HUY, "Electro-magnetic field exposure aware radio thanks to reconfigurable intelligent surfaces and backscatters." Talk, December 2023. Talk given during the UCLouvain workshop *B5G wireless communications*.

[51] J. G. Andrews, F. Baccelli, and R. K. Ganti, "A tractable approach to coverage and rate in cellular networks," *IEEE Transactions on Communications*, vol. 59, no. 11, pp. 3122–3134, 2011.

[52] H. S. Dhillon, R. K. Ganti, F. Baccelli, and J. G. Andrews, "Modeling and analysis of k-tier downlink heterogeneous cellular networks," *IEEE Journal on Selected Areas in Communications*, vol. 30, no. 3, pp. 550–560, 2012.

[53] Z. Ding, R. Schober, and H. V. Poor, "A general mimo framework for noma downlink and uplink transmission based on signal alignment," *IEEE Transactions on Wireless Communications*, vol. 15, no. 6, pp. 4438–4454, 2016.

[54] T. Bai and R. W. Heath, "Coverage and rate analysis for millimeter-wave cellular networks," *IEEE Transactions on Wireless Communications*, vol. 14, no. 2, pp. 1100–1114, 2015.

[55] H. Wei, N. Deng, W. Zhou, and M. Haenggi, "A simple approximative approach to the sir analysis in general heterogeneous cellular networks," in *2015 IEEE Global Communications Conference (GLOBECOM)*, pp. 1–6, 2015.

[56] M. Haenggi, "The mean interference-to-signal ratio and its key role in cellular and amorphous networks," *IEEE Wireless Communications Letters*, vol. 3, no. 6, pp. 597–600, 2014.

[57] H. Wei, N. Deng, W. Zhou, and M. Haenggi, "Approximate sir analysis in general heterogeneous cellular networks," *IEEE Transactions on Communications*, vol. 64, no. 3, pp. 1259–1273, 2016.

[58] H. Wei, N. Deng, and M. Haenggi, "An asappp approach to the spectrum allocation in general heterogeneous cellular networks," *IEEE Access*, vol. 7, pp. 89141–89151, 2019.

[59] S. Wang and M. Di Renzo, "On the meta distribution in spatially correlated non-poisson cellular networks," *EURASIP Journal on Wireless Communications and Networking*, 2019.

[60] S. Wang and M. Di Renzo, "On the mean interference-to-signal ratio in spatially correlated cellular networks," *IEEE Wireless Communications Letters*, vol. 9, no. 3, pp. 358–362, 2020.

[61] E. Turgut and M. C. Gursoy, "Coverage in heterogeneous downlink millimeter wave cellular networks," *IEEE Transactions on Communications*, vol. 65, no. 10, pp. 4463–4477, 2017.

[62] H.-S. Jo, Y. J. Sang, P. Xia, and J. G. Andrews, "Heterogeneous cellular networks with flexible cell association: A comprehensive downlink sinr analysis," *IEEE Transactions on Wireless Communications*, vol. 11, no. 10, pp. 3484–3495, 2012.

[63] H. Q. Ngo, A. Ashikhmin, H. Yang, E. G. Larsson, and T. L. Marzetta, "Cell-free massive mimo versus small cells," *IEEE Transactions on Wireless Communications*, vol. 16, no. 3, pp. 1834–1850, 2017.

[64] S. Buzzi and C. D'Andrea, "Cell-free massive mimo: User-centric approach," *IEEE Wireless Communications Letters*, vol. 6, no. 6, pp. 706–709, 2017.

[65] H. Q. Ngo, A. Ashikhmin, H. Yang, E. G. Larsson, and T. L. Marzetta, "Cell-free massive mimo: Uniformly great service for everyone," in *2015 IEEE 16th International Workshop on Signal Processing Advances in Wireless Communications (SPAWC)*, pp. 201–205, 2015.

[66] E. Björnson and L. Sanguinetti, "Scalable cell-free massive mimo systems," *IEEE Transactions on Communications*, vol. 68, no. 7, pp. 4247–4261, 2020.

[67] A. Papazafeiropoulos, P. Kourtessis, M. D. Renzo, S. Chatzinotas, and J. M. Senior, "Performance analysis of cell-free massive mimo systems: A stochastic geometry approach," *IEEE Transactions on Vehicular Technology*, vol. 69, no. 4, pp. 3523–3537, 2020.

[68] Z. Chen and E. Björnson, "Channel hardening and favorable propagation in cell-free massive mimo with stochastic geometry," *IEEE Transactions on Communications*, vol. 66, no. 11, pp. 5205–5219, 2018.

[69] A. Papazafeiropoulos, H. Q. Ngo, P. Kourtessis, S. Chatzinotas, and J. M. Senior, "Towards optimal energy efficiency in cell-free massive mimo systems," *IEEE Transactions on Green Communications and Networking*, vol. 5, no. 2, pp. 816–831, 2021.

[70] J. Qiu, K. Xu, X. Xia, Z. Shen, and W. Xie, "Downlink power optimization for cell-free massive mimo over spatially correlated rayleigh fading channels," *IEEE Access*, vol. 8, pp. 56214–56227, 2020.

[71] P. Parida and H. S. Dhillon, "Cell-free massive mimo with finite fronthaul capacity: A stochastic geometry perspective," *IEEE Transactions on Wireless Communications*, pp. 1–1, 2022.

[72] S. Elhoushy and W. Hamouda, "Limiting doppler shift effect on cell-free massive mimo systems: A stochastic geometry approach," *IEEE Transactions on Wireless Communications*, vol. 20, no. 9, pp. 5656–5671, 2021.

[73] S. Mukherjee and J. Lee, "Edge computing-enabled cell-free massive mimo systems," *IEEE Transactions on Wireless Communications*, vol. 19, no. 4, pp. 2884–2899, 2020.

[74] S. Chen, J. Zhang, Z. Chen, and B. Ai, "Treating interference as noise in cell-free massive mimo networks," in *ICC 2022 - IEEE International Conference on Communications*, pp. 1385–1390, 2022.

[75] M. Ibrahim, S. Elhoushy, and W. Hamouda, "Uplink performance of mmwave-fronthaul cell-free massive mimo systems," *IEEE Transactions on Vehicular Technology*, vol. 71, no. 2, pp. 1536–1548, 2022.

[76] S. Kusaladharma, W.-P. Zhu, W. Ajib, and G. Amarasuriya, "Performance of swipt in cell-free massive mimo: A stochastic geometry based perspective," in *2020 IEEE 17th Annual Consumer Communications Networking Conference (CCNC)*, pp. 1–6, 2020.

[77] S. Kusaladharma, W.-P. Zhu, W. Ajib, and G. A. A. Baduge, "Stochastic geometry based performance characterization of swipt in cell-free massive mimo," *IEEE Transactions on Vehicular Technology*, vol. 69, no. 11, pp. 13357–13370, 2020.

[78] R. Cai, W. Zhang, and P. C. Ching, "Cost-efficient optimization of base station densities for multitier heterogeneous cellular networks," *IEEE Transactions on Wireless Communications*, vol. 15, no. 3, pp. 2381–2393, 2016.

[79] G. Koutitas and T. Samaras, "Exposure minimization in indoor wireless networks," *IEEE Antennas and Wireless Propagation Letters*, vol. 9, pp. 199–202, 2010.

[80] D. Plets, W. Joseph, K. Vanhecke, and L. Martens, "Exposure minimization algorithm in homogeneous indoor networks," in *2013 7th European Conference on Antennas and Propagation (EuCAP)*, pp. 1497–1501, 2013.

[81] S. K. Goudos, D. Plets, N. Liu, L. Martens, and W. Joseph, "A multi-objective approach to indoor wireless heterogeneous networks planning," in *2015 9th European Conference on Antennas and Propagation (EuCAP)*, pp. 1–5, 2015.

[82] F. Héliot and T. W. C. Brown, "On the exposure dose minimization of multi-antenna multi-carrier system users," *IEEE Transactions on Vehicular Technology*, vol. 71, no. 7, pp. 7625–7638, 2022.

[83] F. Héliot and T. W. C. Brown, "Minimizing the exposure dose of multi-antenna multi-carrier system users," in *2021 Joint European Conference on Networks and Communications 6G Summit (EuCNC/6G Summit)*, pp. 170–175, 2021.

[84] F. Héliot, M. A. Jamshed, and T. W. C. Brown, "Exposure modelling and minimization for multi-antenna communication systems," in *2020 IEEE 91st Vehicular Technology Conference (VTC2020-Spring)*, pp. 1–6, 2020.

[85] M. A. Jamshed, O. Amjad, F. Heliot, and T. Brown, "Emf-reduction uplink resource allocation scheme for non-orthogonal multiple access systems," in *2019 IEEE Wireless Communications and Networking Conference Workshop (WCNCW)*, pp. 1–5, 2019.

[86] M. A. Jamshed, F. Héliot, and T. W. C. Brown, "Unsupervised learning based emission-aware uplink resource allocation scheme for non-orthogonal multiple access systems," *IEEE Transactions on Vehicular Technology*, vol. 70, no. 8, pp. 7681–7691, 2021.

[87] G. Hurlbert, *Linear optimization: the simplex workbook*. 2009.

[88] H. A. Ammar, R. Adve, S. Shahbazpanahi, G. Boudreau, and K. V. Srinivas, "User-centric cell-free massive mimo networks: A survey of opportunities, challenges and solutions," *IEEE Communications Surveys Tutorials*, vol. 24, no. 1, pp. 611–652, 2022.

[89] W. Jiang, B. Han, M. A. Habibi, and H. D. Schotten, "The road towards 6g: A comprehensive survey," *IEEE Open Journal of the Communications Society*, vol. 2, pp. 334–366, 2021.

[90] J. Kokkoniemi, J. Lehtomäki, and M. Juntti, "Stochastic geometry analysis for mean interference power and outage probability in thz networks," *IEEE Transactions on Wireless Communications*, vol. 16, no. 5, pp. 3017–3028, 2017.

[91] F. Baccelli, B. Liu, L. Decreusefond, and R. Song, "A user centric blockage model for wireless networks," *IEEE Transactions on Wireless Communications*, vol. 21, no. 10, pp. 8431–8440, 2022.

[92] Y. S. Soh, T. Q. S. Quek, M. Kountouris, and H. Shin, "Energy efficient heterogeneous cellular networks," *IEEE Journal on Selected Areas in Communications*, vol. 31, no. 5, pp. 840–850, 2013.

[93] K. A. Hamdi, "A useful lemma for capacity analysis of fading interference channels," *IEEE Transactions on Communications*, vol. 58, no. 2, pp. 411–416, 2010.

[94] H. Seltman, "Approximations for mean and variance of a ratio." available at stat.cmu.edu.

[95] K. O. Alan Stuart, *Kendall's Advanced Theory of Statistics*, vol. 1. Arnold London, 6th edition ed., 1998.

[96] N. L. J. Regina C. Elandt-Johnson, *Survival Models and Data Analysis*. John Wiley and Sons NY, 1980.

[97] E. Weisstein, "Circle-circle intersection." available at mathworld.wolfram.com/Circle-CircleIntersection.html.